Doctoral Dissertation (Shinshu University)

Study on eco-friendly and energy-efficient treatments of nanofibers for advanced textile applications

環境にやさしいかつ優れたエネルギー効率を持つ先端テキスタイル用ナノファイバーに関する研究

March 2021

KHATRI MUZAMIL

ABSTRACT

Study on eco-friendly and energy-efficient treatments of nanofibers for advanced textile applications

環境にやさしいかつ優れたエネルギー効率を持つ先端テキスタイル用ナノファイバーに関する研究

Conventionally, Textile processes consume a high amount energy and release bulk waste effluent to the environment. Sustainable growth of chemical processes is in urge to address serious environmental issues by the development of eco-friendly and energy-efficient processes, which will be simultaneously advantageous to industries.

Our first project states the improvement in aesthetic properties of nanofibers as important property next to functional properties of nanofibers, which has remained with a big research gap.

Because of higher surface area of nanofibers, improvement in their aesthetic properties such as achieving a good color yield had remained a challenging task.

Thus, we reported a successful ultrasonic-assisted dyeing of cellulose and silk fibroin nanofibers with a deep comparison to conventional dyeing, where ultrasonic-assisted dyeing showed a better color yield and improved color fastness properties over conventional dyeing for each nanofiber-based textile substrate.

The reason behind improved coloration properties was ultrasonication which help in rapid aggregation of dye molecules compared to conventional dyeing techniques. Ultrasonic energy produces cavitation and increase intramolecular collisions within the dye molecules which plays an important role to enhance the efficiency of dyeing process and assist the effective improvements in color yield properties.

Continuous cavitation also results in uniform dye transfer and achieving even coloration at a low temperature with less dye discharge into the environment.

After achieving color yield properties on nanofibers, we attempted to improve color fastness properties of cellulose nanofibers, by using vat dyes, which are famous for attaining very good color fastness properties on conventional textiles.

Utilization of vat dyes resulted excellent color fastness properties with almost no color bleeding during washing off, which are ultimately beneficial to keep environment eco-friendly.

Dope-dyeing of polyurethane and polystyrene with indole-based photochromic dye have been reported with different dye concentrations, change in chemical/physical properties and stimuli-sensibility to ultraviolet and halogen light (temperature).

Additionally, photochromic nanofibers also mimic like a sensor that can be used for security of food/drug during transportation.

After achieving energy-efficient and environment friendly coloration of advanced textile materials, we attempted to develop an eco-friendly process to prepare nanofibers.

In our research, we focused to reduce the textile waste effluent by means of adsorption on novel super-hydrophilic Zein nanofibers.

Zein has attracted a great deal of attention due to its biocompatibility, biodegradability, non-toxicity and its wide abundance on earth. Electrospinning of Zein has yet been challenged by the limitation of reusability of the polymer solution and frequent clogging of spinneret when its dissolution occurs in aqueous-ethanol (Aq-EtOH) or its preparation using hazardous solvents, such as DMF.

Recently deep eutectic solvents (DES) are widely recognized as non-volatile and non-hazardous solvents. Therefore, we prepared Zein nanofibers using deep eutectic solvents (DES-Zein) for the first time, thanks to the cedar leaf morphology and the abundant presence of -NH and -OH groups on the surface of DES-Zein nanofibers, which allow it to be used for

the applications, where super hydrophilicity is required such as biosensors, drug release and adsorption of dyes and heavy metals.

The proposed method of preparing Zein nanofibers using DES opens a new door to continuous electrospinning with tunable morphology, having potential to be used for environmental, biomedical and advanced textile applications.

All chapters separately discuss necessary characterizations with a relation to chemical and physical properties.

Keywords: Electrospinning, nanofibers, energy-efficient, coloration, adsorption, dye removal, deep eutectic solvents, Cellulose, Silk fibroin, Zein, Polyurethan, Polystyrene, textile, environmental applications.

TABLE OF CONTENTS

LIST OF TABLES

LIST OF FIGURES

LIST OF SCHEMES

CHAPTER 1 General Introduction

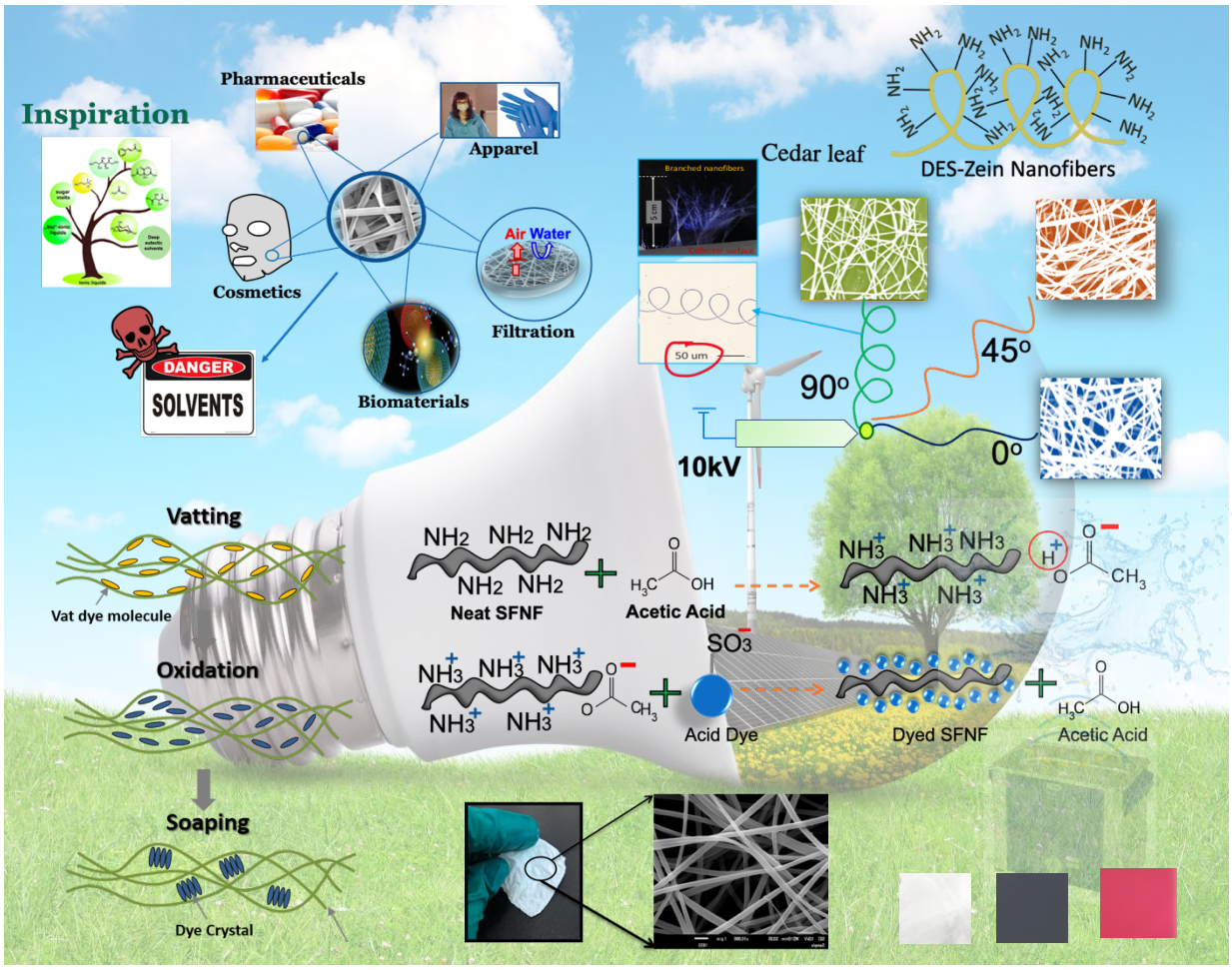

1.1. **Background and Literature**

Nanofibers have been utilized for a variety of advanced textile applications. Due to their lightweight, flexibility of function, three-dimensional structure, and ease of production using the electrospinning method [1-12].

Nanofibers have been utilized for aerospace, advanced apparel, environmental, biomedical, sensor, agriculture, tissue engineering, face mask against bacteria, pollen and viruses, filtration, batteries, cosmetic, food, pharmaceutical but there is still a big research gap to be addressed [8-14].

Cellulose nanofibers have gained a great deal of attention due to their unique properties of lighter weight, higher surface area, breathability, thermal stability, chemical resistance, and biodegradability and widespread applications in separation membranes, biosensors, chemosensory, wound dressing materials, reinforced composites, smart wearables, surgical gowns and advanced apparels [1,2].

Although there are many methods to obtain cellulose nanofibers from lignocellulosic sources by mechanical and chemical methods or enzymatic treatments, but their yield and production are low [2].

In contrast, producing cellulose nanofibers via electrospinning technique has attracted much interest due to its ease of processing and high production rate. Most commonly, cellulose nanofibers are synthesized by direct electrospinning of cellulose using N-methyl morpholine-N-oxide (NMMO) hydrate. In the typical process, cellulose/NMMO hydrate solutions are electrospun at high temperature (80–130°C) [2].

Another route to get cellulose is the deacetylation of cellulose Acetate nanofibers but this process required 30 hours of treatment with an alkali solution to complete. Due to having prolonged treatment time, it is expensive and a hectic route, deacetylation has an adverse effect too, especially on nanofibers morphology that becomes irregular. So, there is an acute need to develop a rapid deacetylation method that can reduce treatment time significantly [2]. Silk is one of them, which is an eco-friendly natural biomaterial abundantly available on Earth having distinctive properties such as high strength and good biocompatibility and is frequently used for different applications such as sensors, tissue engineering, drug release, filters, and protective clothing.

Silk fibroin nanofiber (SFNF) is a protein-based substrate mainly composed of beta-sheets with repeating varying amines and hydrogen bonds, which make silk amorphous and provides good wettability. SFNF is one of the soft, breathable, and lightweight materials and best fit

for the functional textile substrate. It is environment friendly, hygienic, non-allergenic, and has a smooth lustrous surface, its human skinlike chemical structure makes it ideal for manufacturing advanced textile.

Dyeing of SFNF requires a high temperature and longtime which releases a bulk waste after coloration by the textile industries, therefore, it was an urge to develop an energy-efficient method to save energy and the environment [3].

The coloration of the textile substrate using the ultrasonic technique is getting more attention due to better performance in the improvement of aesthetic properties of different types of nanofibers. Ultrasonic energy produces cavitation and breaks dye aggregate fast with rapid and uniform dye exhaustion on the nanofibers.

Improvement in aesthetic properties of nanofibers are as important as functional properties and this research area has remained with a big gap. Because of the higher surface area of nanofibers, improvement in their aesthetic properties such as color yield had remained a challenging task. Reactive dyes for cellulosic substrate and acid dyes for silk have always a better selection for dyers [4-7].

After achieving a good color yield, the issue of color fastness properties was in the urge to be resolved. There were many reports on dyeing of cellulose nanofiber but the color fastness properties especially the washing fastness of cellulose nanofiber remained a big problem with resultin in increased discharge of dye effluent.

Conventionally, vat dyes are famous for overcoming color fastness issues but have never been utilized on cellulose nanofibers up to date [4].

Doped dyeing is an alternate dyeing method to save time, prevent dye loss to effluents, energy, and chemicals. This technique is advantageous to achieve a uniform and even coloration for very long runs [7].

Using the dope-dyeing technique, we prepared photosensitive nanofibers which undergo a reversible structural change when irradiated with UV light, the photosensitive spiropyran (SP) dye [1′ -30′ -Dihydro-8- methoxy-1′ ,3′ ,3′ -trimethyl-6-nitrospiro [2H-1-benzopyran- 2,2′-(2H)-Indole] has been extensively considered leading to interconversion between a colorless, closed-ring, less polar SP form to a colored, ring-opened, more polar merocyanine (MC) form.

Polyurethane (PU) due to its shape memory, dyeability, and good mechanical properties have been investigated for several advanced and functional application and compared to a Polystyrene (PS) which is quite stiffer compared to PU [6].

Zein has attracted a great deal of attention due to its biocompatibility, biodegradability, non-toxicity, and its wide abundance on earth. Electrospinning of Zein has yet been challenged by the limitation of reusability of the polymer solution and frequent clogging of spinneret when its dissolution occurs in aqueous-ethanol (Aq-EtOH) or its preparation using hazardous solvents, such as DMF [8].

The use of organic solvents for the preparation of nanofibers is challenged due to their volatile and hazardous behavior.

Recently deep eutectic solvents (DES) are widely recognized as non-volatile and non-hazardous solvents which never been utilized directly for nanofabrication via electrospinning [8].

The effluents generated from industries, particularly the textile industry, contain approximately 15% of total dye that deteriorates not only the environment but also reduces availability of drinkable water resources. Therefore, it is the utmost task to prevent the discharge of industrial effluents to an aquatic environment from an eco-toxicological and aesthetic point of view. Conventionally, various chemical and biological processes are employed to remove dyes from wastewater such as photochemical, coagulation, ozonation,

membrane filtration, and adsorption. Nevertheless, the use of these techniques is limited by high operation cost, generation of waste sludge, and ineffectiveness in treating effluent with low dye concentrations. Adsorption has proven the best in terms of ease of operation, low cost, simple design, and flexibility towards the type of adsorbent used in the process [9,10-13].

1.2. **Electrospun Nanofibers**

Nanotechnology not only depends on overcoming scientific barriers in developing a novel method by addressing numerous environmental and textile concerns.

In this regard, the most important challenges are the maximized use of "green" materials (concerning the type of chemistry involved) in the generation of nanoscale-based products.

Electrospinning is an efficient technique that produces continuous nanofibers with lengths in the range of 5–100 nm, which is 100–10000 times smaller than fibers fabricated by solution or melt spinning. This method can be used for synthetic and natural polymers, polymer blends and nanoparticles [1-10].

For example, nanofibers from any polymer, which can be synthetic or natural can be produced by electrospinning with sizes at the nanoscale [11-16].

The electrospinning is a high voltage supply to a specifically prepared polymer solution, neat or with any external guest molecule which can be shaped into nanofibers by keeping Infront of a negatively charged collector where the fibers can be collected produced with the flow of electrons from positively charged electrode to the negatively charged cathode.

During electrospinning, spherical pendant polymer droplets of the polymer solution are transferred to a conical shape with high stretch characteristics. Additionally, fast solvent evaporation happens at the time of polymer discharge from the tip of the syringe where the solution is poured prior to a voltage supply.

Electrospinning is an effective technique for bulk production of a range of non-woven textiles using a variety of polymers [17].

1.3. **Nanofibers for dye adsorption**

Nanofibers with a porous structure, surface functionalities, and high specific surface area show promise for adsorptive applications. The removal of pollutants, including heavy metals and dyes, is of paramount importance.

Water contamination by dyes and other impurities has remained one of the big global concerns. Scientists are trying to develop various techniques to remove these contaminants from water using advanced materials with adsorption technique, which as per literature is efficient enough and eco-friendly approach.

Bio-based natural polymers with green and benign features and potential for commercial applications have been employed as feasible alternatives to replace synthetic polymers and reduce environmental impacts [8-14].

With unique chemical composition, molecular weights, and functional chemical groups such as amines, hydroxyl, and in some cases carboxyl groups, show a multitude potential for dye and metal ion removing capability [12].

The adsorption technique is one of the most energy-efficient, simple, and fast approaches for separating contaminants from wastewater adsorption relates to the accumulation of substances at the interfaces of different phases, and desorption is the process of regenerating the adsorbents by removing adsorbates from their surface. Adsorption is very efficient for heavy metal and dye elimination with respect to cost-effectiveness, regeneration, and performance [15].

1.4. **Deep eutectic solvents (DES)**

Deep eutectic solvents (DESs) were introduced in 2003 as low-melting-point eutectics that are liquid at room temperature. DESs are eutectic mixtures composed of two or more components having melting point lower than that of the individual components such as hydrogen bond donors (HBDs) and hydrogen bond acceptors (HBAs).

Usually, DESs are formed through hydrogen bonding. The physicochemical properties of DESs are similar to those of ionic liquids (ILs). These properties include non-flammability, low volatility, and designability. Preferable to ILs, DESs are regarded as green solvents owing to their biodegradability, low toxicity, facile synthesis, and low cost.

These desirable properties such as Pharmaceuticals, cosmetic, environmental, and biomedical applications for ensuring public health can be achieved by using DES. In compliance with the current trend towards green analytical chemistry, the replacement of conventional toxic organic solvents with eco-friendly and safe solvents has been pursued in developing sample pretreatment methods. DES has been increasingly applied as desirable alternative solvents in numerous types of sample pretreatment methods for different eco-friendly and bio-friendly applications [20-30].

1.5. **Ultrasound energy**

Ultrasound processing is an environment-friendly, safe and inexpensive technology used as a versatile tool in a wide range of scientific and technological applications, for instance: biology, chemistry, physics, medicine, material science, and industrial applications. Nanomaterials can be obtained and modified using ultrasonic irradiation to assist synthetic methods in aqueous solution.

The acoustic cavitation produced by ultrasonic irradiation in water generates transient bubbles, within which different physical and chemical phenomena generated by their implosion play an essential role in the formation of nanostructures. Combining the ultrasound physical effects such as cavitation arises of temperature and local pressure differential and ultimately enhance the efficiency of any chemical reaction or process including exhaustion rate and uniform distribution of dyes on nanofibers during dyeing [1,2,3,17].

1.6. **Objectives**

In our research, we focused to reduce the textile waste effluent (dyes and heavy metals) utilizing advanced energy-efficient coloration techniques, reducing/removing industrial discharge from water, and eco-friendly production of nanofibers.

The main objectives of the research are listed below;

1- Preparation of appropriate nanofiber substrates via electrospinning method.
2- The eco-friendly and energy-efficient coloration of cellulose nanofiber to improve color yield properties.
3- Improvement in color fastness properties of cellulose nanofibers using vat dyes.
4- The energy-efficient coloration of SFNF nanofibers at room temperature with less discharge of dye effluent and overcoming the issue of shrinkage during dyeing of SFNF.
5- Dope dyeing of polyurethane and polystyrene nanofibers to save energy and the environment for apparel and food security applications.
6- Replacing hazardous solvents with DES for electrospinning of nanofibers for advanced textile, environmental applications.

The highlighted outcomes of the research chapter-wise are given below.

CHAPTER 1

The first chapter gives an overview of the thesis book, including background literature, the introduction of the technologies used for the research such as nanotechnology, electrospinning, ultrasonication, deep eutectic solvents system, dope dyeing.
Short description of effecting parameters of processing and a general description of applications of electrospun nanofibers.

CHAPTER 2

Improvement in aesthetic properties of cellulose nanofibers are as important as functional properties and this research area has remained with a big gap. Because of the higher surface area of nanofibers, improvement in their aesthetic properties such as enhancing the color yield remained a challenging task. Reactive dyes for cellulosic substrate have always a better selection for dyers.
Therefore, we reported successful ultrasonic-assisted dyeing of cellulose nanofibers with a deep comparison to conventional dyeing results, ultrasonic-assisted dyeing showed better color yield and much-improved color fastness properties over conventional dyeing of cellulose nanofibers. This is because the Ultrasonic energy aggregates the dye rapidly compared to conventional techniques for dyeing processes in which cavitation plays an important role to enhance the efficiency and improve the color yield with uniform dye transfer and even coloration. Exhaust dyeing method was used with mass: liquor ration 1:20, and, Ultrasonic equipment with an output power 320w and the intensity of sonicating bath 0.98 W/cm2 (intensity = power/bath area: 320–328) with a frequency of 38 kHz were used for dyeing.

CHAPTER 3

After achieving a good color yield, the issue of color fastness properties was in the urge to be resolved. There were many reports on dyeing of cellulose nanofiber but the color fastness properties especially the washing fastness of cellulose nanofiber remained a problem with results in more dye effluent.

We chose vat dyes because of their good color fastness properties towards the cellulose-based textile substrate. We chose two types of vat dyes for coloration of cellulose nanofibers to enhance color fastness properties and several dyeing parameters were optimized to dye cellulose nanofibers using vat dyes. Ultimately, enhanced crystallinity was achieved when dye using vat dyes.

CHAPTER 4

Silk is an eco-friendly natural biomaterial abundantly available on Earth, Silk fibroin nanofiber (SFNF) is one of the soft, breathable, and lightweight materials and best fit for the functional textile substrate. It is environment friendly, hygienic, non-allergenic, and has a smooth lustrous surface, its human skinlike chemical structure makes it ideal for manufacturing advanced textile.

SFNF are most suitable for acid dyeing due to their high substantive behavior towards them. The SFNF is dyed in an acidic solution having pH 6, the SFNF contains NH_2 as a functional compound which is protonated by acetic acid, and as a result, NH_3^+ is formed, which ionically interacts with the negatively charged acid dye resulting in hydrogen bonds, dipolar bonds and van der Waals forces between the acid dye and positively charged SFNF. As a result, acetic acid is reformed and washed off during the soaping of resultant dyed samples.

The SFNF were prepared by dissolving silk solution of 7 w/v % in HFIP and carried for electrospinning. Ultrasonic-assisted dyeing of silk fibroin nanofibers using acid dyes at room temperature was reported for the very first time. SFNF has been intensively investigated for various textile industries. Ultrasonic dyeing was carried at mass: liquor ration 1:20, and this method improved 60% of dyeing efficiency with 62.28% electrical and 64.28% thermal energy saving. It potentially enhanced color yield properties and reduction in dye effluent compared to the conventional dyeing process. The dyed SFNF showed smooth morphology and the shrinkage problem in the dyeing of SFNF was resolved by using Ultrasonic energy.

CHAPTER 5

Dope dyeing also has the potential to produce nanofibers with photosensitive properties which undergo a reversible structural change when irradiated with UV light, the photosensitive spiropyran (SP) dye [$1^{/}$ -$30^{/}$ -Dihydro-8- methoxy-$1^{/}$,$3^{/}$,$3^{/}$ -trimethyl-6-nitrospiro [2H-1-benzopyran- 2,$2^{/}$-(2H)-Indole] has been extensively considered leading to interconversion between a colorless, closed-ring, less polar SP form to a colored, ring-opened, more polar merocyanine (MC) form.

Polyurethane due to its shape memory, dyeability, and good mechanical properties have been investigated for several advanced and functional application. Therefore, Photo-responsive dye incorporated polyurethane nanofibers were prepared via electrospinning for the QR code data recording/erasing applications. The resultant polyurethane nanofibers were UV printed with QR code data which was easily readable via Smartphones at the area of 1 cm^2. The resultant nanofibers were found to be multiple times photo-switchable upon alternating UV (365 nm) and 40^{o}C irradiations and optimized for smart apparel applications.

Hence, various types of dyes have been applied/optimized using different dyeing techniques for aesthetic improvements in aesthetic properties of nanofibers for advanced apparel applications.

CHAPTER 6

Zein has attracted a great deal of attention due to its biocompatibility, biodegradability, non-toxicity, and its wide abundance on earth. Electrospinning of Zein has yet been challenged by the limitation of reusability of the polymer solution and frequent clogging of spinneret when its dissolution occurs in aqueous-ethanol (Aq-EtOH) or its preparation using hazardous solvents, such as DMF.

Recently deep eutectic solvents (DES) are widely recognized as non-volatile and non-hazardous solvents Therefore, we prepared Zein nanofibers using deep eutectic solvents (DES-Zein) for the first time. , thanks to the cedar leaf morphology and the abundant presence of -NH and -OH groups on the surface of DES-Zein nanofibers, which allow it to be used where super hydrophilicity is required.

The proposed method of preparing Zein nanofibers using DES opens a new door to continuous electrospinning with tunable morphology, having the potential to be used for environmental and biomedical applications.

1.7. **References**

[1] Muzamil Khatri, Farooq Ahmed, Abdul Wahab Jatoi, Rasool Bux Mahar, Zeeshan Khatri and Ick Soo Kim "Ultrasonic Dyeing of cellulose nanofiber" Ultrasonics sonochemistry (2016), 31, 350-354

[2] Farooq Ahmed, Alvira Ayoub Arbab, Abdul Wahab Jatoi, Muzamil Khatri, Najma Memon, Zeeshan Khatri and Ick Soo Kim "Ultrasonic-assisted deacetylation of cellulose acetate nanofibers: A rapid method to produce cellulose nanofibers" Ultrasonics sonochemistry (2017), 36, 319-325.

[3] Muzamil Khatri, Nadir Hussain, Sofia El-Ghazali, Takayuki Yamamoto, Shunichi Kobayashi, Zeeshan Khatri, Farooq Ahmed, and Ick Soo Kim "Ultrasonic-assisted dyeing of silk fibroin nanofibers: an energy-efficient coloration at room temperature" Applied Nanoscience (2019) 1-14

[4] Muzamil Khatri, Farooq Ahmed, Irfan Shaikh, Duy Nam Phan, Qamar Khan, Zeeshan Khatri, Hoik Lee and Ick Soo Kim "Dyeing and characterization of regenerated cellulose nanofibers with vat dyes" Carbohydrate Polymers (2017), 174, 443-449

[5] Zeeshan Khatri, Farooq Ahmed, Awais Khatri, Muzamil Khatri, Umair Ahmed Qureshi and Ick Soo Kim "Screen-printed electrospun cellulose nanofibers using reactive dyes" Cellulose (2017), 24, 4561-4568

[6] Muzamil Khatri, Farooq Ahmed, Shamshad Ali, Mujahid Mehdi, Sana Ullah, Phan Duy-Nam ,Zeeshan Khatri and Ick Soo Kim "Photosensitive nanofibers for data recording and erasing" The Journal of the Textile Institute (2020), 1754-2340

[7] Mujahid Mehdi, Faraz Khan Mahar, Umair Ahmed Qureshi, Muzamil Khatri, Zeeshan Khatri, Farooq Ahmed, Ick Soo Kim "Preparation of colored recycled polyethylene terephthalate nanofibers from waste bottles: Physicochemical studies" Advances in Polymer Technology (2018), 37 (8), 2820-2827

[8] Muzamil Khatri, Zeeshan Khatri, Sofia El-Ghazali, Nadir Hussain, Umair Ahmed Qureshi, Shunichi Kobayashi, Farooq Ahmed and Ick Soo Kim "Zein nanofibers via deep eutectic solvent electrospinning: tunable morphology with super hydrophilic properties "Scientific Reports (2020), 10, 1-11

[9] Umair Ahmed Qureshi, Zeeshan Khatri, Farooq Ahmed, Abdul Sameeu Ibupoto, Muzamil Khatri, Faraz Khan Mahar, Rafi Zaman Brohi and Ick Soo Kim "Highly efficient and robust electrospun nanofibers for selective removal of acid dye" Journal of Molecular Liquids (2017), 244, 478-488

[10] Qureshi, Umair Ahmed, Zeeshan Khatri, Farooq Ahmed, Abdul Sameeu Ibupoto, Muzamil Khatri, Faraz Khan Mahar, Rafi Zaman Brohi, and Ick Soo Kim. "Highly efficient and robust electrospun nanofibers for selective removal of acid dye." Journal of Molecular Liquids 244 (2017): 478-488.

[11] Phan, D.N., Rebia, R.A., Saito, Y., Kharaghani, D., Khatri, M., Tanaka, T., Lee, H. and Kim, I.S., 2020. Zinc oxide nanoparticles attached to polyacrylonitrile nanofibers with hinokitiol as gluing agent for synergistic antibacterial activities and effective dye removal. Journal of Industrial and Engineering Chemistry.

[12] Phan, D.N., Khan, M.Q., Nguyen, N.T., Phan, T.T., Ullah, A., Khatri, M., Kien, N.N. and Kim, I.S., 2020. A review on the fabrication of several carbohydrate polymers into nanofibrous structures using electrospinning for removal of metal ions and dyes. Carbohydrate Polymers, p.117175.

[13] Qureshi, U. A., Khatri, Z., Ahmed, F., Khatri, M., & Kim, I. S. (2017). Electrospun zein nanofiber as a green and recyclable adsorbent for the removal of reactive black 5 from the aqueous phase. ACS Sustainable Chemistry & Engineering, 5(5), 4340-4351.

[14] Hashmi, M., Ullah, S., Ullah, A., Khan, M. Q., Hussain, N., Khatri, M., ... & Kim, I. S. (2020). An optimistic approach “from hydrophobic to super hydrophilic nanofibers” for enhanced absorption properties. Polymer Testing, 90, 106683.

[15] Najafi, M., & Frey, M. W. (2020). Electrospun Nanofibers for Chemical Separation. Nanomaterials, 10(5), 982.

[16] Khan, M. Q., Lee, H., Khatri, Z., Kharaghani, D., Khatri, M., Ishikawa, T., ... & Kim, I. S. (2017). Fabrication and characterization of nanofibers of honey/poly (1, 4-cyclohexane dimethylene isosorbide trephthalate) by electrospinning. Materials Science and Engineering: C, 81, 247-251.

[17] Khatri, M., Qureshi, U. A., Ahmed, F., Khatri, Z., & Kim, I. S. (2018). Dyeing of electrospun nanofibers. In Handbook of nanofibers (pp. 1-16). Springer.

[18] X. Zhou, W. Jin, C. Sun, S.H. Gao,C. Chen, Q. Wang, & Q.Wang, "Microbial degradation of N, N-dimethylformamide by Paracoccus sp. strain DMF-3 from activated sludge." Chemical Engineering Journal 343 (2018): 324-330.

[19] K. Baskar, J. Ananthi & S. Ignacimuthu, "Toxic effects of Solanum xanthocarpum Sch &Wendle against Helicoverpa armigera (Hub.), Culex quinquefasciatus (Say.) and Eisenia fetida (Savigny, 1826)." Environmental Science and Pollution Research 25.3 (2018): 2774-2782.

[20] E.L. Smith, A.P. Abbott, K.S. Ryder, Deep eutectic solvents (DESs) and their applications." Chemical reviews 114.21 (2014): 11060-11082.

[21] C.A. Nkuku, R.J. J. LeSuer. "Electrochemistry in deep eutectic solvents." The Journal of Physical Chemistry B 111.46 (2007): 13271-13277.

[22] A. Paiva, R. Craveiro, I. Aroso, M. Martins, R.L. Reis, A.R.C. Duarte, "Natural deep eutectic solvents–solvents for the 21st century." ACS Sustainable Chemistry & Engineering 2.5 (2014): 1063-1071.

[23] Y.P Mbous, M. Hayyan, A. Hayyan, W.F.Wong, M.A. Hashim, M. A., & C.Y. Looi, , "Applications of deep eutectic solvents in biotechnology and bioengineering—promises and challenges." Biotechnology advances 35.2 (2017): 105-134.

[24] A. Abo-HamadM. Hayyan, M.A. AlSaadi, M. A. Hashim, ”Potential applications of deep eutectic solvents in nanotechnology." Chemical Engineering Journal273 (2015): 551-567.

[25] Chatterjee, M., Ishizaka, T., & Kawanami, H. (2018). Accelerated decarbonylation of 5-hydroxymethylfurfural in compressed carbon dioxide: a facile approach. Green chemistry, 20(10), 2345-2355.

[26] Paulino, P. N., Perez, R. F., Figueiredo, N. G., & Fraga, M. A. (2017). Tandem dehydration–transfer hydrogenation reactions of xylose to furfuryl alcohol over zeolite catalysts. Green Chemistry, 19(16), 3759-3763.

[27] L. Millia, V. Dall'Asta, C. Ferrara, V. Berbenni, E. Quartarone, F.M. Perna & P. Mustarelli, "Bio-inspired Choline chloride-based deep eutectic solvents as electrolytes for lithium-ion batteries." Solid State Ionics 323 (2018): 44-48

[28] Wang, Y., Niu, Z., Zheng, Q., Zhang, C., Ye, J., Dai, G., ... & Zhang, X. (2018). Zn-based eutectic mixture as anolyte for hybrid redox flow batteries. Scientific reports, 8(1), 5740

[29] Li, G., Li, N., Zheng, M., Li, S., Wang, A., Cong, Y., ... & Zhang, T. (2016). Industrially scalable and cost-effective synthesis of 1, 3-cyclopentanediol with furfuryl alcohol from lignocellulose. Green Chemistry, 18(12), 3607-3613.

[30] Perez, R. F., & Fraga, M. A. (2014). Hemicellulose-derived chemicals: one-step production of furfuryl alcohol from xylose. Green Chemistry, 16(8), 3942-3950.

CHAPTER 2

Ultrasonic dyeing of cellulose nanofibers

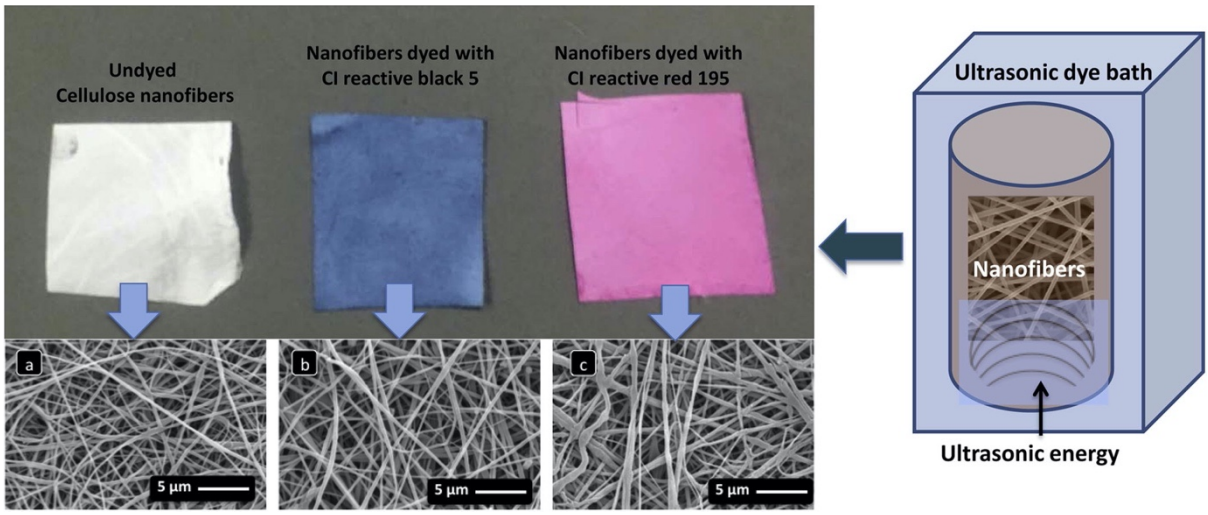

2.1. Introduction

Nanofiber for use in apparel has attained a great deal of interest recently due to its breathable characteristics, lighter in weight, and ease of production via electrospinning. Apart from the intensive research on functional characteristics of nanofibers [1], [2], [3], [4], [5], the exploration of dyeability of nanofibers has also been initiated for obtaining aesthetic property.

For the past couple of years, dyeing of nanofibers by various methods has been reported. Most recent works include dyeability of cationic cellulose nanofibers with reactive dyes by the batch-wise method [6], dyeing of cellulose acetate (CA) nanofibers with disperse dye by the pad-dry-bake method [7], cold-pad-batch dyeing method of nanofiber [8], dyeing of nanofibers by dual padding method [9] and dyeing of polyurethane nanofibers by the pad-dry-bake method [10]. Despite consistent progress in this area, nanofiber dyeing remains a challenge due to lower color yield in comparison to conventional fibers.

This is mainly due to the higher surface to volume ratio that scatters more light and results in lower color yield values. Since this factor is out of dyer's control, the only possible way is to develop a method that would be able to introduce more dye into nanofibers.

In our opinion, the color yield may improve if the nanofiber dyeing were assisted by ultrasonic energy, thanks to the sonication that breaks the dye aggregates. Later, this was proved through our experiments to be a better option to improve color yield.

Ultrasonic assisted dyeing of cellulosic fibers has already proved to be a better choice among conventional dyeings. For instance, low-temperature dyeingg of knitted cotton fabric using ultrasonic energy [11], ultrasonic-assisted dyeing of bamboo fibers [12], ultrasound-assisted dyeing of cellulose acetate [13], cold-pad-batch dyeing of cotton fiber using ultrasonic energy [14], ultrasonic natural dyeing [15]; ultrasonic dyeing of cellulosic fabric [16], ultrasonic dyeing of cationized cotton fabric [17], [18]. Dyeing of cotton fabrics with Crocus sativus using the ultrasonic method [19], ultrasonic-assisted dyeing of cationic cotton with lac natural dye [20]. Therefore, we attempted to optimize the ultrasonic-assisted dyeing method for cellulose nanofiber and report improvement in terms of color yield.

There has always been a choice for dyers to dye cellulosic fiber with reactive dyes, direct dyes, sulfur dyes, and vat dyes [21]. We chose reactive dyes due to the wide range of inexpensive brilliant colors with excellent color fastness to washing [22]. The cellulose nanofibers were dyed with CI reactive black 5 and CI reactive red 195 by ultrasonic-assisted batch-wise dyeing method. The ultrasonic dyeing parameters optimized were dyeing temperature, dyeing time, dye concentrations, and color fastness properties. The optimized results of conventional dyeing have also been presented in the article. The morphologies of optimum samples were investigated under scanning electron microscopy (SEM).

2.2. Experimental

2.2.1. Materials

Cellulose acetate, CA (39.8% acetyl content having an average Mw = 30 kDa), was obtained from Sigma–Aldrich Chemical Co. and used without further purification. Two dyes used were namely, CI reactive black 5 (bis-sulphatoethylsulphone) (Mw = 991.82 g/mol) and CI reactive red 195 (Aminochlorotriazine-sulphatoethylsulphone) (Mw = 1136.32 g/mol), supplied by the Sumitomo Chemical Co., Ltd., Japan; the corresponding dye structures are shown in Scheme 3.1. Sodium carbonate and sodium sulphate used were of Analar grade.

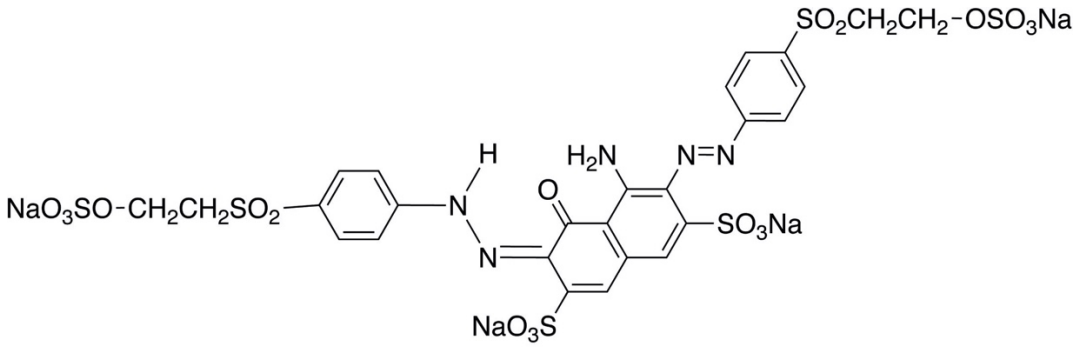

CI Reactive Black 5

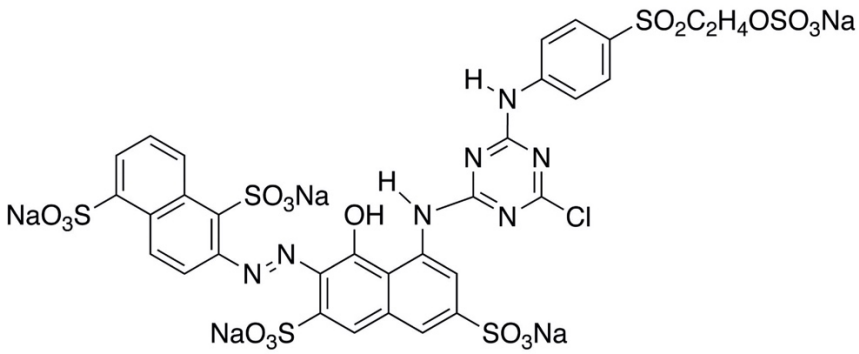

CI Reactive Red 195

Scheme 2.1. Chemical structures of reactive dyes.

2.2.2. Preparing cellulose nanofibers

For cellulose nanofiber preparation, cellulose acetate (CA) was electrospun followed by deacetylated to remove acetyl group. Our previous method [14] was followed for electrospinning of CA nanofibers. A 17% of CA solution was prepared using acetone:DMF solvents (2:1) and electrospun using a high-voltage power supply (Har-100*12, Matsusada Co., Tokyo, Japan). The voltage applied was 12.5 kV and 15 cm distance from needle-tip to collector was fixed. The nanofibers were then dried in air for 48 h. For deacetylation, conversion of CA into cellulose, the CA nanofiber samples were soaked for 30 h in 0.05 M NaOH followed by rinsing with distilled water till neutral pH of cellulose nanofibers was obtained. Before ultrasonic dyeing, all cellulose nanofibers were dried at 50 °C for 4 h.

2.2.3. Dyeing of cellulosic nanofibers

All nanofiber webs were dyed by batchwise method using Ultrasonic equipment (Model: Elmasonic E30H, Elma, Germany) with precise control of time and temperature. The dyeing was carried out at 320 W power output using fixed frequency of 37 kHz. The internal area of the bath was 24 × 13.7 cm2. The ultrasonic intensity to the dye bath was 0.97 W/cm2 (Intensity = Power/ bath area; 320/328). At low ultrasonic intensities less than 3 W/cm2, forms stable cavitation bubbles, which breaks dye aggregates at nanofibers surface as a result, dye diffusion is enhanced. The ratio of dye liquor to the mass of nanofibers was maintained at 20:1. Nanofibers dyeing was carried out to investigate the effect of dyeing temperatures (40–80 °C), effect of dyeing times (10–70 min) and effect of dye concentrations (2–6% on mass of web, omw) on color yields of dyed nanofibers. After dyeing, each sample was finally given a gentle rinse separately with warm then cold water followed by soaping-off with anionic detergent. The wash was continued until no dye

bleeding was observed. In order to compare ultrasonic dyeing with conventional dyeing of nanofibers, we selected optimum dyeing conditions based on our previous work [6]. Briefly, conventional dyeing of cellulose nanofibers was carried out without using ultrasonic energy at 70 °C for 60 min. The dye concentration selected was 3% omw for each dye.

2.2.4. Measurement of color

The K/S values that determine the color yield of dyed nanofibers, were assessed for each dyed sample using Datacolor Spectrophotometer. The relative color yields (K/S values) were calculated using Eq. (2. 1):

$$K/S = \frac{(1-R)^2}{2R} \qquad (2.1)$$

where R = decimal fraction of the reflectance of the dyed nanofibers, K = absorption coefficient and S = scattering coefficient.

2.2.5. Fourier transform infrared spectroscopy

The chemical structure of dyed and undyed nanofibers were analyzed using FTIR spectroscopy on an IR Prestige-21 by Shimadzu, Japan. All nanofibers samples were analyzed using ATR-FTIR mode.

2.2.6. Scanning electron microscope

The dyed nanofibers were examined under scanning electron microscope (SEM) by JEOL model JSM 6010LA with accelerating voltage of 30 kV and maximum magnification of 300,000×. All samples were sputtered with Pd–Pt before assessment.

2.2.7. Color fastness tests

Color fastness to washing of dyed nanofibers were performed using Gyrowash (James H. Heal Co., UK) by following ISO 105-C10:2006 method, whereas, the color fastness to light were performed using Apollo (James H. Heal Co., UK) by following ISO 105-BO2 light fastness test.

2.3. Results and discussion

2.3.1. Effect of dyeing temperature on color yield

Since the ultrasonic dyeing of nanofibers is very first time, therefore, it was necessary to optimize dyeing parameters such as temperature and time. To begin with, effect of temperature was studied first, keeping the dyeing time constant for 80 min. Fig. 2. 1 shows the effect of temperature on color yield of nanofibers dyed with CI reactive black 5 and CI reactive red 195. The color yield of CI reactive black 5 increased gradually with increasing dyeing temperature from 40 °C to 60 °C with a slower increase from 60 °C to 70 °C. The color yield at higher dyeing temperature (80 °C) remained same. This may be due to higher dyeing temperature that lowers the substantivity ratio of the dye and lead to accelerate dye hydrolysis [21], [22]. It is worth considering the optimum dyeing temperature of 70 °C because of higher color yield. Irrespective to the dyeing temperature, the color yield of CI reactive black 5 obtained higher than the CI reactive red 195. This may be due to the difference of molar extinction coefficient, affinity and reactivity between both dyes. On the other hand, dye uptake of CI reactive red 195 slowly increased from 40 °C to 60 °C and reached higher yield at 70 °C. This steady profile of CI reactive red 195 is due to lowering of substantivity ratio caused by increasing temperature [21], [22].

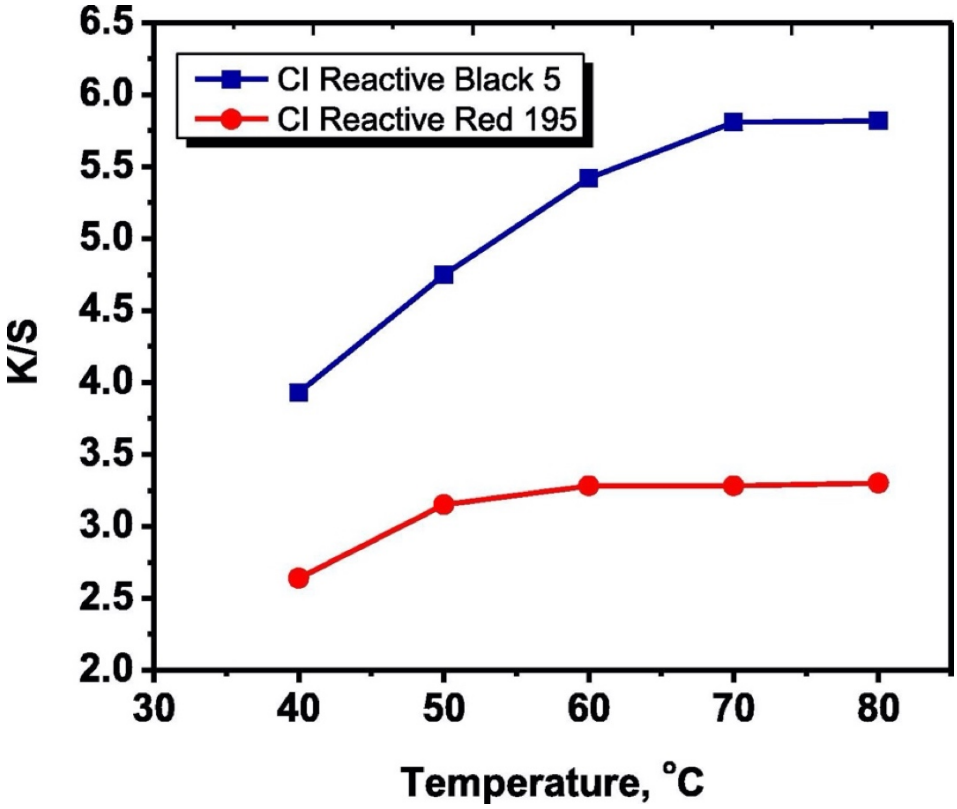

Fig. 2.1. Effect of dyeing temperature on color yield (dyeing time 60 min; dye conc. 2% omw).

2.3.2. Effect of dyeing time on color yield

Owing to higher dye uptake and optimum dyeing of cellulose nanofibers at 70 °C, this temperature was used for determining optimum dyeing time and the results are reported in Fig. 2. 2. For CI reactive black 5, a notably higher increase in color yield can be observed from 10 min to 20 min thereby maximum color yield obtained until 30 min of dyeing time. This may be due to ultrasonic cavitation that breaks the dye aggregates and helps to increase dye uptake [11]. The color yield of nanofibers dyed with CI reactive red 195 also increased from 10 min to 20 min with substantial increase and higher color yield at 30 min. Hence, 30 min was chosen as optimum time for CI reactive black 5 as well as CI reactive red 195.

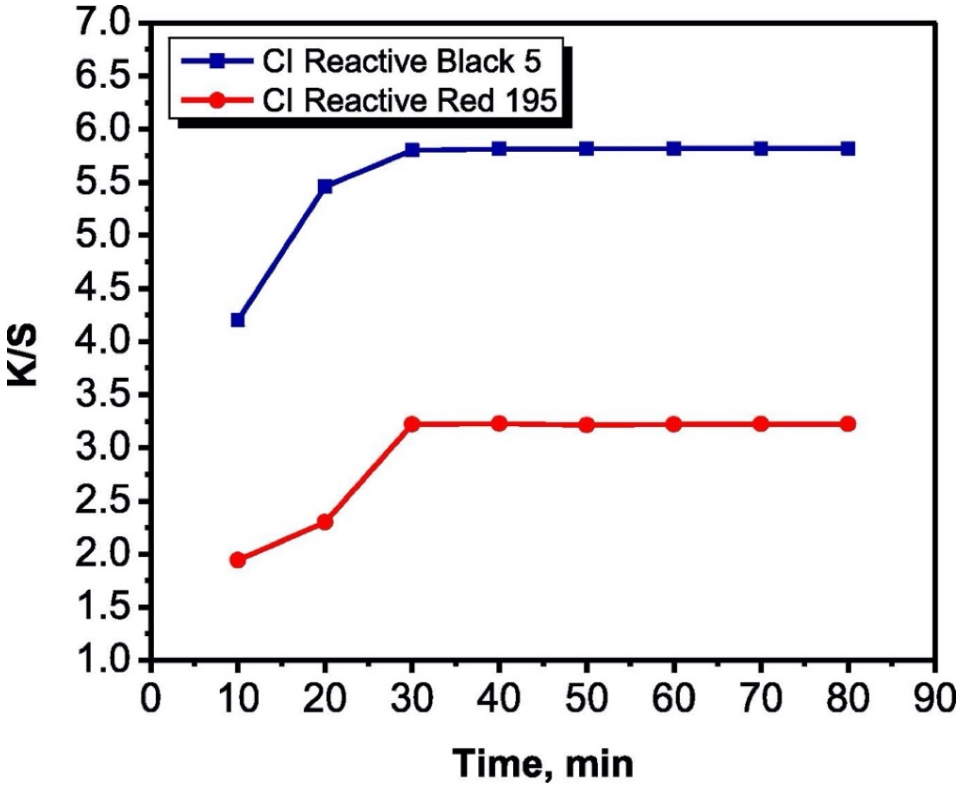

Fig. 2.2. Effect of dying time on color yield (dyeing temperature 70 °C; dye conc. 2% omw).

2.3.3. Color build-up property of nanofibers

To investigate the buildup property of CI reactive black 5 and CI reactive red 195, the effect of dye concentrations on color yield was studied for each dye as demonstrated in Fig. 2. 3. A build-up characteristic of each dye was investigated measuring K/S values at each dye concentrations (2%, 3%, 4%, 5% and 6%) using temperature and time optimized in previous steps. The results demonstrated in Fig. 2. 3 depict gradual increase of K/S values with higher dye concentration for both the dyes. Increasing dye concentration during ultrasonic dyeing showed a linear relationship that demonstrates cellulose nanofibers has a very good ability to dye build up characteristic. It can be seen from the Fig. 2. 3 that the K/S values for

CI reactive black 5 was higher than the CI reactive red 195. The reason for higher color yield values is quite obvious due to the molar extinction coefficient; affinity and reactivity for each dye are different, resulting in different color yield values [22].

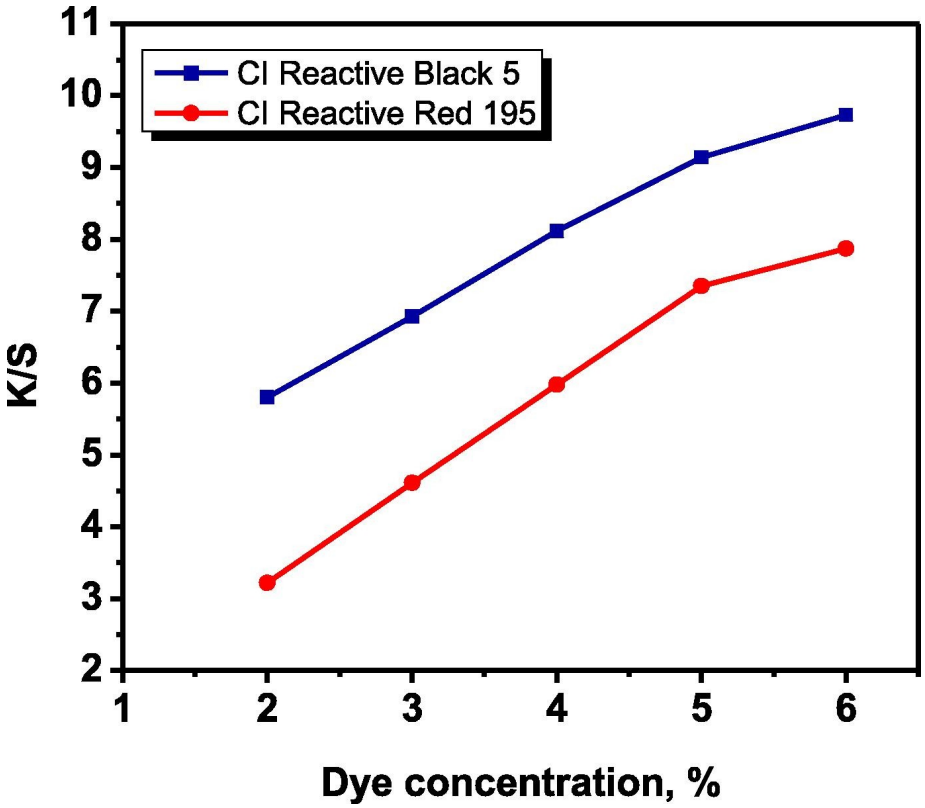

Fig. 2. 3. Effect of dye concentrations on color yield (dyeing time 60 min; dyeing temperature 70 °C).

2.3.4. Comparison of color yield between ultrasonic dyed nanofibers and conventional dyed nanofibers

Comparison of ultrasonic dyeing and conventional dyeing of cellulose nanofibers has been given in Fig. 2. 4. The results of ultrasonic dyeing show higher color yield than the conventional dyeing for both dyes. Color yield of nanofibers dyed with CI reactive black 5 by ultrasonic dyeing showed 20.35% higher than those nanofiber dyed by conventional

dyeing, whereas, CI reactive red 195 showed 14.53% higher color yield. The higher K/S value with ultrasonic supported dyeing may be attributed to breaking of dye aggregates at nanofiber surface by ultrasonic energy and establishment of resultant equilibrium in a shorter time period [11].

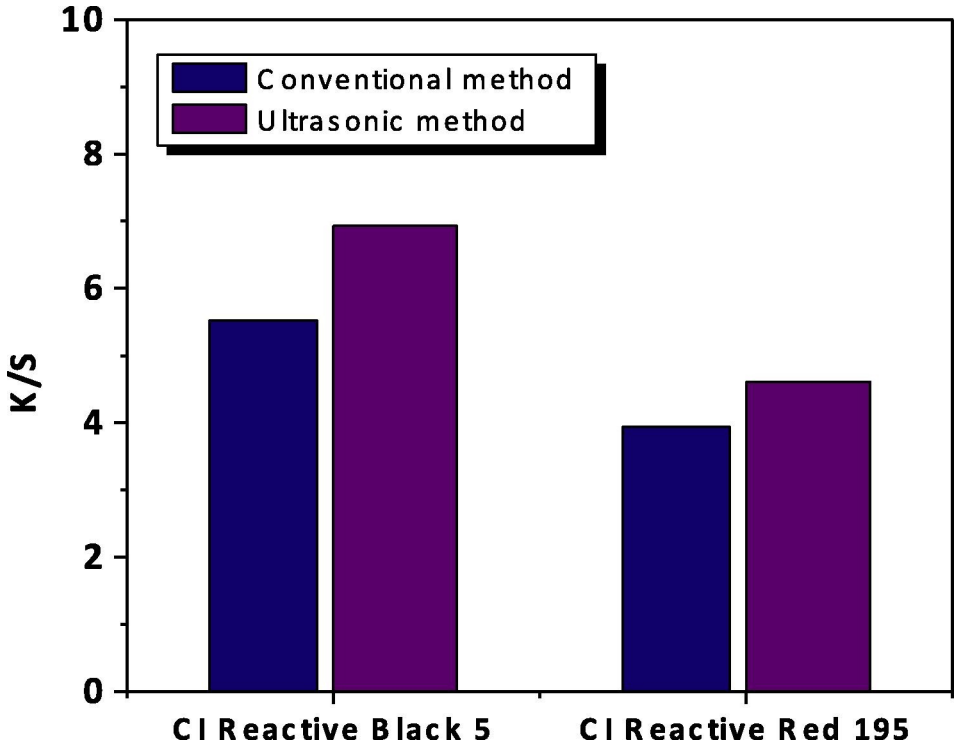

Fig. 2.4. Comparison of color yield between ultrasonic dyed nanofibers and conventional dyed nanofibers (dye conc. 3%).

2.3.5. Chemical structural changes in dyed and undyed nanofibers

The characteristic adsorption peaks of cellulose acetate attributed to the vibrations of the acetate group C–O at 1745 cm^{-1} , C–CH_3 at 1375 and C–O–C at 1235 cm^{-1} disappeared, whereas an absorption peak at 3500 cm^{-1} attributed to O–H increased confirmed that the cellulose acetate has been converted completely into cellulose (Fig. 2. 5a and b). In addition, cellulose nanofibers showed characteristic absorption peaks of cellulose structure at around 1000–1200 cm^{-1} [23]. The characteristic bands for hydrogen-bonded O–H

stretching at 3550–3100 cm^{-1}, the C–H stretching at 2917 cm^{-1}, and the C–H wagging at 1316 cm^{-1} attributed to cellulose can be observed before and after ultrasonic dyeing. This substantiates that the ultrasonic energy do not change chemical structure of cellulose nanofibers during reactive dyeing. However, the dye interaction with cellulose nanofibers could not be identified due to small ratio of dye concentration to the nanofiber mass. Therefore, FTIR spectra for cellulose nanofibers dyed with CI reactive black 5 (Fig. 2. 5c) and CI reactive red 195 (Fig. 2. 5d) are similar to cellulose.

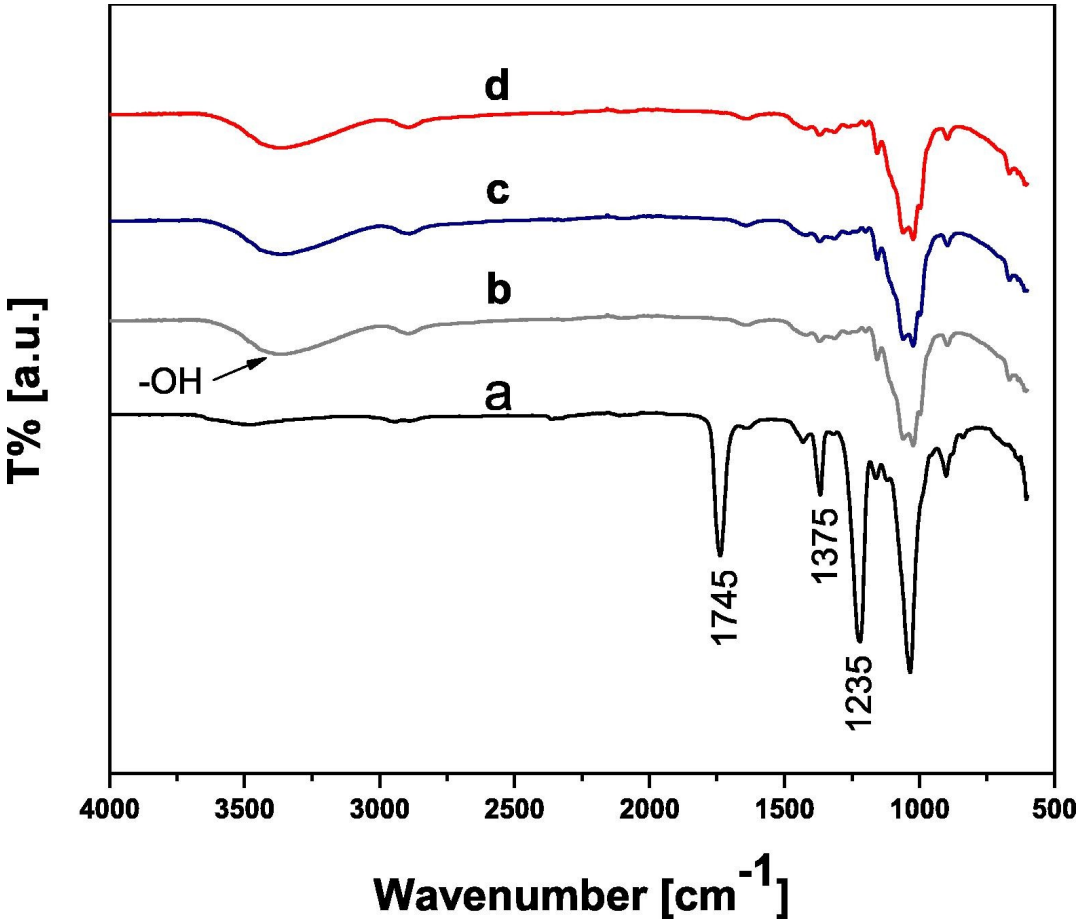

Fig. 2.5. FTIR spectra of (a) neat cellulose acetate nanofibers (b) cellulose nanofibers without dye, (c) cellulose nanofibers dyed with CI reactive black 5 and (d) cellulose nanofibers dyed with CI reactive red 195.

2.3.6. Effect of ultrasonic energy on morphology of dyed nanofibers

The morphology of dyed and undeyed cellulose nanofibers were observed under SEM and their corresponding images have been shown in Fig. 2. 6a–c. The image for undyed cellulose nanofibers (Fig. 2. 6a) shows smooth and regular morphology. The cellulose nanofiber dyed with CI reactive black 5 (Fig. 2. 6b) and with CI reactive red 195 (Fig. 2. 6c) exhibit a slight increase in nanofiber diameter, whereas surface becomes irregular in comparison to undeyed cellulose nanofibers. This slight morphological change during ultrasonic dyeing may be due to nanofiber swelling by ultrasonic energy.

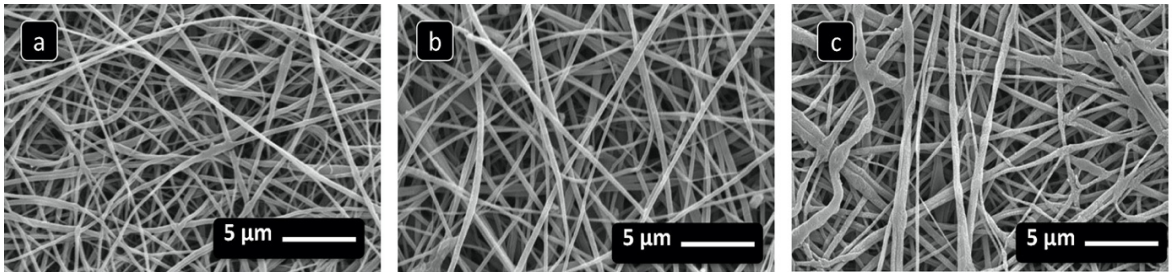

Fig. 2.6. SEM images of (a) cellulose nanofibers without dye, (b) cellulose nanofibers dyed with CI reactive black 5 and (c) cellulose nanofibers dyed with CI reactive red 195.

2.3.7. Color fastness performance of nanofibers

The color fastness to washing (shade change and staining) and light fastness tests were conducted on the cellulose nanofibers dyed with 3% dye concentrations of CI reactive black 5 and CI reactive red 195 at 70 °C for 30 min and the results have been given in Table 2. 1. The staining in washing fastness test for CI reactive black 5 has attained maximum rating, which indicates no color bleeding and therefore good dye fixation. The staining of CI reactive red 195 demonstrates half rating less than the CI reactive 5 dyes obtained. The

color changes were observed to be very good rating of 4/5 for both dyes. The light fastness results on the other hand, demonstrated average ratings. The cellulose nanofibers dyed with CI reactive black 5 has shown better light fastness than the cellulose nanofibers dyed with CI reactive red 195. The fastness to light of a dyed fiber depends on many factors. The probable reason to this may be due to the inherent stability of the dye chromogen of CI reactive black 5.

Table 2. 1. Color fastness to light test ISO 105-BO2 and color fastness to washing test ISO 105-C10:2006.

Dye conc. (3%)[a]	**Light fastness (20 h)**	**Washing fastness (change of shade)**	**Washing fastness (staining on multi fiber)**[b]					
			CT	**CO**	**PA**	**PES**	**PAC**	**Wo**
CI reactive black 5	3/4	4/5	5	5	5	5	5	5
CI reactive red 195	2	4/5	4/5	4/5	4/5	4/5	4/5	4/5

[a]Dyeing conditions: dyeing temperature 70 °C and dyeing time 30 min.
[b]CT, cellulose triacetate; CO, cotton; PA, polyamide; PES, polyester; PAC, polyacrylic; Wo, wool.

2.4. Conclusion

Cellulose nanofibers were successfully dyed with CI reactive black 5 and CI reactive red 195 dyes by ultrasonic batch-wise dyeing method. Irrespective to the class of dyes, ultrasonic dyeing showed a higher color yield than conventional dyeing. In comparison, the color yield of nanofibers dyed with CI reactive black 5 by ultrasonic dyeing showed 20.35% higher than the nanofibers dyed by conventional dyeing, whereas, CI reactive red 195 showed 14.53% higher color yield. The morphology under SEM showed a slight change in the surface of nanofibers and increased the diameter of nanofibers in the case of ultrasonic

dyeing. The color fastness results for both reactive dyes revealed no dye bleed during washing that indicates good dye fixation.

2.5. References

[1] F. Hamano, H. Seki, M. Ke, G. Mayakrishnan, C.T. Lim, I.S. Kim Cellulose acetate nanofiber mat with honeycomb-like surface structure Mater.
Lett. (2015), 10.1016/j.matlet.2015.11.069

[2] L. Sumin, D. Kimura, A. Yokoyama, K. Lee, J.C. Park, I.S. KimThe effects of laundering on the mechanical properties of mass-produced nanofiber web for use in wear Text. Res. J., 79 (2009), pp. 1085-1090

[3] F. Ahmed, S. Saleemi, Z. Khatri, M.I. Abro, I.S. KimCo-electrospun poly (ε-caprolactone)/cellulose nanofibers-fabrication and characterization
Carbohydr. Polym., 115 (2015), pp. 388-393

[4] Y.K. Kang, C.H. Park, J. Kim, T.J. KangApplication of electrospun polyurethane web to breathable water-proof fabrics Fiber Polym., 8 (2007), pp. 564-570

[5] S. Iwamoto, A. Isogai, T. IwataStructure and mechanical properties of wet-spun fibers made from natural cellulose nanofibers Biomacromolecules, 12 (3) (2011), pp. 831-836

[6] Z. Khatri, G. Mayakrishnan, Y. Hirata, K. Wei, I.S. KimCationic-cellulose nanofibers: preparation and dyeability with anionic reactive dyes for apparel application Carbohydr. Polym., 91 (2013), pp. 434-443

[7] Z. Khatri, U. Saleem, G. Mayakrishnan, B.S. Kim, K. Wei, I.S. KimPad dyeing of cellulose acetate nanofibres with disperse dyes Color. Technol., 128 (2012), pp. 1-5

[8] Z. Khatri, F. Ahmed, A.K. Jhatial, M.I. Abro, G. Mayakrishnan, I.S. KimCold pad-batch dyeing of cellulose nanofibers with reactive dyes Cellulose, 21 (2014), pp. 3089-3095

[9] Z. Khatri, R.A. Arain, A.W. Jatoi, G. Mayakrishnan, K. Wei, I.S. KimDyeing and characterization of cellulose nanofibers to improve color yields by dual padding method Cellulose, 20 (2013), pp. 1469-1476

[10] A. Khatri, S. Ali, A.K. Jhatial, S.H. KimDyeability of polyurethane nanofibres with disperse dyes Color. Technol., 131 (2015), pp. 374-378

[11] N.D. Tissera, R.N. Wijesena, K.N. de SilvaUltrasound energy to accelerate dye uptake and dye–fiber interaction of reactive dye on knitted cotton fabric at low temperatures Ultrason. Sonochem., 29 (2016), pp. 270-278

[12] S.A. Larik, A. Khatri, S. Ali, S.H. KimBatchwise dyeing of bamboo cellulose fabric with reactive dye using ultrasonic energy Ultrason. Sonochem., 24 (2015), pp. 178-183

[13] C. Udrescu, F. Ferrero, M. PeriolattoUltrasound-assisted dyeing of cellulose acetate Ultrason. Sonochem., 21 (2014), pp. 1477-1481

[14] Z. Khatri, M.H. Memon, A. Khatri, A.U. TanwariCold Pad-Batch dyeing method for cotton fabric dyeing with reactive dyes using ultrasonic energy Ultrason. Sonochem., 18 (2011), pp. 1301-1307

[15] A. Guesmi, N. Ladhari, F. SakliUltrasonic preparation of cationic cotton and its application in ultrasonic natural dyeing Ultrason. Sonochem., 20 (2013), pp. 571-579

[16] E. Öner, I. Başer, K. AcarUse of ultrasonic energy in reactive dyeing of cellulosic fabricsJ. Soc. Dyers Colour., 111 (1995), pp. 279-281.

[17] M.M. Kamel, M.M. El Zawahry, N.S.E. Ahmed, F. AbdelghaffarUltrasonic dyeing of cationized cotton fabric with natural dye. Part 1: cationization of cotton using Solfix E Ultrason. Sonochem., 16 (2009), pp. 243-249

[18] M.M. Kamel, M.M. El Zawahry, N.S.E. Ahmed, F. AbdelghaffarUltrasonic dyeing of cationized cotton fabric with natural dye. Part 2: cationization of cotton using Quat 188 Ind. Crops Prod., 34 (2011), pp. 1410-1417

[19] M.M. Kamel, H.M. Helmy, N.S. El HawarySome studies on dyeing properties of cotton fabrics with Crocus sativus (Saffron flowers) using an ultrasonic method J. Nat. Fibers, 6 (2009), pp. 151-170.

CHAPTER 3

Dyeing and characterization of regenerated cellulose nanofibers with vat dyes

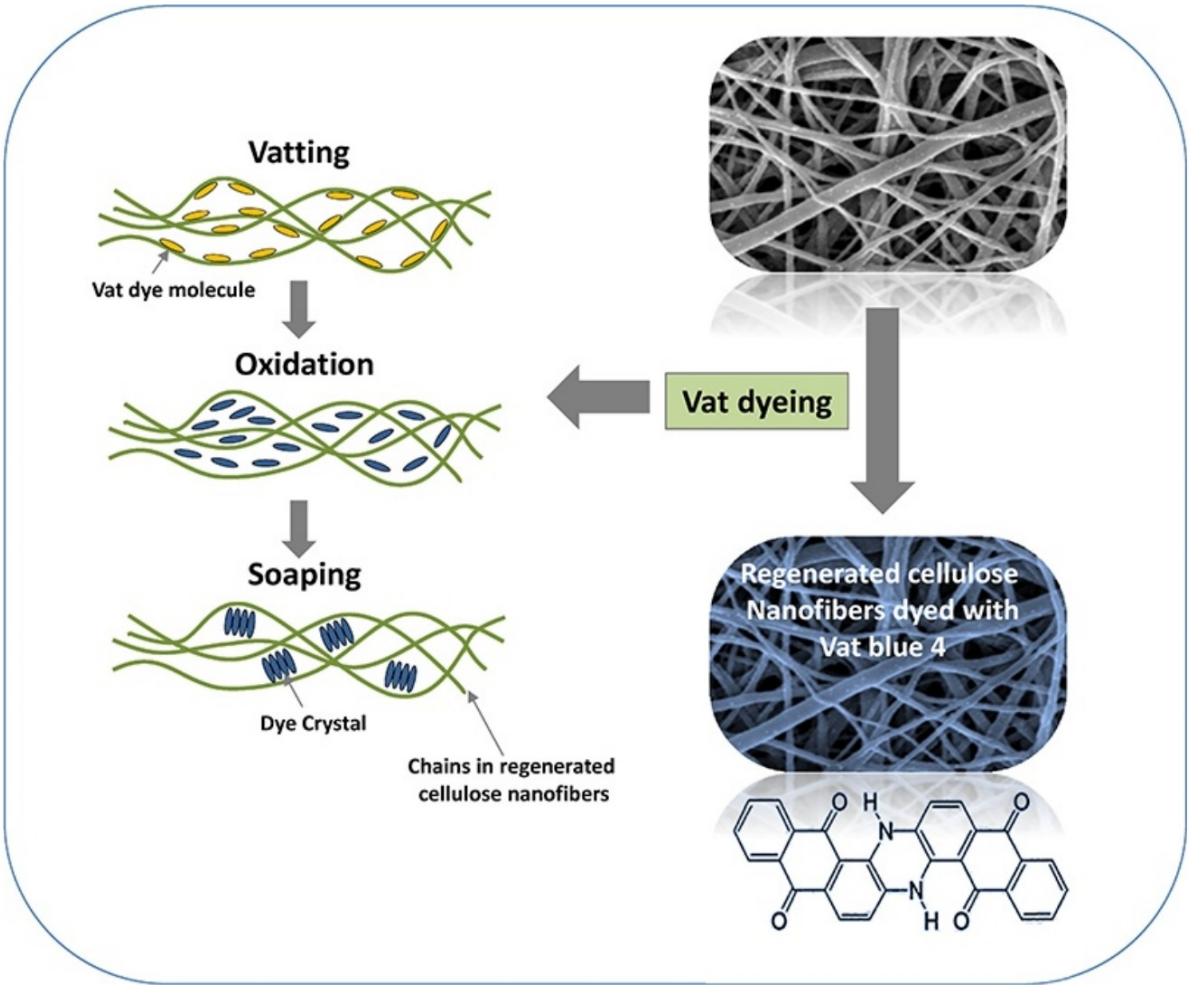

3.1. Introduction

Development of functional nanofibers for technical as well as apparel applications has been investigated since past few years, because they offer unique properties at nanoscale level [1-5] and Nanofibers for apparel application have been proved to be breathable, lightweight, permeable and can be produced in bulk [6-11].

Besides functional properties of apparel, the aesthetic property is equally important. Recent advancement in dyeing of nanofibers has been accelerated to improve their aesthetic properties [8]. used disperse dyes of cellulose acetate nanofibers using pad bake method and they showed good dyeability. Another report on polyurethane nanofibers dyed by using pad, dry-bake method [9-12] and dyeing of nylon 6 nanofibers using ultrasonic energy [6].

To date, cellulose nanofibers (CNF) has been reported dyeing with reactive dyes only. The dyeing of cellulose nanofibers pad batch dyeing of CNF [11], ultrasonically dyed CNF [13], dyeing of cationic-CNF nanofibers [9] nanofibers dyeing using dual and pad method [10]. Although CNF dyeing with reactive dyes produced good color yield, however, the color fastness is not satisfactory due to limits of reactive dye chemistry. In order to overcome the drawback of reactive dyeing, we therefore, chose to dye CNF with vat dyes due to having an edge of better color fastness over reactive dyes.

Vat dyes possess affinity towards cellulose [1]. vat dye is one of the well know carbonyl class of dyes having coplanar and multiring sing system [14]. These rings contribute in strengthening the Van-der-Waals forces between dye and the substrate [15]. This is the main reason why vat dye offers better color fastness than the reactive dyes.

We electrospun cellulose acetate nanofibers and converted into regenerated cellulose nanofibers (RCNF) by deacetylation [13]. RCNF were dyed with two different vat dyes namely C.I vat blue 4 (VB4) and C.I vat green 1 (VG1) by batch wise dyeing method. Dyeing parameters such as temperature, time and dye concentrations were optimized and characterized by color yield (Reflectance spectrophotometer), color fastness, Wide Angle X-ray diffraction spectroscopy (WAXD), Fourier transform infrared spectroscopy (FTIR), Scanning electron microscopy (SEM).

3.2. Experimental

3.2.1. Materials

Cellulose Acetate (CA) contained 39.8% acetyl with average molecular weight 30,000 Da was obtained from Sigma-Aldrich, Japan. Two vat dyes (VB4 and VG1) were obtained from Novasol supplied by Huntsman, USA as shown in Scheme 3.1. The dyeing auxiliaries include sodium dithionite, sodium hydroxide, hydrogen peroxide and acetic acid were used analytical grade.

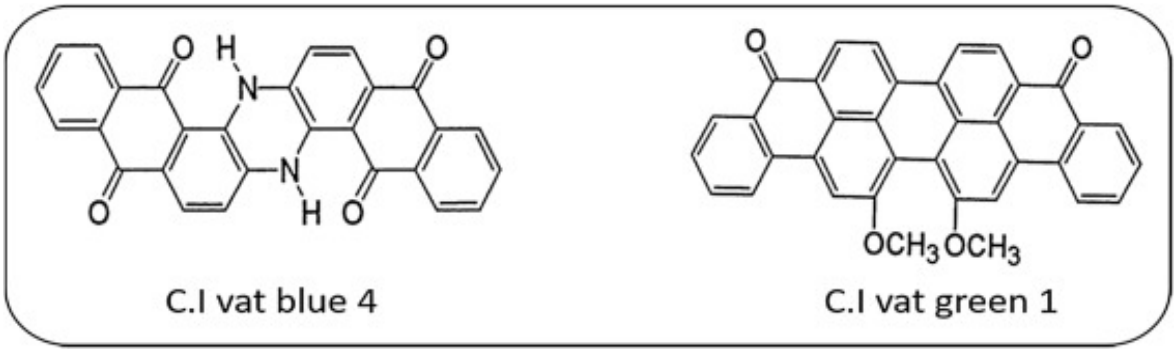

Scheme 3.1. Chemical structures of VB4 and VG1.

3.2.2. Preparation of RCNF

Our previously successful electrospinning method was used to produce CA nanofibers [11]. The polymer solution consists of 17% CA polymer and two solvents acetone: DMF having ratio 2:1 respectively. Har-100*12, Matsusada Co., an electrospinning machine from Tokyo, Japan was used for the production of nanofibers.

For optimum electrospinning voltage supplied to the solution was maintained at 12.5 kV and the distance from tip to collector was kept at 15 cm. After collecting nanofibers on collector sheet, these samples were dried in air for 48 h.

The nanofibers web thickness was maintained between 70 and 80 μm. Dried CA nanofibers were then converted into RCNF by means of a deacetylation process. For deacetylation, CA

nanofiber samples were immersed in a solution of NaOH with a molar concentration 0.05 M in distilled water for 48 h, samples were then washed in distilled water until the liquor reached to neutral pH. RCNF were dried at 40 °C for 5 h before the vat dyeing process. The degree of deacetylation achieved in RCNF was 94%.

3.2.3. Vat dyeing of RCNF

Vat dyeing application on RNCF was studied for the very first time and optimization of dyeing parameters is key step to process dyeing smoothly. RCNF were dyed using two Vat dyes, VB4 and VG1 at given dyeing parameters. At first, effect of temperature was studied at 40, 50, 60 and 70 °C and then effect of time intervals at (10, 20, 30, 40, 50 and 60) minutes was investigated.

The effect of dye concentrations (1%, 1.5%, 2%, 2.5% and 3% omw) on color yield was investigated. RCNF were dyed by batchwise method using liquor ratio 1:20, 1 being mass of nanofibers and 20 is the dye liquor. Vat dyeing of RCNF was completed in three steps, vatting, oxidation and soaping.

Briefly, in vatting step, Vat dyes were solubilized in liquor containing 20 g/L sodium hydroxide (alkali) and 20 g/L sodium dithionite (a reducing agent). The leuco form (solubilized dye) was absorbed by the RCNF during dyeing under controlled temperature and time. After given time, the second step begun, the dyed RCNF were treated with 2 g/L hydrogen peroxide (37%) at 60 °C for 15 min to oxidize dye molecule back to its insoluble form. In third step, soaping of RCNF was carried for completion of the dyeing process, because of soaping the dye molecules are clump together and increase the crystallinity [15].

3.2.4. Measurement of color

A reflectance spectrophotometer (ColorEye 7000A spectrophotometer) was used to measure the K/S values of the dyed RCNF. These K/S values were used to determine color yield of dyed samples and calculated by using equation 1.(1)$K/S = (1-R)^2/2R$In this equation, R represents reflectance decimal fraction dyed RCNF and K denotes the co-efficient of absorption, whereas S is scattering co-efficient.

3.2.5. Fourier transform infrared spectroscopy

The changes in chemical structure of RCNF before and after vat dyeing RCNF were assessed by FTIR spectroscopy (IR Prestige-21 by Shimadzu, Japan). The ATR-FTIR mode was used to investigate all nanofiber samples.

3.2.6. Scanning electron microscopy

Scanning electron microscope (SEM) of JEOL model JSM 6010LA was used to analyze the morphology of vat dyed and undyed RCNF samples. Accelerating voltage of 10 kV and maximum magnification of 500,000×. All nanofiber samples were sputtered with Pd–Pt prior to take imaging.

3.2.7. Wide angle X-ray diffraction

Wide-angle X ray diffractometer (WAXD) Rigaku Miniflex 300, Japan was used to analyze the effect of crystallinity of vat dyed RCNF. Samples were analyzed in the range of 10–50° degree at the scanning speed of $2\theta = 4°$/min.

3.2.8. Color fastness tests

For washing-fastness test of vat dyed samples, Gyrowash (James-H. Heal Co., UK) was used followed by ISO 105C 10:2006 method and for light-fastness test Apollo (James-H. Heal Co., UK) was used followed by ISO 105-BO2 light-fastness test.

3.3. Results and discussion

3.3.1. Effect of temperature on RCNF dyeing

Temperature is most impacting parameter in order to optimize vatting step during vat dyeing of RCNF, we chose maximum time of 70 min that was kept constant and dye concentration was selected 1%. Fig. 3. 1 elaborates that influence of dyeing temperature on color yield (K/S) while using VB4 and VG1 dyes.

Color yield of VG1 showed a rapidly increase with increasing dyeing temperature from 40 °C to 50 °C and slow increments were observed in color yield between dyeing temperature from 50 °C to 60 °C, whereas dyeing temperature of 70 °C show no significant increment in color yield. This may be because higher temperatures lower the ratio of dye substantivity [14].

Using vat dye VG1 showed higher color yield on RCNF comparing to vat dye VB4 regardless of the dyeing temperature because of difference in molar extinction coefficient of vat dye. In contrast to dye uptake of VB4, the VG1 started to increase slowly from 40 °C to 50 °C and obtained higher color yield at 60 °C. Increasing temperature to 70 °C did not show any increment in color yield value. Dyeing temperature was optimized at 60 °C because it showed maximum color yield at constant time and dye concentration.

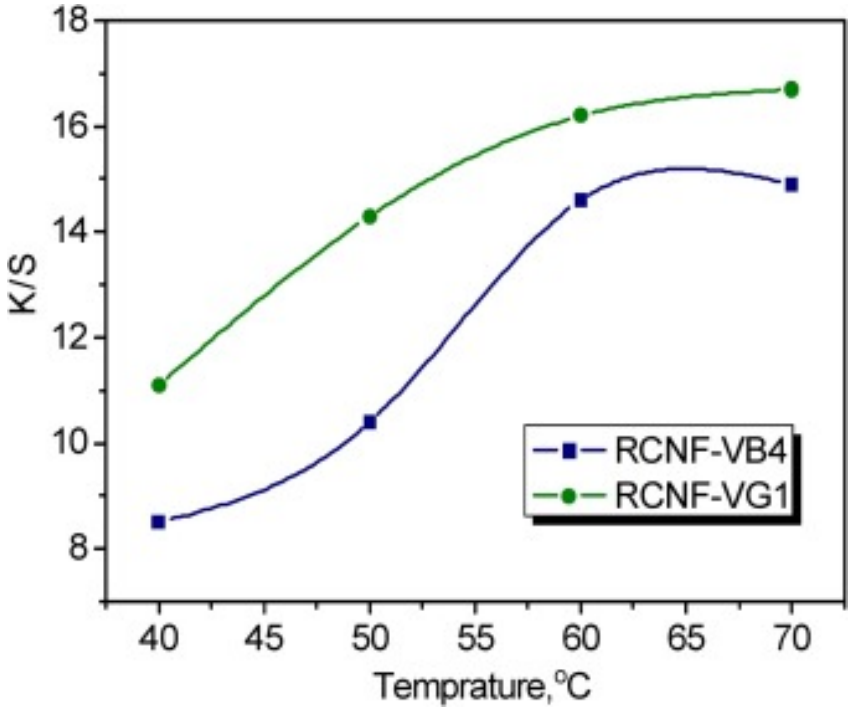

Fig. 3. 1. Effect of dyeing temperature on color yield (dyeing time 60 min; dye conc. 1% omw).

3.3.2. Time optimization for vat dyeing

Effect of time on color yield was optimized using optimized temperature (60 °C) from the previous step and dye concentration (1%). The dye VG1 in Fig. 3. 2 showed noticeably higher color yield comparing to VB4 over dyeing time between 20–40 min. The maximum color yield obtained when the dyeing carried out for 50 min, after which, no further increased in color yield was observed.

Similar trend was observed for the RCNF dyed with VB4. Hence, the dyeing time for both dyes was optimized at 50 min. The results of time study conclude 50 min as an optimum dyeing time for both dyes.

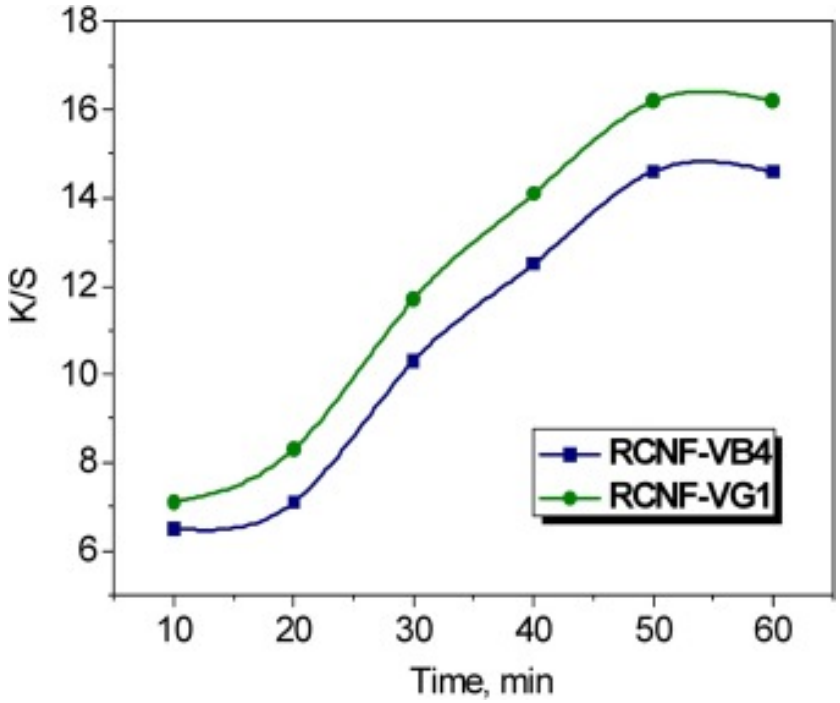

Fig. 3. 2. Effect of dying time on color yield (dyeing temperature 60 °C; dye conc. 1% omw).

3.3.3. Color build-up property of RCNF

Color build-up property of both VB4 and VG1 on RCNF were investigated using different dye concentrations (1%, 1.5%, 2%, 2.5% and 3%) at optimized time and temperature, 50 min and 60 °C respectively. Fig. 3. 3 demonstrates that irrespective to the type of dye, increasing dye concentration resulted higher K/S values and has a linear relationship. The dye VG1 resulted higher K/S values than the dye VB4; it is mainly due to higher molar extinction coefficient of VG1. VB1 dye resulted 20.5 K/S at 3% dye concentration, which is twice as higher than 1% dye concentration.

Similarly, VG4 dye resulted 22.5 K/S at 3% dye concentration, which is also twice as higher than 1% dye concentration. Since K/S values are continuously increased with increasing dye concentrations of both vat dyes, thus the vat dyes have good color build up properties for RCNF.

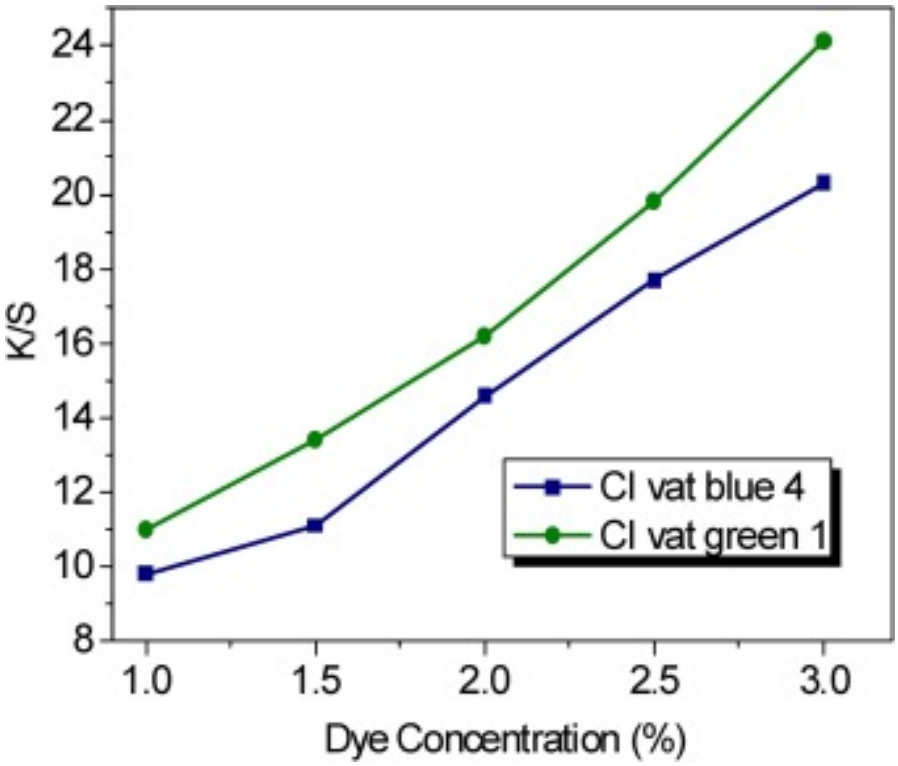

Fig. 3. 3. Effect of dye concentrations on color yield (dyeing time 50 min; dyeing temperature 60 °C).

3.3.4. Chemical change in vat dyed and undyed samples

Since vat dyes were applied on RCNF or the very first time so it was necessary to know the chemical compatibility of vat dyes with RCNF. FTIR was also very important to confirm the conversion of cellulose acetate into RNCF after deacetylation.

In Fig. 3. 4 (a) FTIR spectra of acetate group C–O at 1745 cm^{-1}, C–CH3 at 1375 cm^{-1} and C–O–C at 1235 cm^{-1} confirms the presence of cellulose acetate whereas in Fig. 3. 4 (b) deacetylation of cellulose acetate is given as an additional absorption peak at 3500 cm^{-1} can be observed which confirm the presence of O–H and the peak at 1235 cm^{-1} vanished so it can be said that the cellulose acetate has successfully changed to RCNF.

Additionally, RCNF showed FTIR spectra absorption peaks between 1000-1200 cm^{-1}. The hydrogen-bonded O–H is stretching at 3550–3100 cm^{-1}, the C–H is wagging at 2917 cm^{-1}, and the C–H is stretching at 1316 cm^{-1} attributed to cellulose can be observed before application of vat dyes and after application of vat dyes.

Though vat dyes interaction with RCNF can be easily observed by comparing RCNF spectrum against both vat dyed RCNF spectra. For VB4 in Fig. 3. 4 (c) some additional peaks can be observed at 1016 cm^{-1}, 1285 cm^{-1}, 1492 cm^{-1}, 1580 cm^{-1} and 1652 cm^{-1} which show the presence of C–O–C, C–H, (CC aromatic ring), C=O and NH respectively, whereas, in Fig. 3. 4 (b) some additional peaks can also be seen in the FTIR spectra of VG1 at 1022 cm^{-1}, 1294 cm^{-1}, 1573 cm^{-1} and 1636 cm^{-1}, which depicts the presence of C–O–C, C–CH3, C=C and C=O respectively.

The adsorption band of C-O-C at 1070 cm^{-1} (Fig. 3. 4d) shifted to 1016 cm^{-1} (Fig. 3. 4c) and 1022 cm^{-1} (Fig. 3. 4d) in spectra of VB1 and VG4 respectively, indicating a strong interaction (van der Waals interaction) between dye and RCNF. The hydrogen-bonded O–H is stretching at 3550–3100 cm^{-1} peaks of RCNF retained even after dyeing that shows successful application of vat dyes on RCNF without changing chemical structure of CNF.

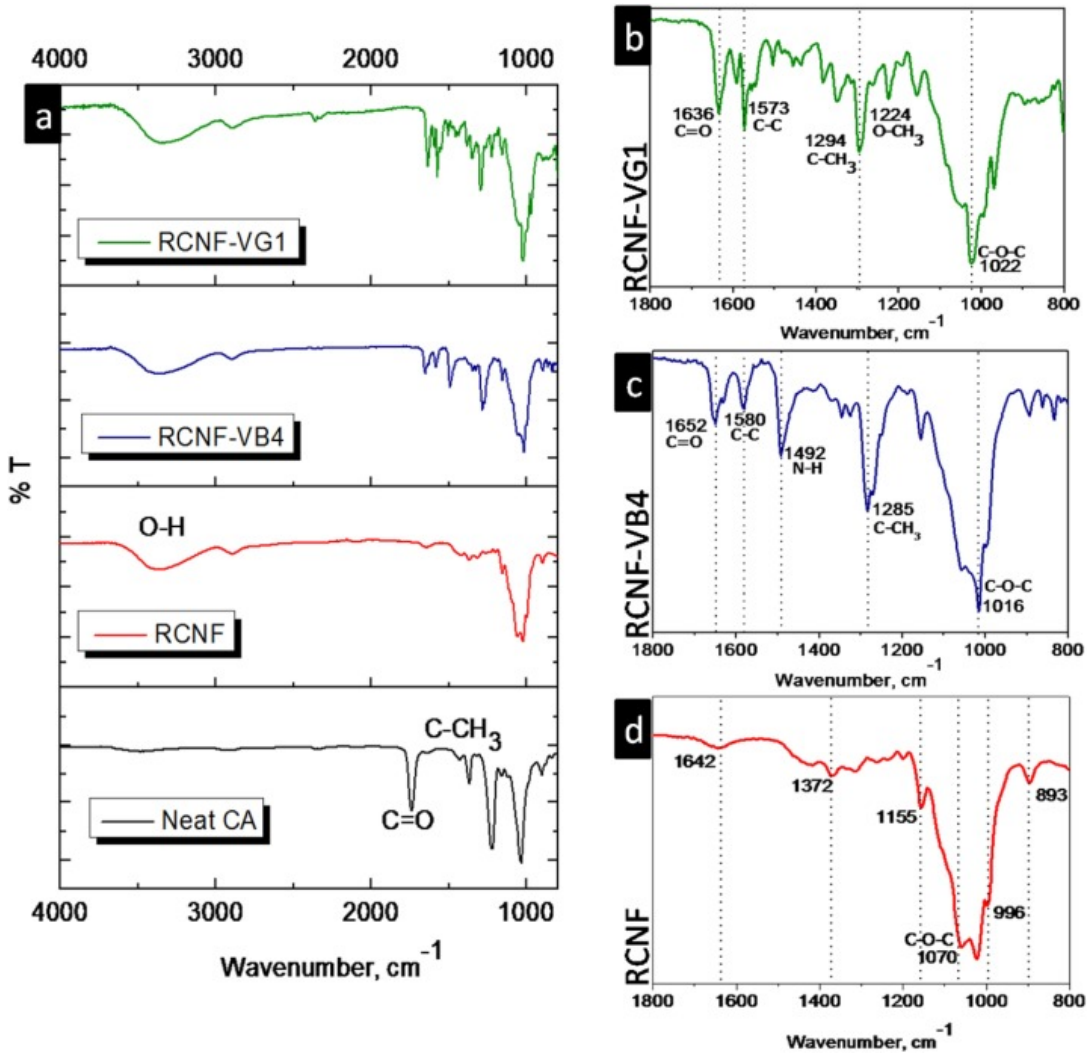

Fig. 3. 4. FTIR spectra of (a) stacked neat CA, dyed and undyed RCNF with vat dyes (b) RCNF dyed with VB4 and (c) RCNF dyed with VG1 and (d) undyed RCNF

3.3.5. X-ray diffraction spectroscopy (WAXD)

It is well known that the vat dye increase crystallinity of cellulose after dyeing, more specifically after soaping. Therefore, we obtained WAXD patterns of dyed and undyed RCNF and compared their crystallinity. Fig. 3. 5 demonstrates that number of obvious crystalline peaks in RCNF dyed with VB4 and VG1 increased in comparison to undyed

RCNF. The crystalline peak intensity for RCNF appeared at 2θ angle of 12.1°, 20.0° and 22.1° [15,16].

The RCNF dyed with VB4 has more intensive peaks at 2θ angle of 11.8°, 15.9° and 22.5° comparing to undyed RCNF due to crystal planes of VB4 dye in nanofibers chain. Whereas, RCNF dyed with VG1 show different patterns appeared at 2θ angle of 12.9°, 21.6° and 25.3°. Due to formation of dye crystal during soaping of vat dyed RNCF, the 2θ angles became intensive and the crystallinity was increased.

Three steps reduction, oxidation and soaping are portrayed in Fig. 3. 6 better understand the movement of dye molecules towards RCNF during each step, specifically the aggregation of molecules after soaping to form crystals. The rearrangement of vat dye molecule within the cellulosic polymer chains contributes to better washing and light fastness results [1].

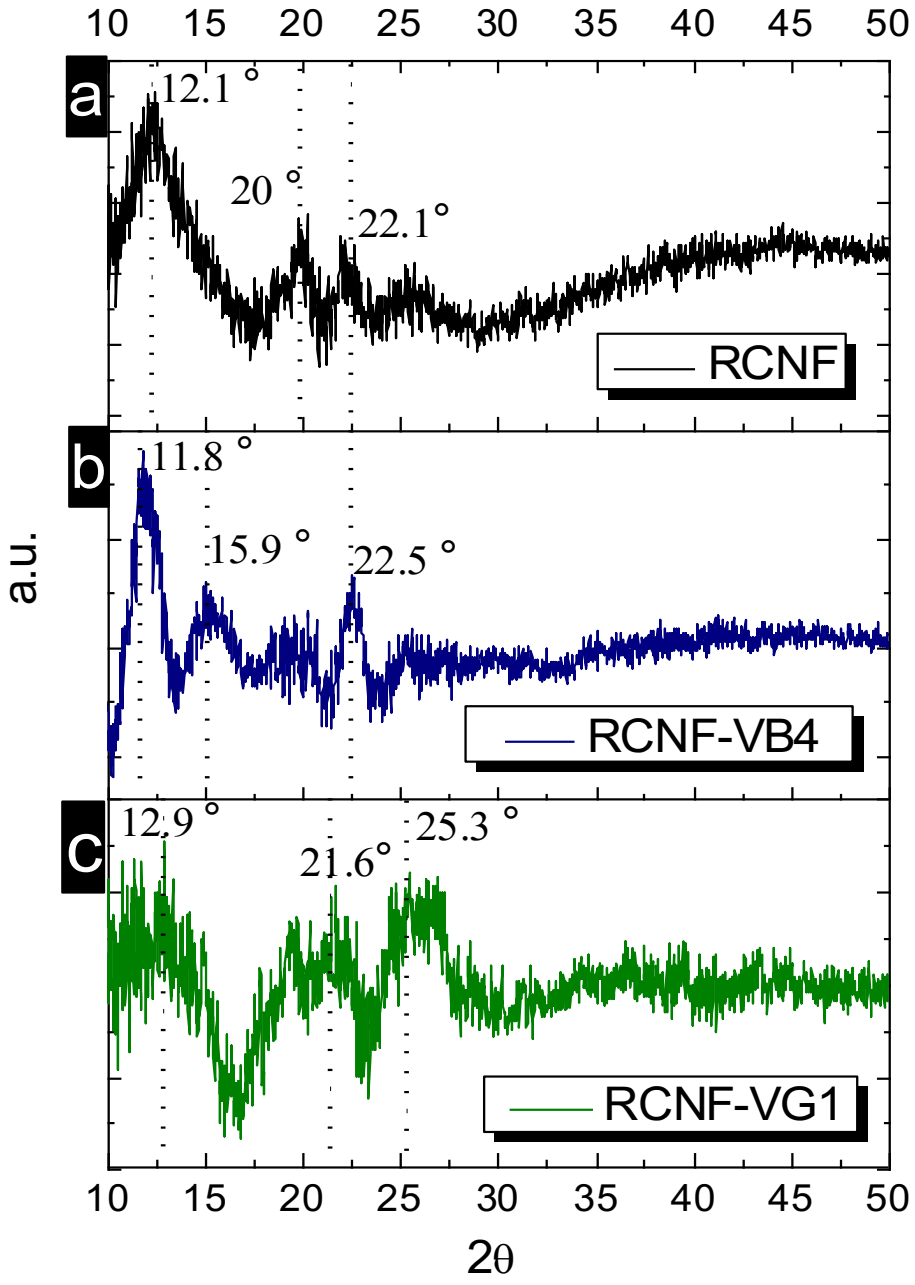

Fig. 3. 5. X ray diffraction results of (a) RCNF (b) RCNF dyed with VB4 (c) RCNF dyed with VG1.

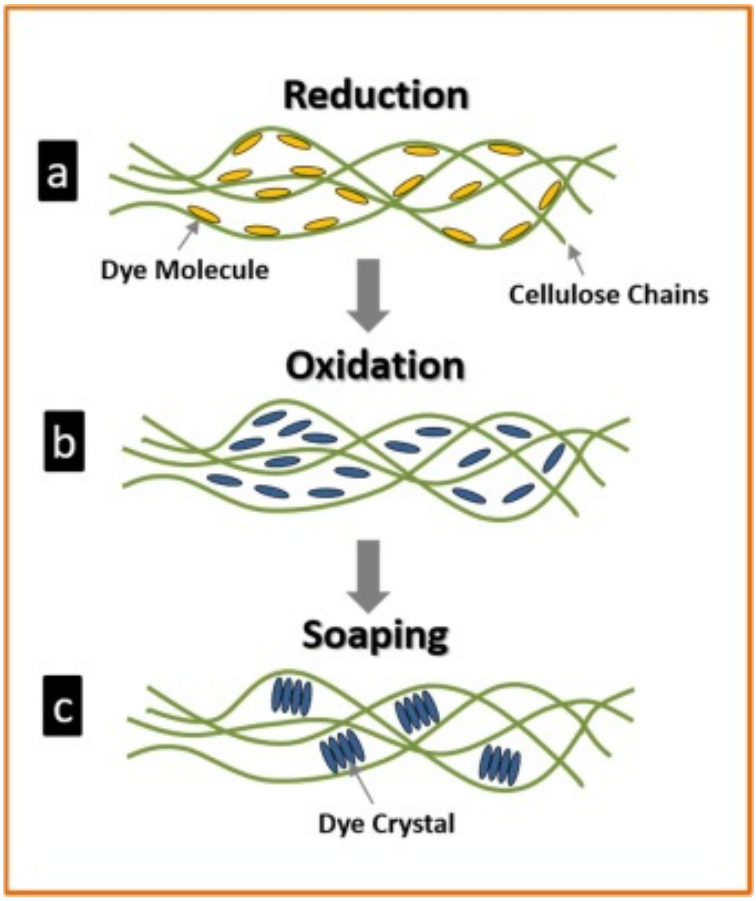

Fig. 3. 6. Changes in molecular configuration during (a) vatting (reduction), (b) oxidation and (c) soaping.

3.3.6. Morphological study of RCNF

The SEM image in Fig. 3. 7(a)–(c) shows smooth morphology of neat RCNF, whereas, the morphology of dyed RCNF slightly irregular after dyeing. The diameter distribution of RCNF before dyeing can be observed from Fig. 3. 7(d) that showed an average diameter of 400 ± 30 μm. The diameter slightly increased after dyeing, for instance RCNF with VB4 (Fig. 3. 7e) increased to 440 ± 30 μm and RCNF with VG1 (Fig. 3. 7 f) increased to 480 ± 30 μm. The probable reason for increasing diameter is due to the formation of dye crystals within the nanofibers, as discussed in previous section (Fig. 3. 6).

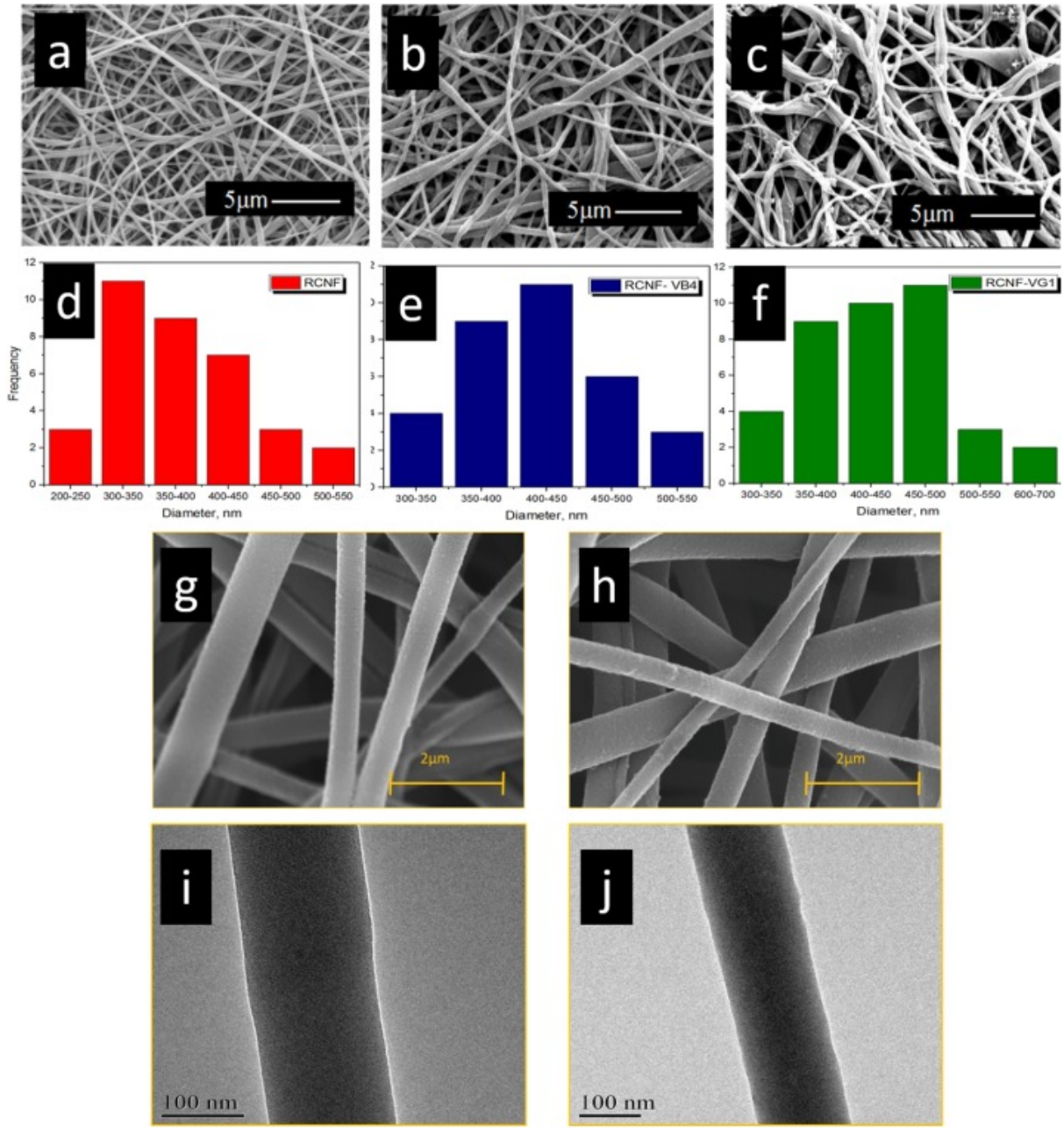

Fig. 3. 7. SEM images of (a) neat RCNF (b) RCNF dyed with VB4 and (c) RCNF dyed with VG1; Diameter distribution graph of (d) neat RCNF (e) RCNF dyed with VB4 and (f) RCNF dyed with VG1; FE-SEM images of (g) CA nanofibers before deacetylation (h) RCNF after deacetylation; TEM images of (i) CA nanofibers before deacetylation (j) RCNF after deacetylation.

To investigate the effect of deacetylation on morphology of RCNF, FE-SEM images were taken before and after deacetylation as shown in Fig. 3. 7 (g) and (h), where RCNF showed smooth morphology with slight decrease in diameter after deacetylation. Further examining any effect of deacetylation on single nanofiber, TEM images were obtained as shown in Fig. 7(i) and (j). The TEM show no cracking or phase separation as result of deacetylation treament.

3.3.7. Color fastness performance of dyed RCNF

Fastness properties of both vat dyes VB4 and VG1 on were checked by testing fastness to light and fastness to washing separately (staining and change of shade). It can be seen from Table 3. 1 that the staining in washing fastness test for VB4 obtained high ratings because it indicated no color bleed, which is evidence of good dye fixation. The staining observed on VB4 dyed nanofibers obtained more than half of the fastness ratings compared to RCNF dyed using VG1 due to different molar extinction coefficient of vat dyes [17]. Color change rating in case of both vat dyes is 4/5, which is very good rating for washing fastness test. Results of color fastness to light were assessed against Blue wool scale (1–9), 1 being very poor and 9 being excellent. Light fastness of dyed RCNF also shows that is 7 blue wool scale ratings. The overall color fastness performance of RCNF dyed with vat dyes obtained very good and therefore, results safely propose the use of RCNF in advanced apparel.

Table 3. 1. Color fastness to light test ISO 105-BO2 and color fastness to washing test ISO 105-C10:2006.

[a]Dye conc. (1%)	[b]Light fastness (20 hours)	[c]Washing fastness (Change of shade)	[d]Washing fastness (Staining on multifiber)					
			CT	CO	PA	PES	PAC	Wo
VB4	7	4/5	5	4/5	5	5	5	5
VG1	7	4/5	5	4/5	5	5	5	5

[a]Dyeing conditions: Dyeing temperature 60 °C and time 50 min.
[b]Blue wool scale 1–9, being 1 is poor and being 9 is excellent.
[c]Grey scale 1–5, being 1 is poor and being 5 is excellent.
[d]CT, cellulose triacetate; CO, cotton; PA, polyamide; PES, polyester; PAC, polyacrylic; Wo, wool.

3.4. Conclusion

We conclude a successful dyeability of RCNF with two different vat dyes, VB4 and VG1 by batchwise method. The optimum dyeing temperature and time obtained were 60 °C and 50 min respectively. RCNF showed a very good buildup property for both VB4 and VG1, which VG1 showed 15% higher color yield than the VB4. FTIR spectra confirmed the conversion of RCNF and Van der Walls interaction between dye and RCNF. SEM images revealed smooth morphology and after dyeing of RCNF with both dyes VB4 and VG1 the diameter increased. slightly. FE-SEM images showed that after deacetylation, diameter of nanofibers decreased. The TEM show no cracking or phase separation as result of deacetylation treament. Crystallinity of RCNF increased after dyeing with VB4 and VG1 as revealed by XRD pattern. Color fastness, in general, found from very good to excellent for both dyes, since no dye bleeding was observed during washing; this showed that the dye fixation was very good. Based on results obtained, we safely conclude that vat dyes for RCNF would be a better choice for advanced apparel applications.

3.5. References

[1] Aspland, J. R. (1992). vat dyes and their application. Textile Chemist and Colourists, 24, 22-24.

[2] Ahmed, F., Saleemi, S., Khatri, Z., Abro, M. I., & Kim, I. S. (2015). Co-electrospun poly (ε-caprolactone)/cellulose nanofibers-fabrication and characterization. Carbohydrate polymers, 115, 388-393.

[3] Ahmed, F., Arbab, A. A., Jatoi, A. W., Khatri, M., Memon, N., Khatri, Z., & Kim, I. S. (2017). Ultrasonic-assisted deacetylation of cellulose acetate nanofibers: A rapid method to produce cellulose nanofibers. Ultrasonics Sonochemistry, 36, 319-325.

[4] Hamano, F., Seki, H., Ke, M., Gopiraman, M., Lim, C. T., & Kim, I. S. (2016). Cellulose acetate nanofiber mat with honeycomb-like surface structure. Materials Letters, 169, 33-36.

[5] Iwamoto, S., Isogai, A., & Iwata, T. (2011). Structure and mechanical properties of wet-spun fibers made from natural cellulose nanofibers. Biomacromolecules, 12(3), 831-836.

[6] Jatoi, A, W., Ahmed, F., Khatri. M., Tanwari. A., Khatri. Z., Lee. H and Kim.I.S. (2017). Ultrasonic-assisted dyeing of Nylon-6 nanofibers. Ultrasonics Sonochemistry, DOI:10.1016/j.ultsonch.2017.04.010

[7] Kang, Y. K., Park, C. H., Kim, J., & Kang, T. J. (2007). Application of electrospun polyurethane web to breathable water-proof fabrics. Fibers and Polymers, 8(5), 564-570.

[8] Khatri, Z., Khatri, A., Saleem, U., Mayakrishnan, G., Kim, B. S., Wei, K., & Kim, I. S. (2013). Pad dyeing of cellulose acetate nanofibres with disperse dyes. Coloration Technology, 129(2), 159-163.

[9] Khatri, Z., Mayakrishnan, G., Hirata, Y., Wei, K., & Kim, I. S. (2013). Cationic-cellulose nanofibers: preparation and dyeability with anionic reactive dyes for apparel application. Carbohydrate polymers, 91(1), 434-443.

[10] Khatri, Z., Arain, R. A., Jatoi, A. W., Mayakrishnan, G., Wei, K., & Kim, I. S. (2013). Dyeing and characterization of cellulose nanofibers to improve color yields by dual padding method. Cellulose, 20(3), 1469-1476.

[11] Khatri, Z., Ahmed, F., Jhatial, A. K., Abro, M. I., Mayakrishnan, G., & Kim, I. S. (2014). Cold pad-batch dyeing of cellulose nanofibers with reactive dyes. Cellulose, 21(4), 3089-3095.

[12] Khatri, A., Ali, S., Jhatial, A. K., & Kim, S. H. (2015). Dyeability of polyurethane nanofibres with disperse dyes. Coloration Technology, 131(5), 374-378.

[13] Khatri, M., Ahmed, F., Jatoi, A. W., Mahar, R. B., Khatri, Z., & Kim, I. S. (2016). Ultrasonic dyeing of cellulose nanofibers. Ultrasonics sonochemistry, 31, 350-354.

[14] Shore, J. (1995). Cellulosic dyeing. Society of Dyers and Colourists.

[15] Shore, J. (2002). Colorants and auxiliaries: organic chemistry and application properties, Society of Dyers and Colourists. London, England.

[16] Ju, X., Bowden, M., Brown, E. E., & Zhang, X. (2015). An improved X-ray diffraction method for cellulose crystallinity measurement. Carbohydrate polymers, 123, 476-481.

[17] Sumin, L., Kimura, D., Yokoyama, A., Lee, K., Park, J. C., & Kim, I. (2009). The effects of laundering on the mechanical properties of mass-produced nanofiber web for use in wear. Textile Research Journal, 79(12), 1085-1090.

CHAPTER 4

Ultrasonic-assisted dyeing of Silk fibroin nanofibers: An energy-efficient coloration at room temperature

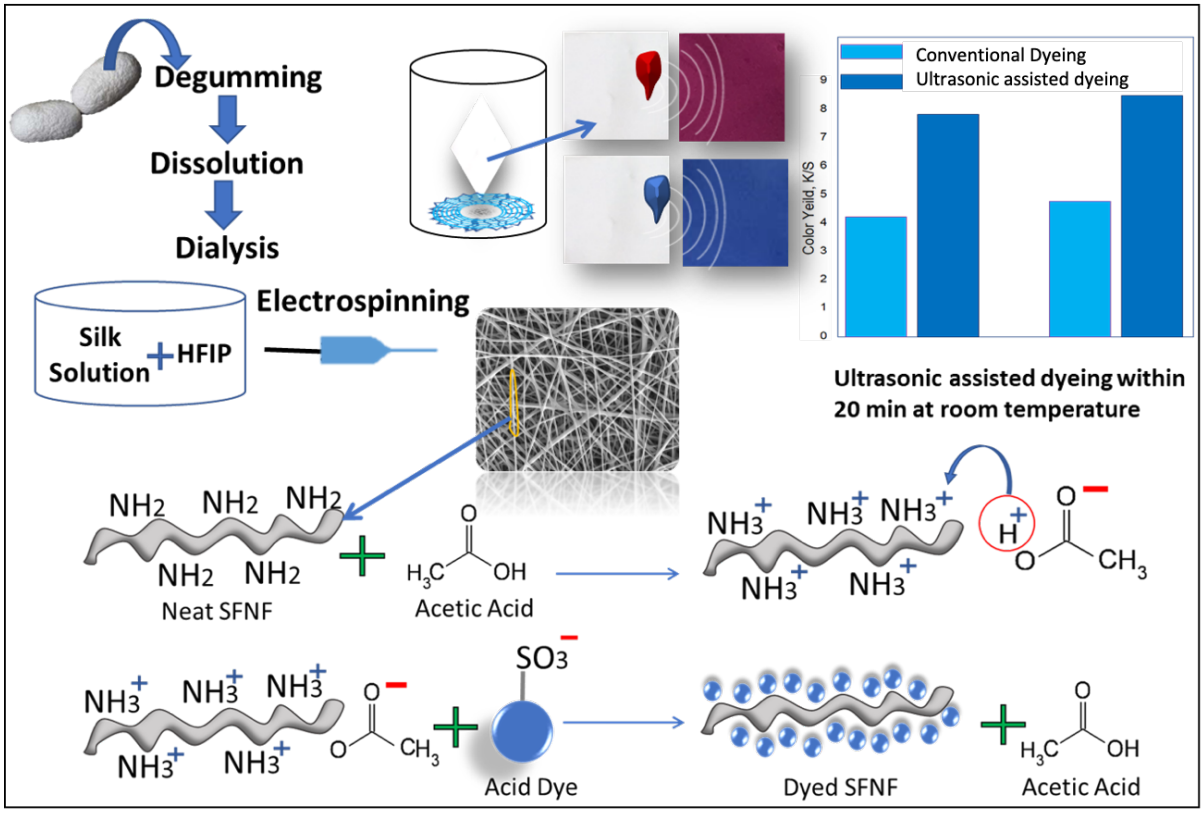

4.1. Introduction

Nanofibers are being promoted because of their unique characteristics, fine diameter, high surface area and multifunctional properties such as biomedical, surgical, filtration, tissue engineering, membranes engineering, sensors [1,2], In parallel to functional enhancement of nanofibers [3], aesthetic properties are also important.

Recently, many scientist are trying to improve aesthetic properties of different nanofibers such as, dyeing of cellulose acetate (CA) nanofibers with acid dyes using different dyeing techniques[3-6] and dyeing of polyurethane nanofibers using pad-dry-bake method [7],

plasma treatment for increasing dyeability of textile substrates[8], doped dyeing of different nanofibers using different dye types [9] are reported but the problems such as the lower color yield and the color fastness are still remained as a challenge due to its nanoscale diameter and higher surface area.

Coloration of textile substrate using ultrasonic technique is getting more attentions due to its better results in improvement of aesthetic properties of nanofibers. Ultrasonic energy aggregates the dye rapidly compared to conventional techniques for dyeing processes in which cavitation plays important role to enhance the efficiency and improve the color yield with uniform dye transfer for even coloration. Recently many works related to ultrasonic assisted dyeing are reported such as cellulose, lyocell, CA, cotton, bamboo, fibers, yarns, nonwoven and fabrics dyed using ultrasonic energy with different dye types [10-20]. Dyeing of nanofibers induced by ultrasonic energy such as ultrasonic-assisted dyeing of cellulose [21], nylon [22], polyurethane [23] and polyacrylonitrile nanofibers [24].

Silk is eco-friendly natural biomaterial abundantly available on earth, [25] having distinctive properties such as, high strength good biocompatibility [26] frequently used for different applications such as sensors, tissue engineering, drug release, filters and protective clothing [27].

Silk fibroin nanofiber (SFNF) is a protein-based substrate mainly composed of beta-sheets with repeating variative amines and hydrogen bonds which make silk amorphous and provides good wettability [25,28]. SFNF is one of the soft, strong, breathable, and lightweight materials and best fit for functional textile substrate, its environment friendly, hygienic, non-allergenic, smooth lustrous surface and its human skin like chemical structure make it ideal for advanced textile [25,29,30]. SFNF are most suitable for acid dyeing due to their high

substantive behavior with them [31], Acid dyes are highly water soluble, and offer good coloration and fastness properties to a range of protein fibers [31-33].

In previous reports the ultrasonic-aided (UA) dyeing of different textile substrates showed better results compared to conventional dyeing processes, some also proved that the dyeing can be carried at low temperature using ultrasonic energy [29,34], where UA dyeing of SFNF at room temperature never reported up to date.

Therefore, we report Ultrasonic-aided (UA) dyeing of SFNF with an efficient approach for coloration at room temperature. Two different acid dyes selected for SFNF coloration. UA dyeing and conventional (C) dyeing for SFNF were optimized with respect to temperature, time and concentration for dyeing. Conventional dyeing of silk needs different auxiliaries and chemicals and it produces bulk dye effluent [30,31], but we attempted to make process eco-friendlier and used a slight amount of acetic acid as auxiliary only to maintain the acidic pH during dyeing of SFNF. UA dyeing resulted better performance over C dyeing of SFNF. Production rate of UA dyeing technique observed as 60% more than the production rate of C dyeing, because ultrasonic energy produce cavitation within dye bath which enhance the breakage rate of acid dye aggregates, resulting increased rate of dye penetration and uniform migration of dye into the SFNF, this was also the reason that ~43% higher color yield achieved by UA dyeing carried at room temperature. C dyeing of SFNF optimized at 70℃ temperature and its maximum color yield was compared to UA dyed SFNF at room temperature. Shrinkage in silk has been considered as one of the major problems in C dyeing of Silk [34,36], whereas the residual shrinkage was observed as 29% more in C dyed SFNF compared to UA dyed SFNF. The shrinkage was resisted ultimately by ultrasound waves because of sonication and bubble formation in order to remove the entrapped gas/air from the SFNF results in interstices points within the nanofiber substrate which make dye migration

easier and consequently cavitation facilitates an rapid and uniform transfer of acid dye molecules to SFNF, this is also the reason of increased color yield and exhaustion rate. as a result, UA dyed SFNF maintained smooth morphology, ultimately luster and softness of UA dyed SFNF sustained by cavitation produced by ultrasonic energy even at room temperature, due to more shrinking effect silk the fibers loses its softness and lustrous effect [34]. Ultrasonication is famous for uniform mass transfer which resulted uniformly dyed SFNF compared to C dyed SFNF. UA dyeing have potential to save 62.28% electrical energy and 64.28% thermal energy compared to C dyeing of SFNF. Ultrasonic energy increased exhaustion 9% for dyeing SFNF, as a result 10% less dye effluent formed which made dyeing more economical and ecofriendly. The UA dyed SFNF revealed smooth morphology, unaltered chemical structure and good color fastness properties. The results revealed that the ultrasonic energy has wide potential for enhancement of textile industries which offer efficient, energy saving, cost effective process, higher production rate with enhanced properties. Therefore, UA dyeing of SFNF can potentially be considered by textile industries to produce advanced apparels.

4.2. Experimental

4.2.1. Materials

High voltage-power supplier (Har-100*12. Matsusada Co. Tokyo, Japan, Ultrasonic equipment (Model: elmasonic E3OH, elma Germany), Bombyx mori from China. Sodium carbonate 99.5% molecular weight 105.99 supplied by Sigma Aldrich, USA. Lithium bromide ≥99.995% with molecular weight 86.85 was purchased from Wako, Japan. Ethanol having molecular weight 46.07 purchased from Wako, Japan. Hexafluoroisopropanol HFIP, Cellulose dialysis tubes from Kingfisher, Japan. Acetic acid ≥99.7% with molecular weight 60.05 supplied by Sigma-Aldrich, USA. Acid dyes, Optilon MF-38 (CI Acid Red 38) and

Optilon MF-2RLA (CI Acid Blue-117) obtained from Clariant (Pakistan) shown in Scheme 4.1.

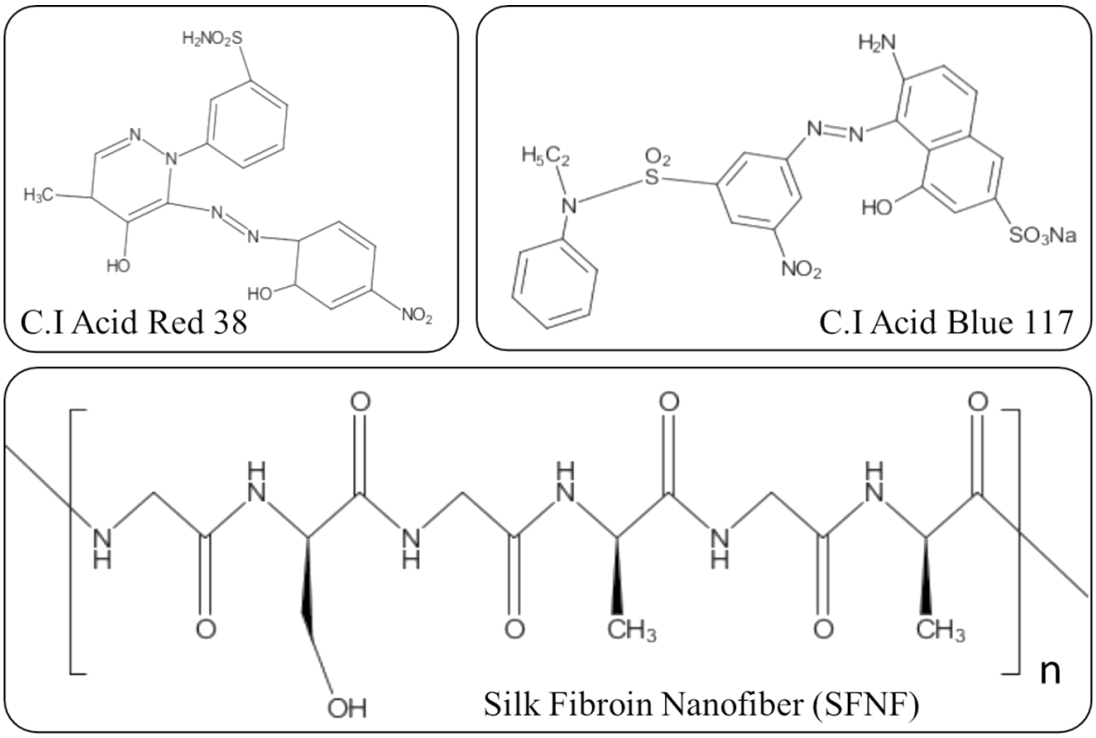

Scheme 4.1. Chemical structures of CI Acid Red and CI Acid Blue

4.2.2. Preparation of SFNF nanofibers

The silk fibroin (SF) solution was prepared by boiling Bombyx mori silk [28] for 30 min in 0.02M solution of sodium carbonate in deionized water and rinsed with warm water to remove the sericin and dried on clean paper. The dried SF then dissolved in a ternary solution of Lithium (bromide: ethanol: deionized water) (1:2:8) respectively at 80°C for 8 h with stirring until the solution color turn into yellowish white. Using a cellulose dialysis tubes, dialysis against deionized water was performed for 80 h days changing the deionized water every 8 h to remove Lithium bromide content from SF solution. The concentration of SF was analyzed by putting different quantities of SF solution on small aluminum plates and dried in oven to

check difference in weight before and after drying SF solution and the mean was calculated, later the concentration of SF solution was maintained at 7 w/v% by dissolving HFIP.

The SF solution was poured in a 5 ml syringe and a high voltage of 11 kV supplied for electrospinning. The SFNF collected on a rotating drum covered with aluminum foil, spaced at 12 cm from the tip to collector. Collected SFNF were then dried overnight prior to dyeing and other characterizations.

4.2.3. Dyeing of SFNF nanofibers

Both C dyeing and UA dyeing carried under batchwise method for dyeing SFNF with two different Acid dyes. The output power 320w, the intensity of sonicating bath 0.98 W/cm^2(intensity = Power/bath area: 320-328) with frequency of 38kHz was used for UA dyeing of SFNF.

Acid dyes usually contains sulphonic-acid groups in the form of sodium-sulphonate salts. These increase solubility in water and give the dye molecules a negative charge. The SFNF is dyed in acidic solution, SFNF contains NH_2 as a functional compound which is protonated and as a results NH_3^+ forms which ionically interacts with the negatively charged acid dye and as result hydrogen bonds, dipolar bonds and van-der-waals forces are formed between acid dye and SFNF and the mechanism can be seen in scheme 4.2. We used 10 mg mas of SFNFs having an average thickness 130 μm for UA and C dyeing, the dye solution to the mass ratio was maintained at 20:1. The temperature (30°C, 40°C, 50°C, 60°C, 70°C and 80°C) for dyeing was checked, The time (10, 20, 30, 40 and 50 min) for dyeing was checked and the dye concentration (2%, 3% and 5% g/l) for dyeing was checked and optimized for UA dyeing and C dyeing of SFNF.

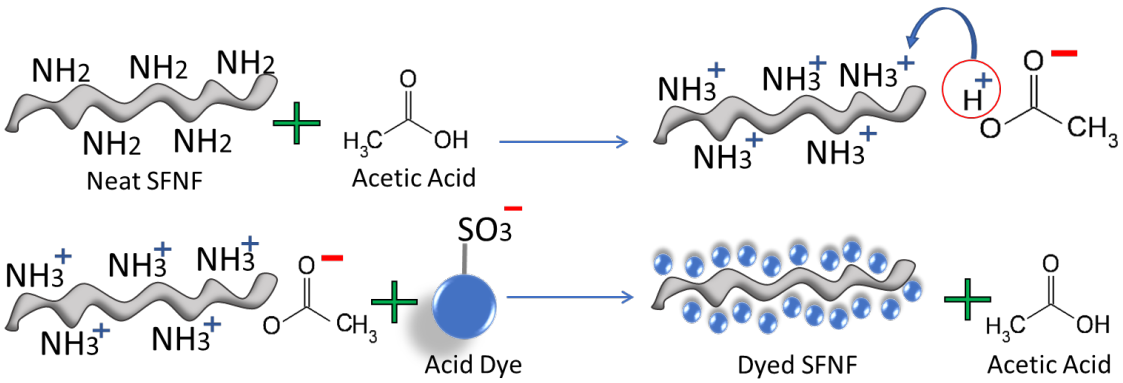

Scheme 4.2. Acid dye application on SFNF using ultrasonic energy

4.2.4. Dye exhaustion percentage

The amount of dye exhaustion % by the nanofibers at end of dyeing process represents the dye fixation and calculated using Eq. (4. 1).

$$\text{Exhaustion } \% = \left[\frac{C_o}{C_f}\right] \times 100 \qquad (4.\ 1)$$

where, C_o and C_f are the initial and final concentration of dye solutions in mg/l. The absorption spectrum of each dye solution before and after dyeing of SFNF was recorded by Lambda 35 UV–vis spectrophotometer (Perkin-Elmer, USA).

4.2.5. Color yield assessment after dyeing

Color yield of C dyed and UA dyed SFNF assessed by data color spectrophotometer and followed by K/S values, calculated using Eq. (4. 2).

$$K/S = \frac{(1-R)^2}{2R} \times 100 \qquad (4.\ 2)$$

Where, R is decimal fraction of the reflectance of dyed SFNF, K denotes the absorption co-efficient and S is the scatting coefficient.

4.2.6. Thermal and electrical energy consumption for dyeing SFNF

Thermal energy utilized by of C dyed and UA dyed SFNF for dyeing process was calculated by Eq. (4.3).

$$Q = m \times c \times \Delta q \qquad (4.3)$$

Where, Q is amount of thermal energy in kcal, m is mass of liquor in grams, Δq is temperature difference in ˚C and c is specific heat capacity of solvents used.

Electrical energy utilized by of C dyed and UA dyed SFNF for dyeing process was calculated by Eq. (4.4).

$$E = Pt \qquad (4.4)$$

Where E is energy consumption in Joules, P is power supplied in Watts and t denotes the time in seconds.

4.2.7. Fourier Transform Infrared Spectroscopy (FTIR)

The changes in chemical structure of dyed SFNF and undyed SFNF assessed by Fourier transform infrared spectroscopy on IR prestige-21(Shimadzu, Japan). All SFNF samples (UA/C-dyed SFNF) assessed using ATR-FTIR mode.

4.2.8. X-ray photo-electron Spectroscopy

XPS measurements were performed with AXIS Ultra by Schimadzu equipped with dual anode X-ray source Al/Mg, HSA hemispherical sector analyzer detector with vacuum pressure maintained at 1.4 × 10 -9 torr. Mg Kα X-ray source (1253.6 eV) was used for XPS measurements.

4.2.9. Scanning electron microscopy (SEM)

Scanning electron microscope model (JEOL JSM 6010LA), given voltage are 30 kV with highest magnification of 500,000x. All dyed and undyed SFNF were sputtered with Pd-Pt before assessing morphology.

4.2.10. Color fatness tests

The color fatness test carried for C dyed and UA dyed SFNF. Color fatness to washing were performed in gyrowash (James H, Heal Co UK), under the standard method of ISO 105, c10: 2006. The light fastness test performed in appollo (James, H Heal co., UK) by the ISO 105 – B02 method.

4.2.11. Crystallinity of SFNF before and after dyeing

Wide-angle X-ray diffractometer (WAXD) Rigaku Miniflex 300, R-AXIPSDS 3C Japan was used Operating at 40 kV, 300 mA using nickel-filtered CuKa radiation to analyze the effect of crystallinity of dyed SFNF and undyed SFNF. The diffraction patterns were measured from 10° to 40° degree at the scanning speed of 4°/min =2θ.

4.2.12. Shrinkage test

Shrinkage test was checked by taking SFNF sample's size 5 cm^2 with constant average thickness 135µm and dyed using acid dyes by both C dyeing and UA dyeing method and the shrinkage was compared before and after dyeing SFNF respectively and calculated using equations (6. 5,6. 6 and 6. 7) (lengthwise shrinkage and widthwise) shrinkage respectively.

$$\lambda_s = \frac{\lambda - \Delta\lambda}{\lambda} \times 100 \qquad (4.\ 5)$$

$$\omega_s = \frac{\acute{\omega} - \Delta\omega}{\acute{\omega}} \times 100 \qquad (4.\ 6)$$

$$R_s = \sqrt{\lambda_s{}^2 + \omega_s{}^2} \qquad (4.\ 7)$$

Where λ_s is lengthwise shrinkage, λ is original length, $\Delta\lambda$ is change in length in Eq. (4. 5), ω_s is widthwise shrinkage, $\acute{\omega}$ is original width, $\Delta\omega$ is change in width in Eq. (4. 6) and R_s is residual shrinkage after dyeing of SFNF in Eq. (4. 7).

4.2.13. Wicking rate

Wicking rate (the increase in height of wicking front per second) was assessed by hanging samples vertically over the petri dish containing 1% (w/v) of dye solution was prepared with CI Reactive Blue 19 (Sumfix Brilliant Blue R, Sumitomo Chemicals, Japan) dissolved in distilled water. The sample size of nanofibers web was cut into 20 mm height and 5 mm width and fixed in a upright stationary clamp, beneath, a petri dish containing dye solution was kept on the jack movable up and down. The lower end of sample was 5 mm below the liquid surface during the wicking test and remaining 15 mm was observed for wicking rise. 90 seconds time

4.2.14. Water contact angle

The static water contact angle (WCA) was determined by Sessile drop measurements using a Contact Shape Analyzer, DSA100 (Krüss, Hamburg, Germany).

4.3. Results and discussion

4.3.1. Effect of dyeing temperature on color yield

For the very first time SFNF dyed with and without UA dyeing method. Basic parameters for acid dyeing, temperature and time were necessary to be optimized for dyeing SFNF. Temperature for UA dyeing of SFNFs was studied constant time 40 min. Fig. 4. 1 shows the effect of dyeing temperature on color yield of SFNF dyed with CI Acid Red using conventional dyeing (CR-SFNF) and using UA dyeing (UR-SFNF) repsectively. The color yield of CI Acid Red increased with increasing dyeing temperature from 30 °C to 70 °C after that a slight increase in K/S observed therefore the optimized temperature for CR-SFNF was selected as 70 °C. In UA dyeing of SFNF showed higher color yield at room temperature compared to C dyeing at 70 °C and UA dyeing of UR-SFNF at room temperature did not affect fiber morphology which will be discussed in morphology section. UA dyeing technique showed higher color yield due to accelerated dye aggregation and rapid mass transfer due to cavitation produced as a result of ultrasonication. [22,39].

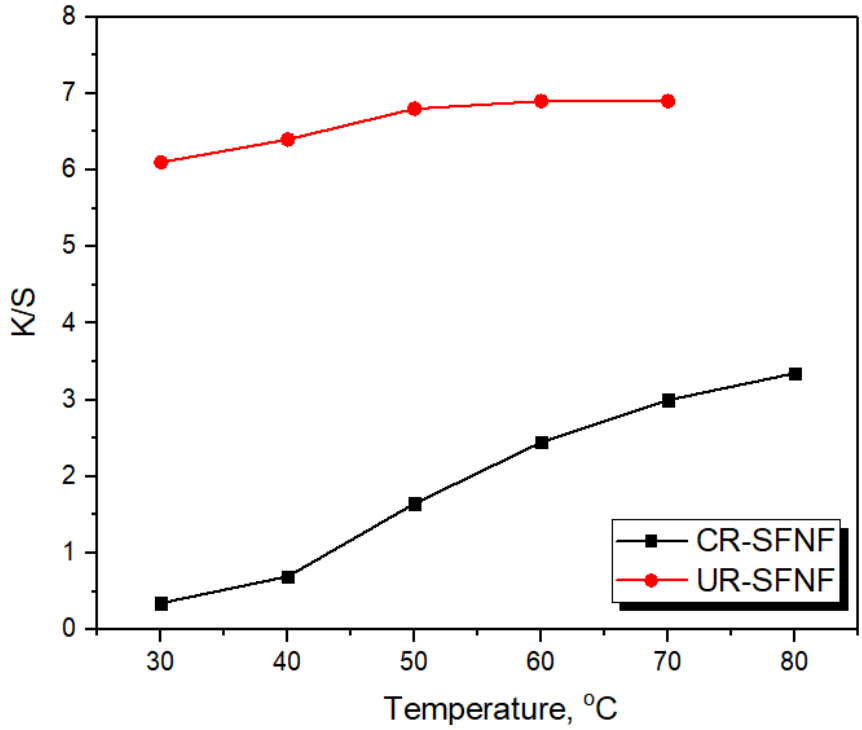

Fig. 4.1. Temperature optimization for UA dyeing of SFNF

4.3.2. Effect of dyeing time on color yield

CR-SFNF showed optimum results at temperature 70°C at time 40 min and the optimization of time was also necessary as this SFNF dyeing never report up to date. Fig. 4. 2. Shows the time optimization to dye SFNF for both C dyeing and UA dyeing. The color yield observed at time (5,10,15,20,30,40,50) min and maximum color yield observed at 50 min for C dyeing of SFNF and selected as optimum, on the other hand the maximum color yield also at 40 min, but after 20 min gradual and slight increase can be observed in color yield of UA dyeing and the optimized time for UA dyeing was selected as 20 min. The reason increased production rate at lower temperature is due to cavitation which breaks dye aggregates and uniformly transfer acid dye towards SFNF rapidly in UR-SFNF [34,35].

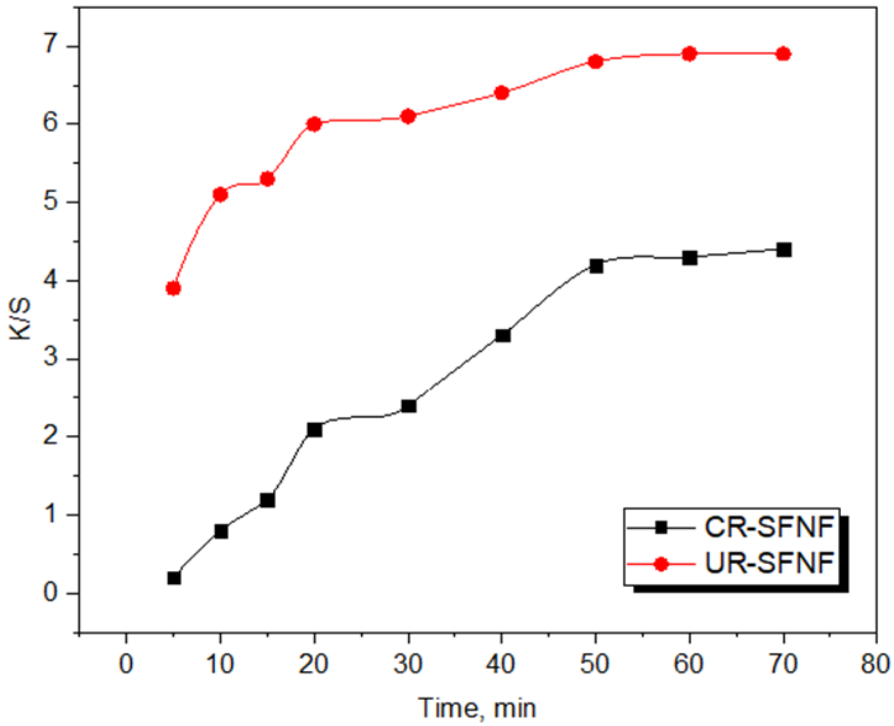

Fig. 4. 2. Time optimization for UA dyeing of SFNFs

4.3.3. Color build-up property of SFNF

Fig. 4. 3. (A). K/S values were taken at concentrations (2%, 3% and 5%) for acid dyes application on SFNF using optimized dyeing parameters for each dyeing method. Fig. 4. 3. (A and B) shows the continuous color buildup as per increasing dye concentration for both acid dyes and techniques. UA dyeing of SFNF depicts a linear relationship that states very good dyeability, color build up and uniform transfer of CR-SFNF, UR-SFNF, CI Acid Blue 117 on SFNF using C dyeing (CB-SFNF) and CI Acid Blue 117 on using UA dyeing (UB-SFNF) respectively. Where in Fig. 4. 3. (B) C dyeing shows hyperbolic curve with good dyeability but non-uniform dye transfer with more dye consumption and less production rate.

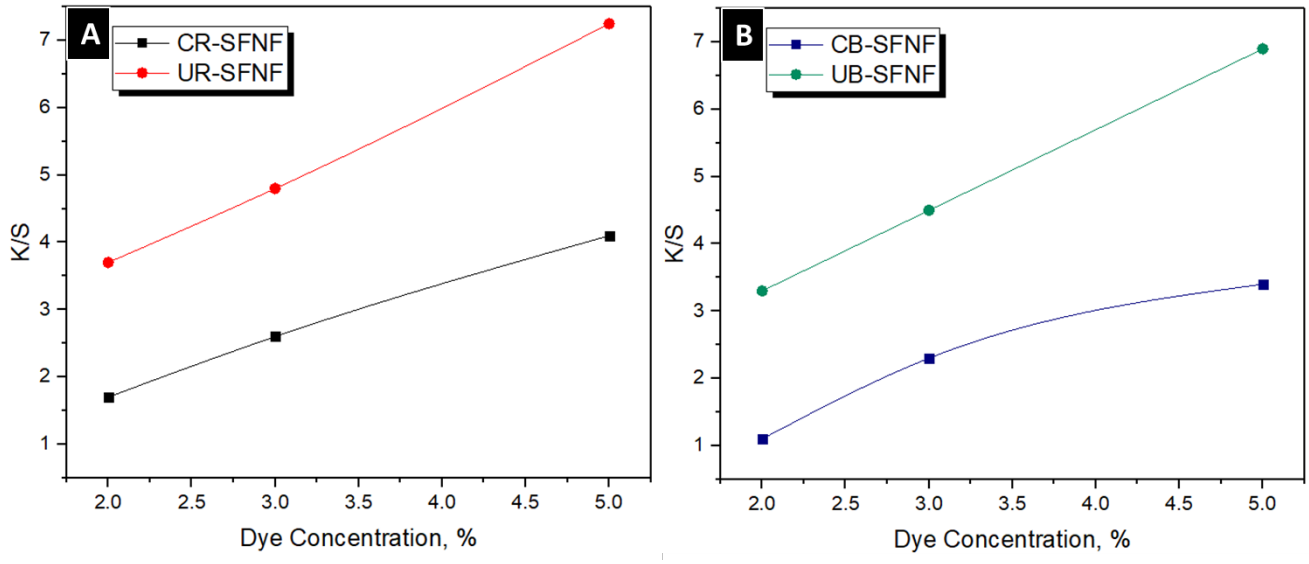

Fig. 4. 3. Enhanced of color buildup properties of SFNF (A) CI Acid red 38 UA dyeing ,(B) UA CI Acid blue117 UA dyeing

4.3.4. Comparison of color yield and exhaustion % between C dyed and UA dyed SFNF

The comparison of color yield between UA dyed and C dyed SFNF is given in Fig. 4. 4(A). UA dyed SFNF with CI Acid red 38 (UR-SFNF) show ~43.9% higher color yield than the C dyed SFNF with CI Acid red 38 (CR-SFNF). UA dyed SFNF with CI Acid blue 117 (UB-SFNF) show ~45.9% higher color yield than the C dyed SFNF with CI Acid blue 117 (CB-SFNF). CR-SFNF showed ~10.9% higher color yield than CB-SFNF.UR-SFNF showed ~7.6% higher color yield than UB-SFNF. The increased color buildup in UA dyeing is due to rapid development of equilibrium because of speedy acid dye aggregates resulted with cavitation [34,35]. The same reason may be attributed for more exhaustion percentage of UA dyeing as revealed in Fig. 4. 4 (B), Ultrasonic energy uniformly transfer the acid dye to SFNF, as a result more exhaustion% and more exhaustion rate can be observed in U dyed SFNF compared to C dyed SFNF. CR-SFNF showed 2.3% more exhaustion than CB-SFNF, UR-SFNF showed 2.1% more exhaustion than UR-SFNF and UA dyed SFNF (in 20 min at room

temperature) showed 9.7% more exhaustion percentage compared to C dyed SFNF (in 50 min at 70°) also the reason of ~10.3% less dye effluent as a waste of industrial production which makes process eco-friendlier and more economical

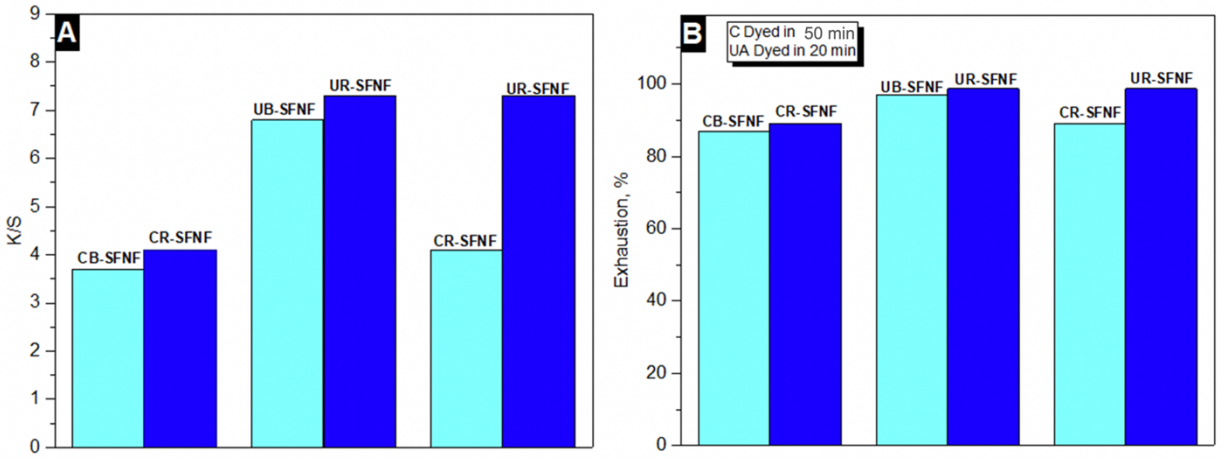

Fig. 4. 4. comparison of (A) Color build up, (B) Exhaustion % of C dyed and UA dyed SFNF

4.3.5. Chemical structure of SFNF after dyeing

4.3.5.1. FTIR Spectroscopy

Fig. 4.5 Shows the FTIR spectra of dyed SFNF and undyed SFNF. The peaks stretching at 1517.46 cm^{-1} shows the presence of N-O (amides), the stretching and bending intensive peaks at 1620.95 cm^{-1} shows beta sheets of SFNF and confirms the presence of C=C and N-H[29,36],the stretching amines can be observed at peak 1226.14 cm^{-1} in the form of C-N and the small peaks at 3285.77 cm^{-1} depicts the presence of NH and OH groups present in all dyed and undyed SFNF samples[30,37]. No significant change observed in dyed and undyed SFNF due to small amount of acid dyes used for dyeing process and rinsed well after for washing. Most of the functional groups of CI Acid red 38 and CI Acid blue 117 are identical such as NH, OH and presence of carbon but specific bonding and type of bonding is unclear, also the presence of sulphur in the form of salt in acid dyes cannot be observed in FTIR spectra.

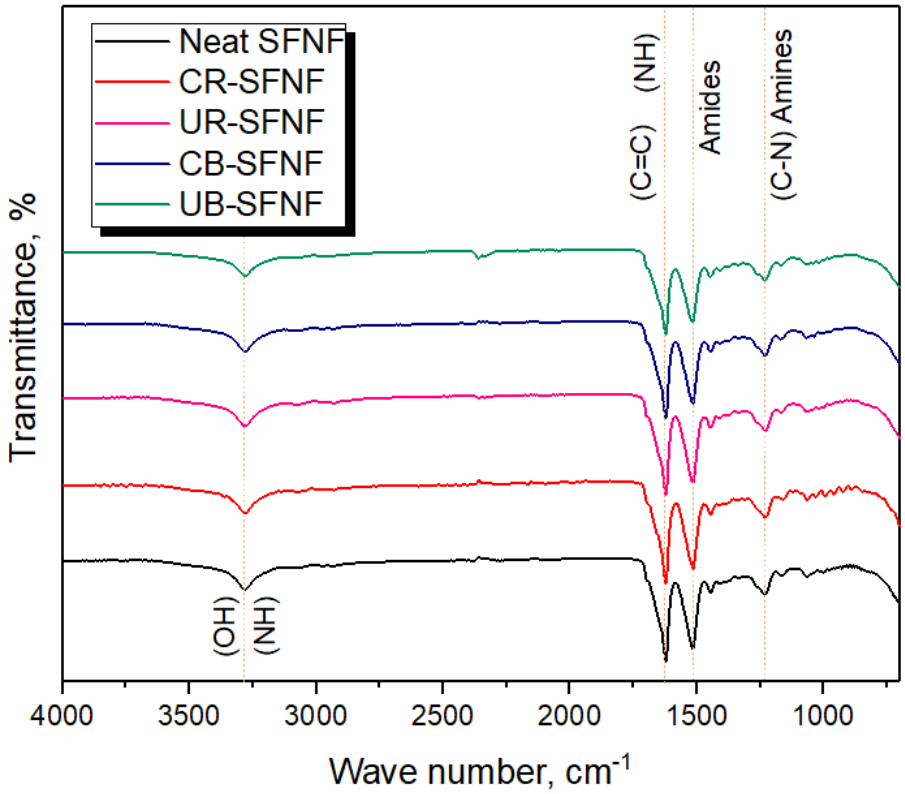

Fig. 4. 5. FTIR spectra of UA dyed and undyed SFNF

4.3.5.2. XPS Spectroscopy

The chemical groups in dyed SFNF, neat SFNF showed no significant peak in S2p region but CR-SFNF and UR-SFNFN show SO_2 where CB-SFNF and UB-SFNF showed SO_2 and SO_3 at binding energy To analyze the presence of specific elements and types of bonds, we choose to characterize dyed SFNF using XPS to confirm the presence of acid dyes elements within dyed SFNF. Fig. 4. 6 (A). shows the wide spectrum of dyed and undyed SFNF in which additional peak at binding energy of (151.84eV) in all dyed SFNF which cannot be observed in the neat SFNF. To confirm presence of nitrogen, oxygen, carbon and sulphur along with their bond types, the XPS results taken separately in their respective region and the respective

range of elements can be seen Fig. 4. 4 (B). In Fig. 4. 6 (C). the XPS spectra at binding energy (398-401eV) of nitrogen (N1s) reveals the presence of NH_2, C-N and C-NH in all dyed

and undyed SFNF but the presence of different functional groups in different samples is different. Neat SFNF shows no C-NH, comparatively less C-N and more NH_2 groups compared to all dyed SFNF. UB-SFNF and CB-SFNF (B dyed SFNF) showed same chemical structure in XPS spectra, N1s shows that B dyed SFNF contain C-N groups, comparatively more C-NH and NH_2 groups due to formation of C-NH after dyeing. UR-SFNF and CR-SFNF (R dyed SFNF) show comparatively less C-NH than B dyed SFNF, C-N same as Neat SFNF and NH_2 slightly less than Neat SFNF. Fig. 4. 6 (D) shows the presence of C=O, C-OH, C-C and C=C in C1s region at binding energy (282-290eV) for all dyed and undyed SFNF. Fig. 4. 6 (E) shows the groups of dyed and undyed SFNF in region O1s at binding energy (528-535eV), Neat SFNF shows more C=O groups compared dyed SFNF. O1s reveals comparatively more SO_2 groups present in B dyed SFNF than R dyed SFNF because of ionic bonding between C=O of neat SFNF, OH and N of CI Acid red 38, As a results slightly C=O can be seen in R dyed SFNF and increased C-OH and C-O-C groups can be observed in O1s of XPS. In Fig. 4. 6 (F) XPS of dyed and undyed SFNF in region S2p can be seen which clearly confirm the presence of different Sulphur 167eV[37].

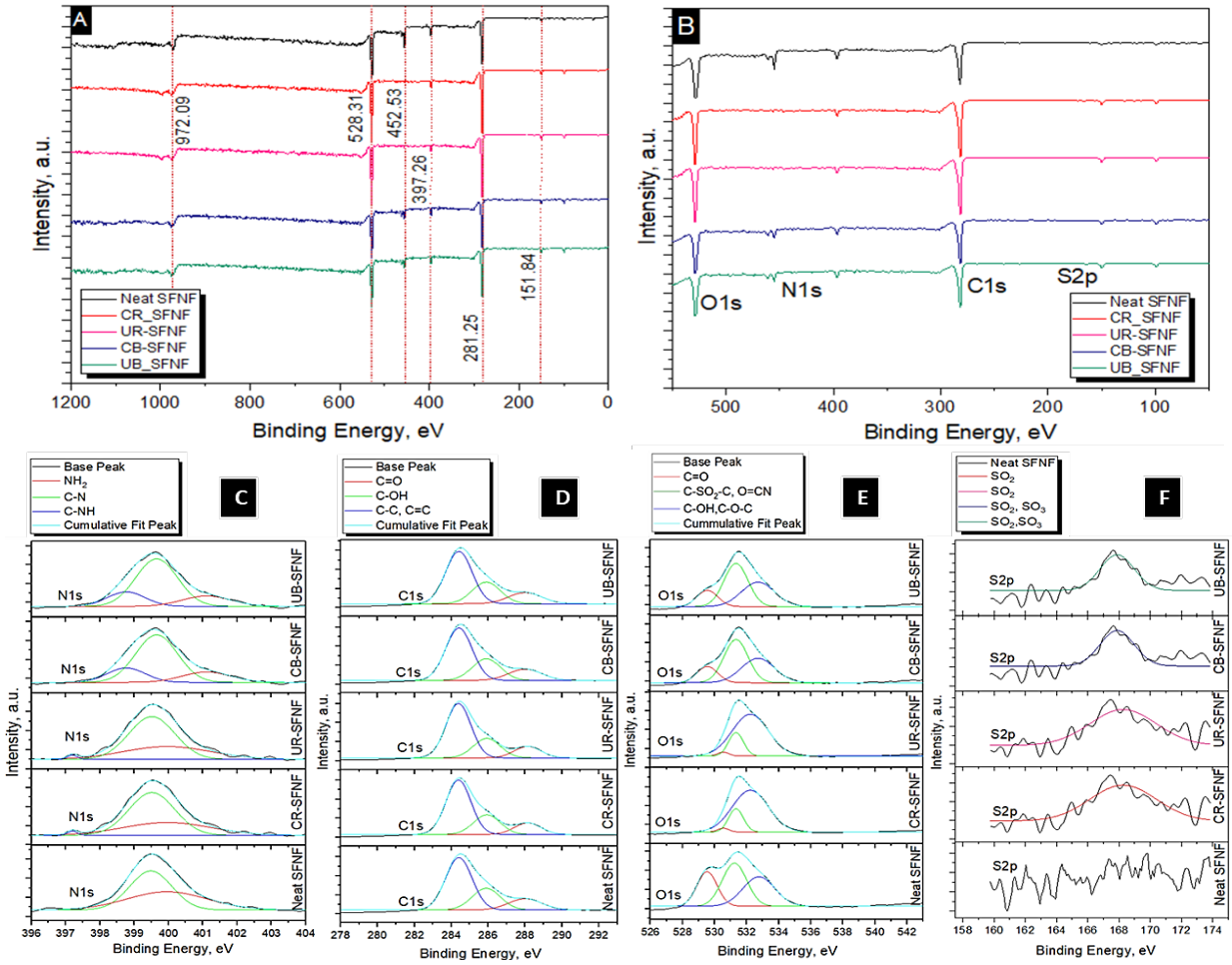

Fig. 4.6. XPS spectra of SFNF before and after UA dyeing (A) Whole wide spectrum (B) Expanded spectrum (C) C1s (D) N1s (E) O1s (F) S2p.

4.3.6. Effect of ultrasonication on morphology of SFNF after dyeing

Fig. 4.7. reveals the regular and smooth morphology of dyed SFNF and undyed SFNF. Fig. 4.7. (A) shows the smooth morphology of Neat SFNF. The C dyed SFNF can be seen in Fig. 4.7 (B and C) which reveals slight increase in fiber diameter of dyed SFNF due to dye diffusion into the nanofibers due to high temperature of 70°C and longer dyeing time 50 min, CB-SFNF shows slightly increased diameter compared to CR-SFNF may be due to bigger molecular size of acid dye type. Fig. 4. 7 (B and C) also shows slight convolution within the nanofibers which ultimately represents the shrinkage in dyed SFNF compared to Neat SFNF

which will be discussed in Shrinkage section 3.9. The SEM images of UA Dyed SFNF can be seen in Fig. 4. 7. (D and E) which reveals stretched smooth morphology after UA dyeing compared to C dyed SFNF because of cavitation within ultrasonic container which stretched the nanofibers webs during dyeing and as a resultant colored nanofiber observed with smooth and un-shrunk morphology. Aligned nanofibers results in increased absorbance rate due to less hindrance in the lengthwise flow within the nanofiber diameter which will later confirmed in wicking test section.

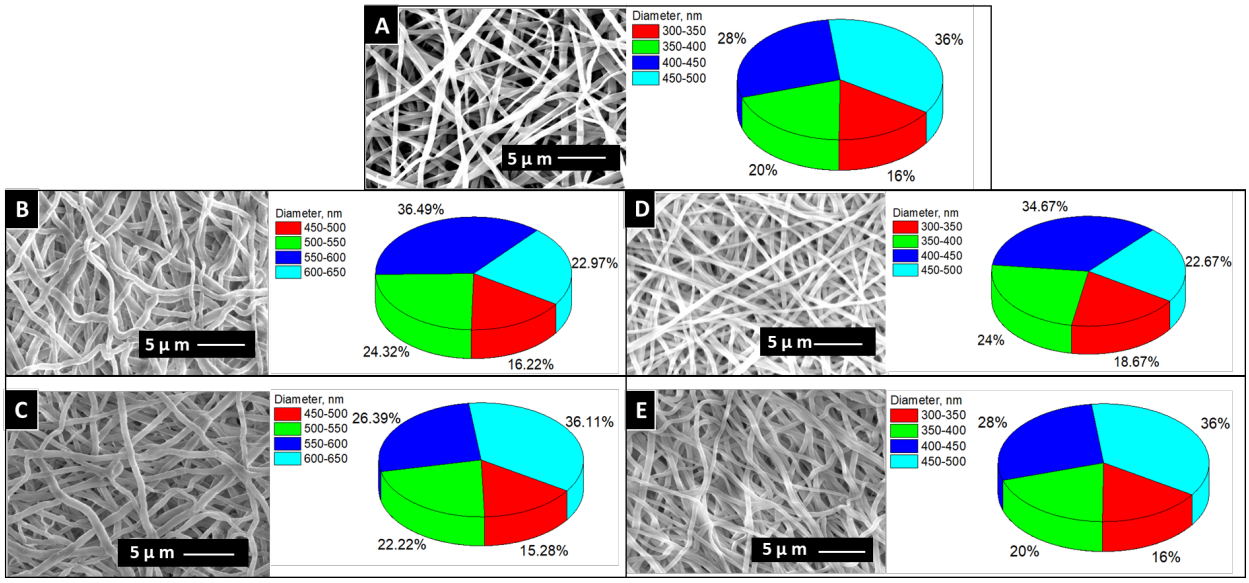

Fig. 4. 7. SEM images of SEM Images of (A)Neat SFNF and Diameter Distribution (B) CR-SFNF and Diameter Distribution (C) CB-SFNF and Diameter Distribution (D) UR-SFNF and Diameter Distribution (E) UB-SFNF and Diameter Distribution

4.3.7. Color fastness properties of SFNF

The color fastness to light and color fastness to washing were carried on the dye SFNFs at 3% dye concentrations in both DES two different Acid dyes, CI Acid red and CI Acid blue. Samples were dyed at 60°C temperature for 40 minutes which are previously optimized dyeing parameters to dye SFNFs. Table 4. 1. Shows the color fastness results, staining in washing fastness for CI Acid blue has attained maximum rating in both conventionally and

ultrasonically dyed SFNFs in CC:FF and staining in washing fastness for Acid red showed slightly lesser than CI Acid blue in both ultrasonically and conventionally in CC:EG which indicates good dye fixation properties for both dyes and medias. The color changes were observed to be very good rating of 4/4 and 4/5 for both dyes irrespective of dyeing medium. Ultimately ultrasonically dyed SFNFs averagely showed better dye fixation to washing fastness test. The conventionally and ultrasonically dyed SFNFs dyed with respect to dye type and medium showed no difference in light fastness test results and achieved as average in all dyed samples.

Table 4. 1. Color fastness to light test ISO 105-BO2 and color fastness to washing test ISO 105-C10:2006

[1]Dye	**Light fastness (20 hours)**	**Washing fastness (Change of shade)**	**[3]Washing fastness (Staining on multifiber)**					
			CT	**CO**	**PA**	**PES**	**PAC**	**Wo**
[1]UR-SFNF	3/4	5	5	5	4/5	5	5	5
[2]CR-SFNF	3	4/5	4	4	4	4/5	4/5	4/5
[1]UB-SFNF	3/4	4/5	5	5	4/5	5	5	5
[2]CB-SFNF	3	4	4/5	4/5	3/4	4/5	4/5	4/5

[1]UA dyeing Conditions: Temperature 25 ^{o}C; time 20 min; Dye concentration 2%
[2]Conventional dyeing Conditions: Temperature 70 ^{o}C; time 40 min; Dye concentration 2%
[3]CT, cellulose triacetate; CO, cotton; PA, polyamide; PES, polyester; PAC, polyacrylic; Wo, wool

4.3.8. Change in crystallinity in SFNF after dyeing

Fig. 4. 8. shows the difference between XRD patterns of C dyed, UA dyed and neat SFNF. C dyed and neat SFNF shows peak at 20.711^{o} where XRD pattern. CR-SFNF showed small additional peak at 29.822^{o} and CB-SFNF showed small additional peak at 12.913 ^{o}. UA dyed SFNF showed only small peaks as it showed increased amorphous region of UA dyed

SFNF which resulted enhanced wettability which will be further confirmed by wicking and water contact angel tests. CR-SFNF showed a similar small additional at 29.822°. The XRD results confirmed that UA dyeing enhance the wettability of SFNF due to ultrasonication which enhance the rate reaction between acid dye and SFNF which may be resisting additional amines and hydrogen bonding on the fiber surface with rapid and proper penetration of dye into the nanofibers, this is also the reason that uniform dye transfer can be achieved in UA dyed SFNF compared to C dyed SFNF [35].

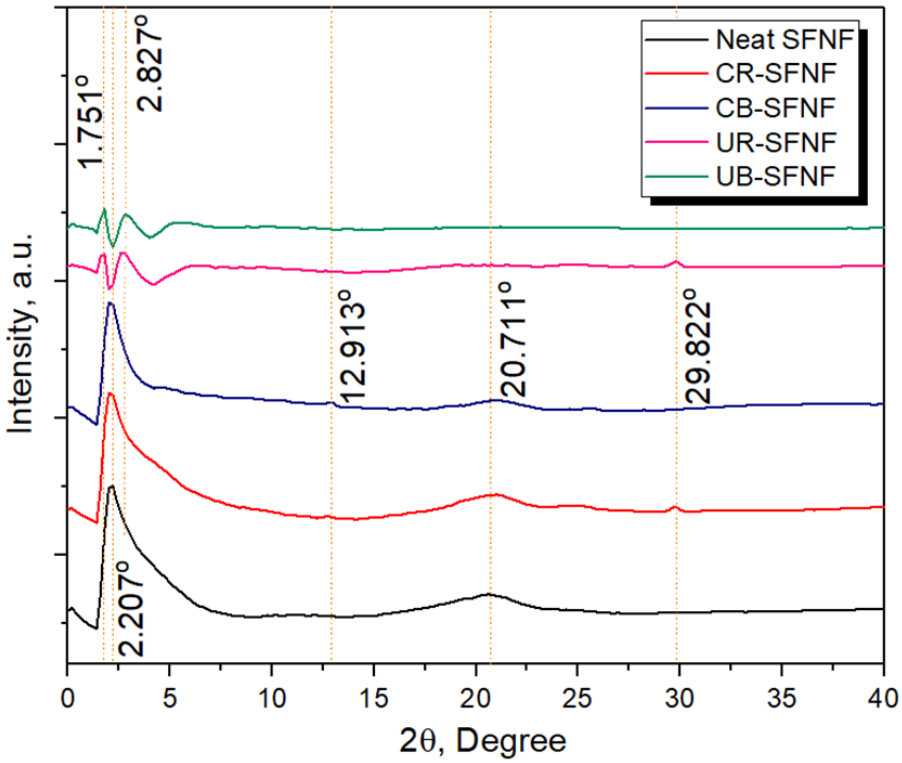

Fig. 4. 8. XRD patterns of UA dyed and Neat SFNF

4.3.9. Cavitation resists shrinkage of SFNF during dyeing

The shrinkage in SFNF observed during interaction with acid dyes. Neat SFNF kept under ultrasonication and at 80°C individually for 20 and 40 min respectively but no shrinkage observed. While interaction with acid dyes the formation and deformation of NH_3 and

Hydrogen ions, the formation of different ionic bonds and wander wall forces maybe a reason of shrinking effect during dyeing of SFNF. Shrinking effect depends on type of dye used and exposure of SFNF to heat as shown in Table 4. 2. Lengthwise shrinkage (λ_s), widthwise shrinkage(ω_s) and residual shrinkage (R_s) calculated accordingly for the comparison. UA dyed SFNF showed slight shrinkage after dyeing where the C dyed SFNF showed higher shrinkage effect this may be due to higher temperature during C dyeing [32].

In Table 4. 2. the samples CB-SFNF shows 8.8% more R_s compared CR-SFNF, UB-SFNF shows 11.5% more R_s compared UR-SFNF and CR-SFNF shows 29.3% more R_s compared UR-SFNF.

Conventionally it is difficult to get satisfactory dyeing results at room temperature because the higher temperature results shrinking effect that cannot be avoided, ultimately cavitation due to ultrasonic energy enhance the chemical reaction, rapid dye aggregation and uniform acid dye transfer to SFNF offer effective and efficient dyeing results at room temperature with a negligible shrinking effect. The results revealed that the cavitation produced by ultrasonication have potential to resist shrinkage during dyeing SFNF.

Table 4. 2. Shrinkage in SFNF after conventional and ultrasonic dyeing

Shrinkage	C Dyeing		UA dyeing	
	CR-SFNF	CB-SFNF	UR-SFNF	UB-SFNF
λ_s	23.2%	28.9%	3%	11.1%
ω_s	24.5%	31.2%	3.3%	11.5%
R_s	33.7%	42.5%	4.4%	15.9%

4.3.10. Effect on wettability of SFNF after dyeing

4.3.10.1. Wicking test

Fig. 4. 9. Shows the wicking behavior of dyed and neat SFNF. As per XRD results the UA dyed samples contain more amorphous region compared to C dyed SFNF and neat SFNF. All dyed and undyed samples showed rapid increase in wicking height until 40 seconds whereas C dyed samples showed increased wicking height compared to neat SFNF and UA dyed SFNF showed increased wicking height compared to C dyed SFNF. All samples reached different wicking heights, Neat SFNF 14.5mm, CR-SFNF 16.5, CB-SFNF 16, UB-SFNF 20 within 90 sec where UR-SFNF reached wicking height of 20mm within 80 sec.

This may be due to presence of more OH groups in CI acid red 38 dye compared to CI acid blue 117 which can be seen in Scheme 4.1. The presence of amines and OH present in acid dyes structure which previously confirmed by FTIR and XPS , resulted in increased wicking of C dyed SFNF compared to neat SFNF where in UA dyed SFNF due to less shrinkage smooth morphology and the uniform migration of dye into the SFNF and rapid dye aggregation due to ultrasonic cavitation, as a result interaction of acid dye bonds with nanofiber increased, ultimately increased wicking and wicking rate compared to C dyed SFNF.

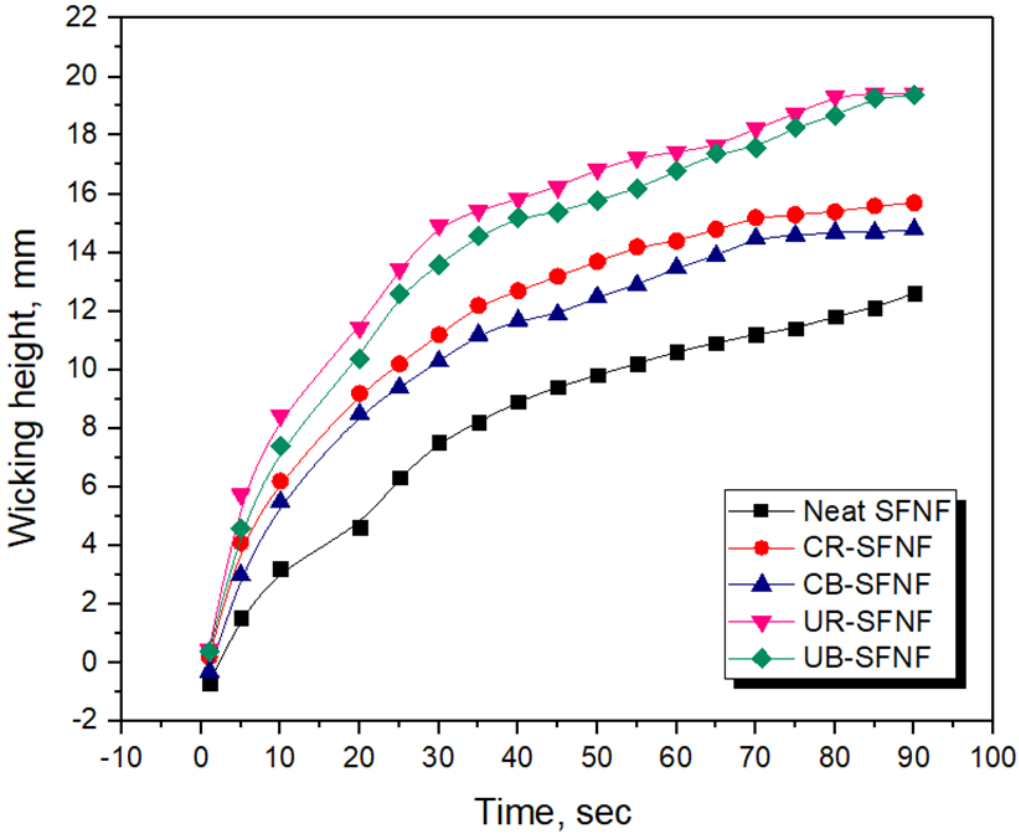

Fig. 4. 9. Wicking test of dyed and Neat SFNF

4.3.10.2. Water contact angle test

Fig. 4. 10. Shows the water contact angle (WCA) of C dyed, UA dyed and neat SFNF, all samples took less than 4 seconds to reach the water drop angle from 115°±10° to 1°±1. Neat SFNF took 3.5 ±1 sec, CR-SFNF and CB-SFNF took 2.5±1 sec where UR-SFNF and UB-SFNF only took 1.5±1 sec to reach the water drop angle from 115° ±10° to 1° ± 1°. Results shows that all samples are hydrophilic. C dyed SFNF showed more hydrophilic behavior compared to neat SFNF and UA dyed SFNF showed more hydrophilic behavior compared to C dyed SFNF and Neat SFNF. The reason behind increased hydrophilicity of C dyed SFNF is the presence of amines and OH on fiber surface compared to neat SFNF where in UA dyed SFNF including the presence of OH and amines on the surface and into the nanofibers due to

increased dye exhaustion due to cavitation which is also the reason of less shrinking effect and smooth morphology of SFNF after UA dyeing.

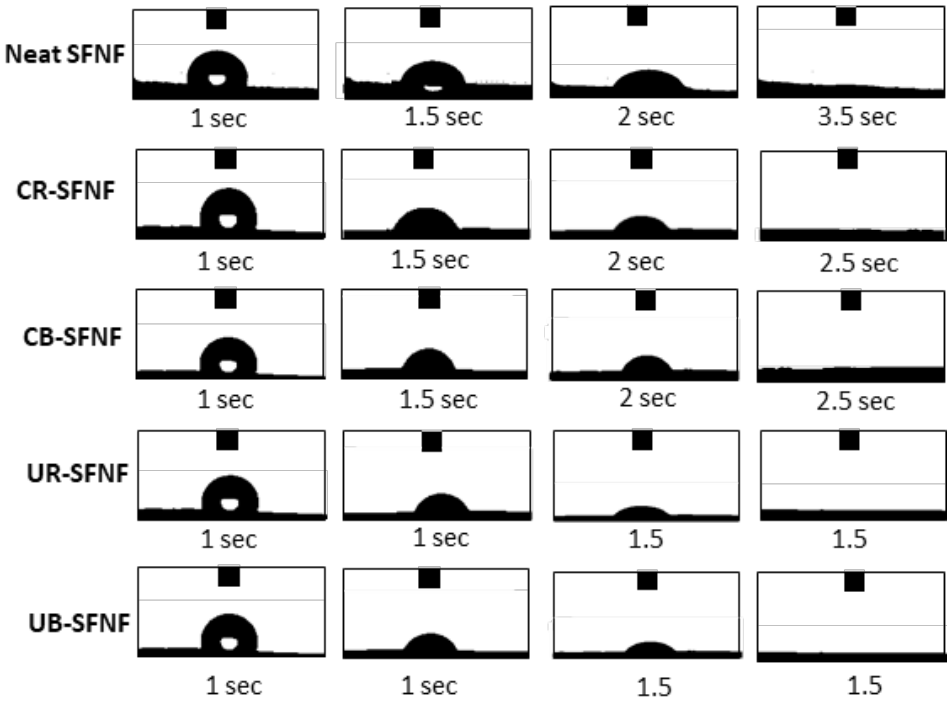

Fig. 4. 10. Water contact angle test of UA dyed and Neat SFNF

4.3.11. Efficiency of ultrasonication on electrical energy consumption for dyeing SFNF

Electrical energy consumption calculated for UA dyed SFNF and C dyed SFNF and compared accordingly. Electrical energy consumption for dyeing SFNF is given in Table 4. 3.

The dyed SFNF samples at optimized conditions for both C dyeing and UA dyeing compared, time and temperature were consumed more than half in C dyed SFNF than UA dyed SFNF. Electrical energy for C dyeing supplied for 50 min maintaining temperature at 70°C where electrical energy used in UA dyeing was only for operating ultrasonic machine because room temperature is enough to dye SFNF while the process aided by ultrasound waves. The results showed UA dyeing have potential to save 62.28% electrical energy with better dyeing results

compared to C dyeing method. Ultimately, room temperature dyeing process saves 64.28% thermal energy as well which was calculate by given experimental methods.

Table. 4. 3. Electrical energy consumption for conventional and Ultrasonic dyeing of SFNF

Method	Temperature (°C)	Time (Min)	Total Consumption (Joules per second)	Saving Energy (%)
CN dyeing	70	50	350000	
UA dyeing	25	20	132000	62.28

The optimum conditions selected for thermal energy consumption comparison between CN dyeing and UA dyeing of SFNF is given in Table 4. 4. The quantity and type of Liquor used for dyeing SFNF was same for both CN dyeing and UA dyeing but the temperature, electrical energy and time for both dyeing methods were different. CN dyeing carried at 70°C temperature where the UA dyeing carried at room temperature, the thermal difference is obvious from the temperature values. The results of thermal energy consumption calculations showed; UA dyeing can potentially save 64.28% of thermal energy with better dyeing results compared to CN dyeing.

The total calculated efficiency for UA dyeing of SFNF is 60% more than the CN dyeing of SFNF. The UA dyed SFNF not only showed better efficiency but uniform and regular dyeing with better properties at room temperature.

Table. 4. 4. Thermal energy consumption for conventional and ultrasonic dyeing of SFNF

Method	Temperature (°C)	Mass of liquor (g)	Total Consumption / (Joules per second)	Saving Energy (%)
CN dyeing	70	0.01	53.809	64.28
UA dyeing	25	0.01	19.21	

4.4. Conclusion

Successful UA dyeing of SFNF using two different acid dyes carried for the very first time. UA dyeing of SFNF showed 60% enhanced efficiency with 10% reduced waste dye effluent production. Ultrasonic energy produces cavitation and promotes dye aggregation which potentially enhanced the 9.7% exhaustion and ~43.9% color yield of SFNF with smooth morphology, low shrinkage and color fastness properties. WAXD, wicking and water contact angle test confirmed enhanced wettability of SFNF. Chemical structures of dyed SFNF confirmed using FTIR and XPS. UA dyeing has potential to save 62.28% electrical, 64.28% thermal energy. Conclusively, UA dyeing of SFNF proved to be better in terms of efficiency, enhanced chemical and physical properties and energy saving over C dyeing of SFNF.

4.5. References

[1] Ahmed, F; Saleemi, S; Khatri, Z; Abro; M, I; I. S. Kim; Co-electrospun poly (ε-caprolactone)/cellulose nanofibers-fabrication and characterization; Carbohyd. Polym. 2015, 115, 388-393.

[2] Khatri, M; Qureshi, U. A; Ahmed, F; Khatri, Z; & Kim, I. S. Dyeing of Electrospun Nanofibers. Handbook of Nanofibers, 2018, 1-16.

[3] Khatri. Z; Saleem, U; Mayakrishnan, G; Kim, B,S; Wei, K and Kim, I, S. Pad dyeing of cellulose acetate nanofibres with Acid dyes, Color. Technol. 128 (2012) 1-5.

[4] Khatri, Z; Mayakrishnan, G; Hirata, Y; Wei, K; Kim, I, S. Cationic-cellulose nanofibers: Preparation and dyeability with anionic reactive dyes for apparel application, Carbohyd. Polym. 2013, 91, 434– 443Z.

[5] Khatri.Z; Arain, R, A; Jatoi, A ,W; Mayakrishnan, G; Wei, K; Kim, I, S., Dyeing and characterization of cellulose nanofibers to improve color yields by dual padding method, Cellulose 2013, 20, 1469–1476.

[6] Khatri, Z; Ahmed, F; Jhatial, A, K; Abro, M, I, Mayakrishnan, G; Kim, I, S. Cold pad-batch dyeing of cellulose nanofibers with reactive dyes, Cellulose. 2014, 21, 3089-3095.

[7] Khatri, A; Ali, S; Jhatial, A,K; Kim, S, H. Dyeability of polyurethane nanofibres with Acid dyes, Color. Technol., 2015, 131, 374-378.

[8] Shahidi, S & Ghoranneviss, M. Effect of Plasma on Dyeability of Fabrics. In Textile Dyeing. 2011

[9] Mehdi, M; Mahar, F, K; Qureshi, U, A; Khatri, M; Khatri, Z; Ahmed, F; & Kim, I. S. Preparation of colored recycled polyethylene terephthalate nanofibers from waste bottles: Physicochemical studies. Advances in Polymer Technology, 2018, 37(8), 2820-2827

[10] Gao, D; Yang, D. F; Cui, H. S.; Huang, T. T.; & Lin, J. X. Synthesis and measurement of solubilities of reactive disperse dyes for dyeing cotton fabrics in supercritical carbon dioxide. Industrial & Engineering Chemistry Research, 2014, 53(36), 13862-13870.

[11] Babar, A. A; Peerzada, M, H.; Naveed, T.; & Dayo, A, Q. Exhaust Reactive Dyeing of Lyocell Fabric with ultrasonic Energy. 2019 Ultrasonics Sonochemistry.

[12] Tissera, N, D; Wijesena, R,N; de Silva, K,N. Ultrasound energy to accelerate dye uptake and dye–fiber interaction of reactive dye on knitted cotton fabric at low temperatures, Ultrason. Sonochem. 2016, 29, 270-278.

[13] Larik S. A; A. Khatri; Ali, S; Kim, S, H. Batchwise dyeing of bamboo cellulose fabric with reactive dye using ultrasonic energy, Ultrason. Sonochem.2015, 24 ,178-183.

[14] Khatri, Z; Memon, M, H; Khatri, A; Tanwari, A. Cold Pad-Batch dyeing method for cotton fabriCN dyeing with reactive dyes using ultrasonic energy, Ultrason. Sonochem. 2011, 18 , 1301–1307.

[15] Guesmi. A; Ladhari, N; Sakli, F. Ultrasonic preparation of cationic cotton and its application in ultrasonic natural dyeing, Ultrason. Sonochem., 2013, 20, 571-579.

[16] Öner, E; Başer, I; Acar, K. Use of ultrasonic energy in reactive dyeing of cellulosic fabrics, J. Soc. Dyers Colour. 1995, 111, 279-281.

[17] Kamel, M, M; El Zawahry; N, S, E; Ahmed; F. Abdelghaffar; Ultrasonic dyeing of cationized cotton fabric with natural dye. Part 1: Cationization of cotton using Solfix E. Ultrason. Sonochem., 2009, 16, 243-249.

[18] Kamel, M, M; El Zawahry, N. S. E; Ahmed, F. Abdelghaffar; Ultrasonic dyeing of cationized cotton fabric with natural dye. Part 2: cationization of cotton using Quat 188, Ind. Crops Prod. 2011, 34, 1410-1417.

[19] Kamel, M,M; Helmy, H,M; N, S, E; Hawary, I. Some Studies on Dyeing Properties of Cotton Fabrics with Crocus sativus (Saffron flowers) Using an Ultrasonic Method, J. Nat. Fibers 2009, 6 , 151-170.

[20] Kamel, M,M; Reda, M, E.; Youssef, B,M; Mashaly, H. Ultrasonic assisted dyeing. IV. Dyeing of cationised cotton with lac natural dye, Dyes and Pigments 2007, 73, 279-284.

[21] Khatri, M; Ahmed, F; Jatoi, A, W; Mahar, R,B; Khatri, Z;& Kim, I, S. Ultrasonic dyeing of cellulose nanofibers. Ultrasonics sonochemistry, 2016, 31, 350-354.

[22] Jatoi, A. W; Ahmed, F; Khatri, M; Tanwari, A; Khatri Z; Lee, H; & Kim, I. S. Ultrasonic-assisted dyeing of Nylon-6 nanofibers. Ultrasonics sonochemistry, 2017, 39, 34-38.

[23] Jatoi, A. W; Kim, I. S; & Ni, Q, Q. Ultrasonic energy-assisted coloration of polyurethane nanofibers. Applied Nanoscience, 2018, 1-10.

[24] Jatoi, A. W; Gianchandani, P. K; Kim, I. S; & Ni, Q, Q. Sonication induced effective approach for coloration of compact polyacrylonitrile (PAN) nanofibers. Ultrasonics sonochemistry, 2019, 51, 399-405.

[25] Robert R Franck Silk, mohair, cashmere and other luxury fibres, LLC , 2001 Woodhead Publishers (ISBN 1 85573 540 7) CRC Press (ISBN 0-8493-1311-2).

[26] Kim, S. H; Yeon, Y. K; Lee, J. M; Chao, J. R; Lee, Y. J; Seo, Y. B; & Hong, I. S. Precisely printable and biocompatible silk fibroin bioink for digital light processing 3D printing. Nature communications,2018, 9(1), 1620.

[27] Mehrotra, S; Chouhan, D; Konwarh, R; Kumar, M; Jadi, P. K; & Mandal, B. B. Comprehensive Review on Silk at Nanoscale for Regenerative Medicine and Allied Applications. ACS Biomaterials Science & Engineering, 2019, 5(5), 2054-2078.

[28] Kim, S. H; Nam, Y. S; Lee, T. S; & Park, W. H. Silk fibroin nanofiber. Electrospinning, properties, and structure. Polymer Journal,2003, 35(2), 185.

[29] Shukla, S. R; & Mathur, M. R. Low-temperature ultrasonic dyeing of silk. Journal of the Society of Dyers and Colourists, 1995, 111(11), 342-345.

[30] Ghaly, A. E; Ananthashankar, R; Alhattab, M. V. V. R; & Ramakrishnan, V. V. Production, characterization and treatment of textile effluents: a critical review. J Chem Eng Process Technol,2014, 5(1), 1-19.

[31] Koh, J. (2011). Dyeing with Acid dyes. In Textile Dyeing. InTech.

[32] Choi, T. S; Shimizu, Y; Shirai, H; & Hamada, K. Acid dyeing of polyester fiber using gemini surfactants containing ammonium cations as auxiliaries. Dyes and pigments, 2001, 50(1), 55-65.

[33] Koh, J., & Greaves, A. J. Synthesis and application of an alkali-clearable azo Acid dye containing a fluorosulfonyl group and analysis of its alkali-hydrolysis kinetics. Dyes and pigments, 2001,50(2), 117-126.

[34] Tissera, N. D; Wijesena, R. N; & de Silva, K. N. Ultrasound energy to accelerate dye uptake and dye–fiber interaction of reactive dye on knitted cotton fabric at low temperatures. Ultrasonics sonochemistry, 21016, 29, 270-278.

[35] Kamel, M. M; Helmy, H. M.; Mashaly, H. M; & Kafafy, H. H.Ultrasonic assisted dyeing: Dyeing of acrylic fabrics CI Astrazon Basic Red 5BL 200%. Ultrasonics Sonochemistry, 2010, 17(1), 92-97.

[36] Yao, C; Li, X; Song, T; Li, Y;& Pu, Y. Biodegradable nanofibrous membrane of zein/silk fibroin by electrospinning. Polymer international, 2009, 58(4), 396-402.

[37] Wang, S; Zhang, Y; Wang, H; & Dong, Z. Preparation, characterization and biocompatibility of electrospinning heparin-modified silk fibroin nanofibers. International journal of biological macromolecules, 2011,

CHAPTER 5

Photosensitive nanofibers for data recording and erasing

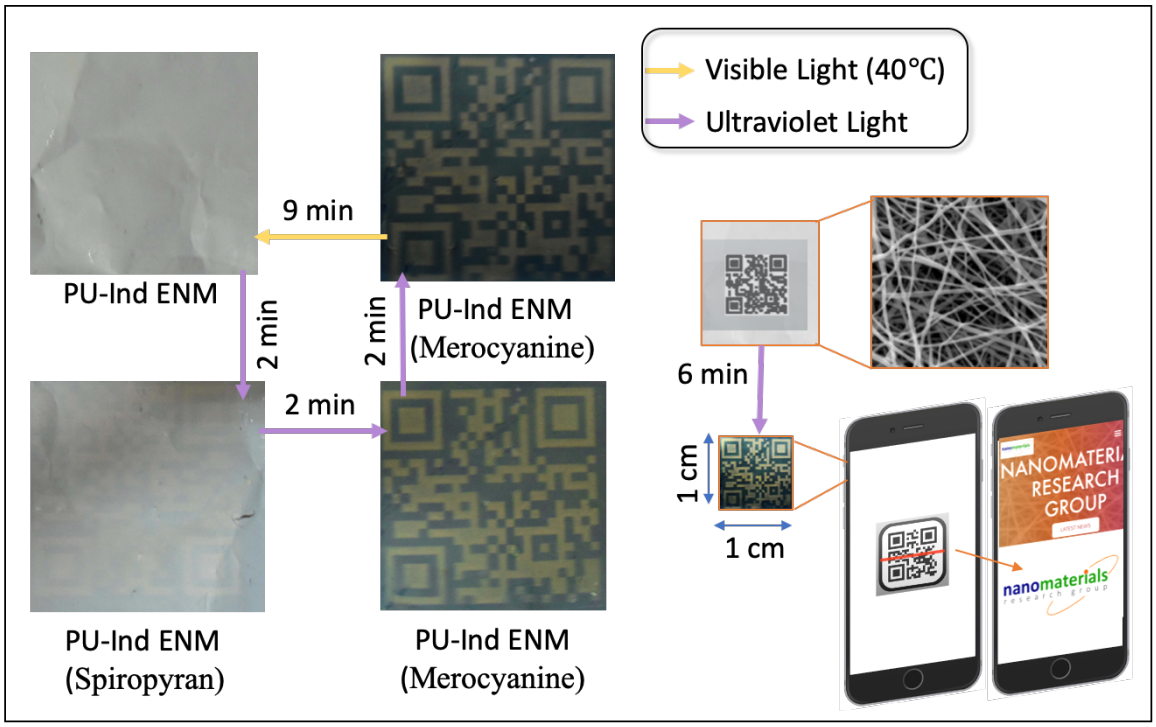

Data recording /erasing mechanism and reading via Smart phone

5.1. Introduction

Electrospinning has been considered as a versatile and viable technique for the preparation of functional nanofibers. A significant progress has been developed to prepare nanofibers with various characteristics. Electrospinning technique have potential to produce the nanofibers with various morphologies, compositions, structures, and functional properties, such as surface treatments, improvement in aesthetic, faster sensation, faster responsive, faster tunability and stimuli switchable, filtration membranes, energy and data storage, electronics, as well as sensor applications, these nanofiber in the form of non-woven webs are being considered for commercialization due to high performance and bulk productivity[1].

Photosensitive materials undergo a reversible structural change when irradiated with UV light and the photosensitive spiropyran dye [1'-3'-Dihydro-8-methoxy-1',3',3'-trimethyl-6-nitrospiro [2H-1-benzopyran-2,2'-(2H)-Indole] (Indole) has been extensively considered, [2] leading to an interconversion between a colorless, closed-ring, less polar spiropyran (SP) form to a colored, ring-opened, more polar merocyanine (MC) form [3]. The reverse transformation to SP form takes place upon irradiation with visible light (Scheme 5.1). Among many photosensitive compounds studied, spiropyran derivatives offer facile synthesis, distinct chromic transition and fluorogenic nature of MC form in certain environments [2, 3]. They have been successfully embedded as a photochrome into various polymers via electrospinning technique including cellulose acetate [4], bacterial cellulose [5], polystyrene (PS) [2], polyethylene oxide [2], polydimethylsiloxane [3], poly (methacrylic acid) [6], poly (methyl methacrylate) [7], and poly(vinylidene fluoride-co-hexafluoropropylene) [8] and polyvinyl alcohol [9] Polyvinylpyrrolidone [11], Polyvinylidene fluoride [12] with different applications [13] .Since previously reports on photosensitive nanofibers have some limitation in either processing or fiber characteristics. Some polymers are hydrophilic in nature and is soluble in water therefore the use of this polymer may limit its application in imaging or recording in moisture environment. Production of some photosensitive nanofibers have been reported as complex and more time consuming and some nanofiber limited due to less flexibility, less durability and less dyeability [1-9].

Polyurethane (PU) has is well known for waterproof and breathable properties, which alternatively have potential to not only protect the goods from sudden interaction with water/moisture/liquid. PU nanofibers has been used for various applications, such as raincoats, sportswear other protective and wearables [14-17]. PU is durable and retain its

shape [16] it has air permeable and breathable properties [17,18]. Electropun nanofiber mates (ENMs) are being explored to enhance aesthetic properties [19-23] and PU ENMs have very good dyeability [24], it has also been used as fire resistant [25], non-toxic and biocompatible [26]. Although, PU ENMs have not been investigated yet for the photosensitive (coloration and decolration) applications.

Therefore, for the very first time we prepared PU ENMs incorporated with Indole dye (Ind-PU) and compared to PS ENMs incorporated with Indole dye (Ind-PS) with respect to the photosensitive properties. PU ENMs showed comparatively better photosensitive properties than the PS ENMs, because of multifunctional characteristics of PU [14-26]. For the production of PU EMNs comparatively lower voltage is required compared to PS EMNs via elecrospinning. For data recording on photosensitive ENMs made of PU and PS, we chose quick-response (QR) codes, which are two-dimensional matrix codes capable of holding 100 times more data than a traditional barcode [10]. The QR data at the area of (1x1cm) could easily be read by smart phone from the surface of PU ENMs in case of rough handling whereas in case of PS ENMs it was okay in soft handling conditions but in case of rough handling the data could easily be read, it may be due the shape memory of PU which retains the shape QR data [27]. Color yield obtained by PU ENMs was higher than the color yield on PS ENMs at 1% Indole dye concentrations and conditions. The SEM images reveals smooth morphology before and after dye incorporation for both PS and PU ENMs. FTIR revealed no chemical influence on the actual chemical structure of either PU or PS due to small amount of dye used only to install photosensitive property. The results revealed that the Ind-PU ENMs has an edge over Ind-PS ENMs, therefore Ind-PU can potentially be considered for data recording and erasing applications such as secure food transportation

under 40°C, UV absorption in protective clothing and UV readable data by military or where such type of photosensitive nanofibers can be utilized.

5.2. Experimental

5.2.1. Materials

PS (M_w: 280,000 g/mol), PU (M_w: 110,000 g/mol), and a photosensitive dye Indole was purchased from Sigma-Aldrich (USA). PS (25 wt.-%) and Indole (1 wt.-%) were dissolved in dimethylformamide at room temperature to prepare Ind-PS solution. Similarly, PU (10 wt.-%) and Indole (1 wt.-%) were dissolved in dimethylformamide-methyl-ethyl ketone at room temperature to prepare Ind-PU solution. Both polymer solutions were stirred overnight before electrospinning.

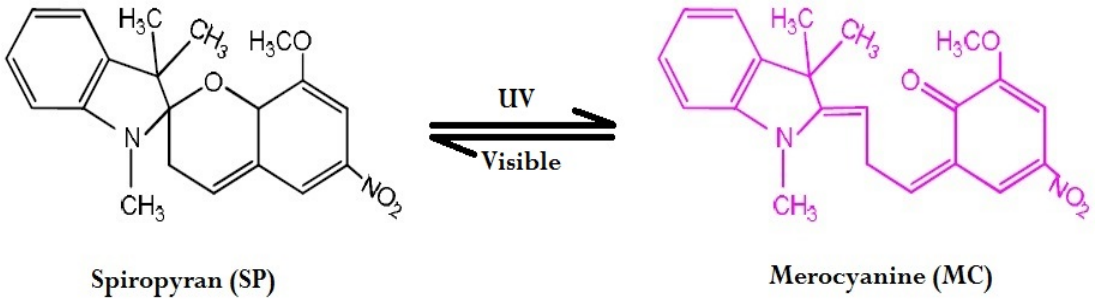

Scheme 5.1. Chemical structure and coloration mechanism of Indole dye

5.2.2. Preparation of photosensitive Ind-PU and Ind-PS ENMs

Electrospinning set up with a high-voltage power supply (Har-100*12, Matsusada Co., Tokyo, Japan), capable of generating voltages up to 100 kV, was used as the source of the electric field. The polymer solutions were supplied through a 5 ml plastic syringe attached to a capillary tip with an inner diameter of 0.6 mm. A copper wire connected to a positive electrode (anode) was inserted into the polymer solution, and a negative electrode (cathode) was attached to a metallic drum (collector). Several parameters were applied in order to

optimize the electrospinning of the solutions and the optimal parameters were chosen as follows: A voltage of 14 kV (Ind-PS) and 12 kV (Ind-PU) was applied, and the tip-to-collector distance was fixed at 12 cm for all electrospinning processes. Nanofibers were deposited continuously over a rotating metallic drum. All the solutions were electrospun at room temperature. All specimens were dried to remove the residual solvent in a vacuum oven at 25^{o}C for a day before use. The thicknesses of ENMs were in between 25 to 30 μm.

5.2.3. Characterizations

The Ind-PS ENM and Ind-PU ENM were measured on Reflectance Spectrophotometer (Datacolor Spectraflash SF 600, USA) under illuminant D65, using 10^{o} standard observer with specular component included and UV component included. The relative color strength was assessed by using the Kubelka-Munk Eq. (5. 1) as described in a previous report [10].

$$\frac{K}{S} = \frac{(1-R)^2}{2R} \quad \text{..... (5. 1)}$$

where R = decimal fraction of the reflectance of the UV irradiated ENM, K = absorption coefficient and S = scattering coefficient.

Photocoloration refers to the color build-up of the Ind-PS ENM and Ind-PU ENM after being UV-irradiated (365 nm); and the reverse process, decoloration, refers to the attainment of actual color of the Ind-PS ENM and Ind-PU ENM (UV-irradiated) upon exposure to visible light (TUNGSTEN BULB). Both photocoloration and decoloration were investigated for different time intervals.

For photocoloration, ENMs were irradiated under UV light (Spectroline ENF 260C/FE, USA) from 0 to 300 s, placed at a distance of 8 cm from the substrate. The samples were measured at 5 s after removal from the UV source. In order to determine decoloration, the samples were UV-irradiated for 300 s and the subsequent color change was measured under the visible light

(TUNGSTEN BULB) after the removal of UV-light source at various intervals (from 2 to 40 min). The photocoloration and decoloration measurements were performed in a controlled temperature room.

The morphology of ENMs was obtained under SEM (JSM 6380LV, JEOL Japan). All samples were sputtered with gold under vacuum before assessment. The average nanofiber diameter was measured from the SEM micrographs using image analysis software (Image Pro® Plus, Version 5.1, Media Cybernetics, Inc.). The average thickness of ENMs was measured by Digital Micrometer MCD130-25 with a measuring sensitivity of 1 μm. Ultraviolet-visible (UV-Vis) absorption spectra of the Ind-PS and Ind-PU solutions were obtained using a UV-Vis spectrophotometer (1800, Shimadzu Japan). The chemical structural changes of neat PU and PS before and after incorporation of Indole was determined by Fourier transform infrared spectroscopy (FTIR) on IR prestige - 21 by shimadzu Japan.

5.3. Results and discussion

5.3.1. Photocoloration and decoloration of ENMs

Fig. 5. 1 shows effect of UV-irradiation time (0 to 300 s) on color strength of Ind-PS ENM and Ind-PU ENM. For comparison, the K/S of ENMs before UV-irradiation (SP form) has been read as Zero. The UV-irradiated ENMs were converted from white to pink color (MC form) under UV irradiation (Photocoloration).Irrespective to the type of polymer used, the K/S was enhanced with increasing UV irradiation time(Fig. 5. 1).This color built-up favors readability of recorded pattern on ENMs[8]. The color conversion of Ind-PS ENM developed white to light blue whereas Ind-PU ENM developed white to deep purple, this is the reason why Ind-PU ENM demonstrated slightly higher K/S in comparison to the Ind-PS ENM. After 300 s UV irradiation time, maximum K/S value of 0.06 was obtained for Ind-PU ENM.

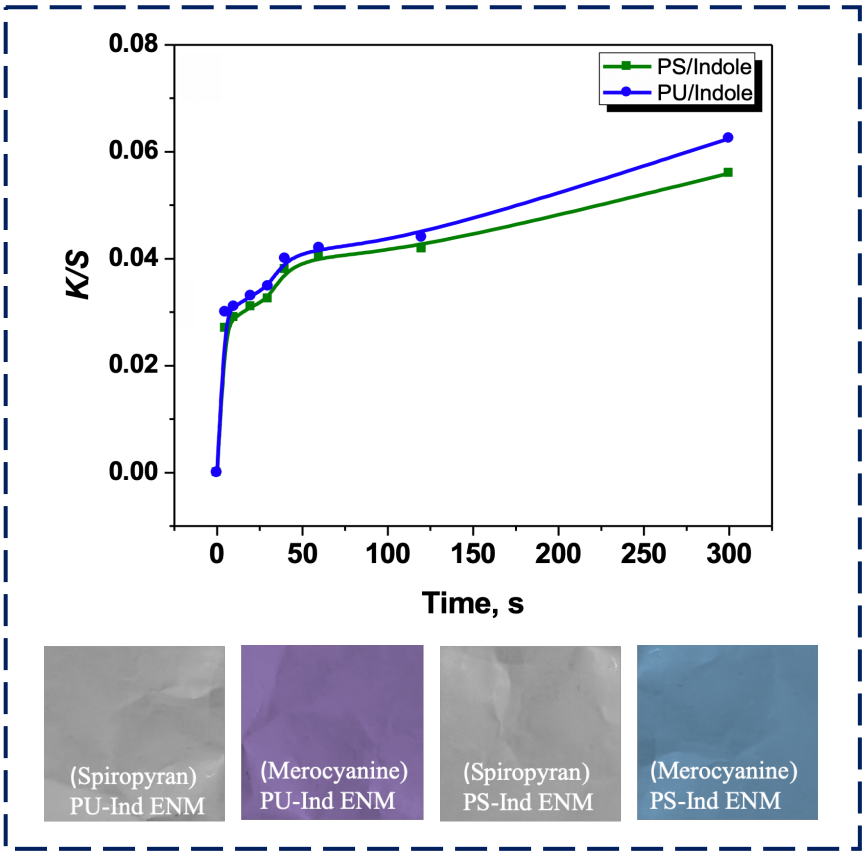

Fig. 5. 1. Effect of UV irradiation time on photocoloration (K/S)

Similarly, in Fig. 5. 2 shows the decoloration of the UV-irradiated (365 nm) samples under visible light. The extent of decolorization was determined by K/S values. Each ENM was UV irradiated for 300 s and after removal of the UV source; the decoloration was measured from 0 to 40 min under the visible light (TUNGSTEN BULB). It can be seen from Fig. 5. 2 that the increasing time resulted into a steady decay in K/S for both Ind-PS ENM and Ind-PU ENM. The transformation of the MC form to the SP form was achieved in 40 min under visible light. Moreover, it was observed that the rate of photocoloration was faster than the rate of decoloration. The results show that proposed photosenstive nanofibers show delay in decoloration as compared to polyvinyl alcohol nanofibers [9] which has the advantage of a prolong data storage.

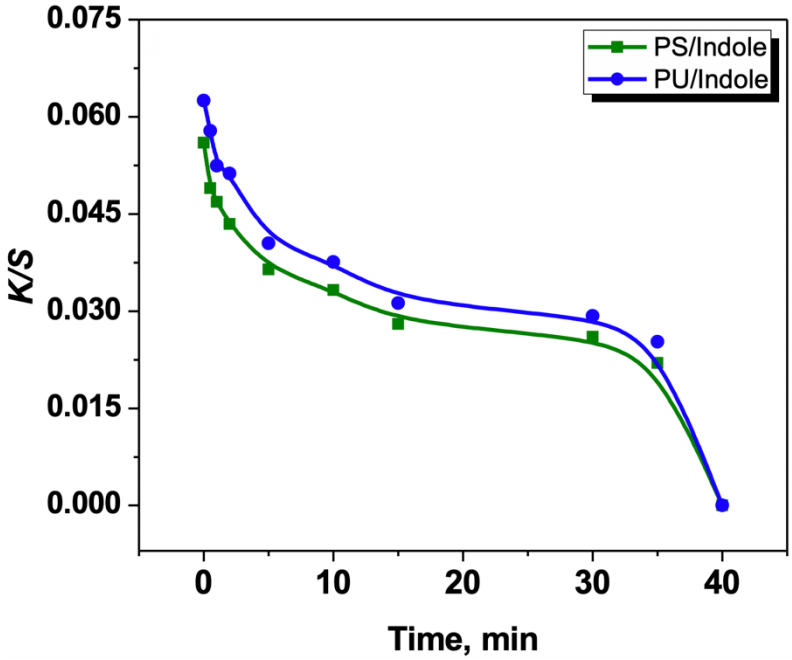

Fig. 5. 2. Effect of time on decoloration (K/S) of PS/Indole ENM and PU/Indole ENM

5.3.2. Data recording and erasing on Ind-PS and Ind-PU ENMs

The data recording and erasing of high-resolution image on Ind-PS ENM and Ind-PU ENM was investigated through record-erase-record mechanism as shown in Fig. 5. 3. Due to the fast readability and large storage capacity, quick-response code has been practiced and used recently [9]. Therefore, we chose quick-response code to be generated as an optical data on Ind-PS ENM and Ind-PU ENM. As an example, we chose a webpage of our research group (http://nanorg.weebly.com/) and recorded it.

Referring Fig. 5. 3, the Ind-PS ENM and Ind-PU ENM were UV-irradiated through a photo-mask (quick-response code image) for 300s generating blue color (MC form) only in the UV-exposed areas. In contrast, the UV-unexposed areas maintained their original color (SP form) producing patterned image on Ind-PS ENM and Ind-PU ENM as shown in Fig. 5. 3.

The recorded QR code on Ind-PS ENM and Ind-PU ENM were scanned via Smartphone (Sony SO-04D) for authentication and validation. Moreover, the erasing of the patterned

image on the Ind-PS ENM and Ind-PU ENM takes place upon visible light irradiation (tungsten bulb) for 600s (Fig. 5. 3). In order to ensure its repeatability, record-erase-record property of the Ind-PS ENM and Ind-PU ENM were performed 10 times and showed comparable results each time.

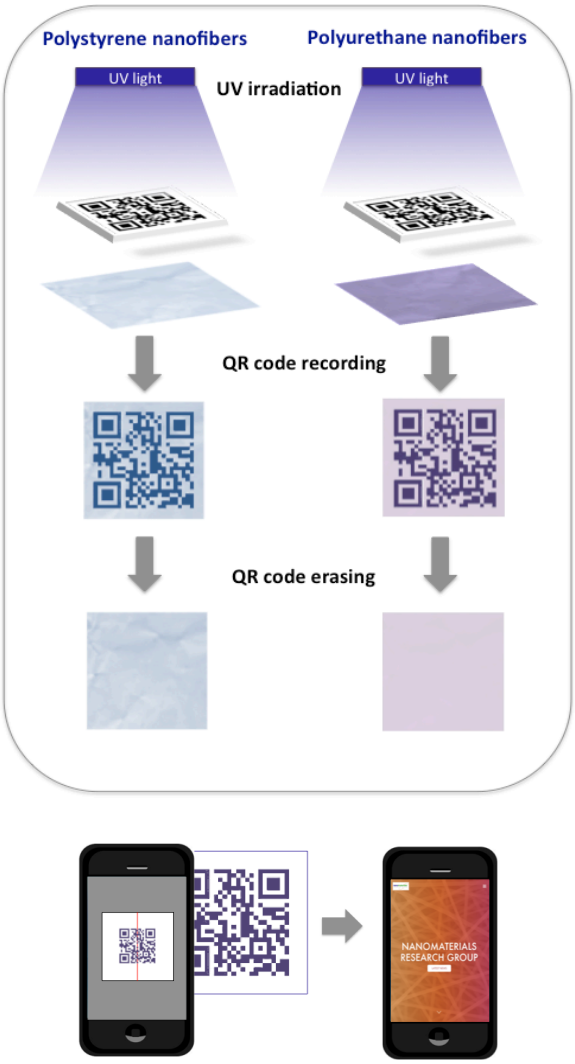

Fig. 5. 3. Recording and erasing of QR code on PS/Indole ENM and PU/Indole ENM (sample was irradiated with UV light of 365 nm for 360 s through a photo-mask followed by visible light irradiation for 600 s)

5.3.3. UV-Vis spectrophotometry of ENMs

Fig. 5. 4a-b shows the UV-Vis absorption spectra of Ind-PS and Ind-PU solutions with and without UV light irradiation of 365 nm. The formation of MC form of the photosensitive molecule is evident by UV light irradiation for 180 s, as a new absorption peak observed at 600 nm (Fig. 5. 4a-b). The color of both Ind-PS and Ind-PU solutions were changed from colorless to blue after UV light irradiation for 180 s. Furthermore, the intensity of peaks presents at 350 nm (Fig. 5. 4a) and 360 nm (Fig. 5. 4b) did not change after UV light irradiation suggesting that there were still a large amount of Indole dyes present in SP form within both Ind-PS and Ind-PU solutions. Our results are in proximity with previous reports[2, 5]. Fig. 5. 4c demonstrates the photo-switchability of Ind-PS and Ind-PU solutions under repeated alternating irradiations with UV light for 3 min and subsequently with visible light (tungsten bulb) for 10 min. We have found good photo-reversibility of both the Ind-PS and Ind-PU solutions from SP form to MC form (photocoloration) and vice versa (decoloration) during many cycles.

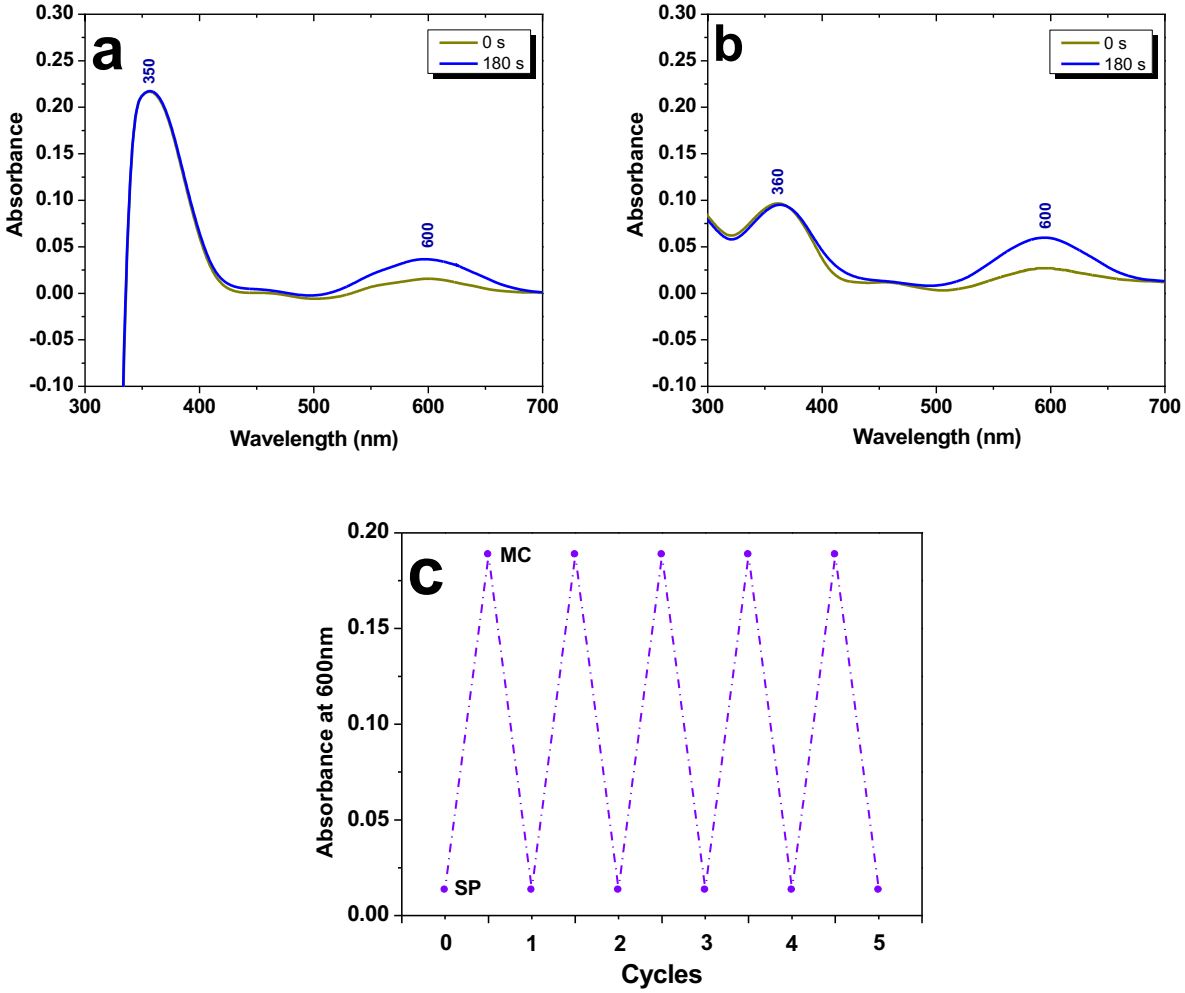

Fig. 5. 4. UV-visible absorption spectra of (a) PS/Indole solution, (b) PU/Indole solution and (c) photo-switchability of PS/Indole and PU/Indole solutions under UV and visible light irradiations.

5.3.4. Morphology of Neat and dyed PU and PS ENMs

The SEM images of un-irradiated and UV-irradiated ENMs are presented in Fig. 5. 5. SEM images of Neat PS and PU ENMS can be seen in the Fig. 5. 5a and 5c which reveals smooth nanofiber morphology having average nanofiber diameter as 350±30 and 400±80 respectively. The Fig. 5. b and d shows that the incorporation of small amount 1% of photosensitive Indole dye in the polymer solutions did not affect the smooth morphology of the resulting Ind-PS ENM and Ind-PU ENM, the respective diameter distribution graphs reveal the average diameter of Ind-Ps and Ind-PU ENMs as 450±80 and 500±80

respectively. Ultimately, after dye incorporation a slight increase in nanofiber diameter observed with bead-free and smooth morphology. Our results are in agreement with some reports [9] and different with other reports. [4, 5]. Results may vary due to chemical compatibility of polymer with the dye or improper dissolution of dye into the solution for electrospinning.

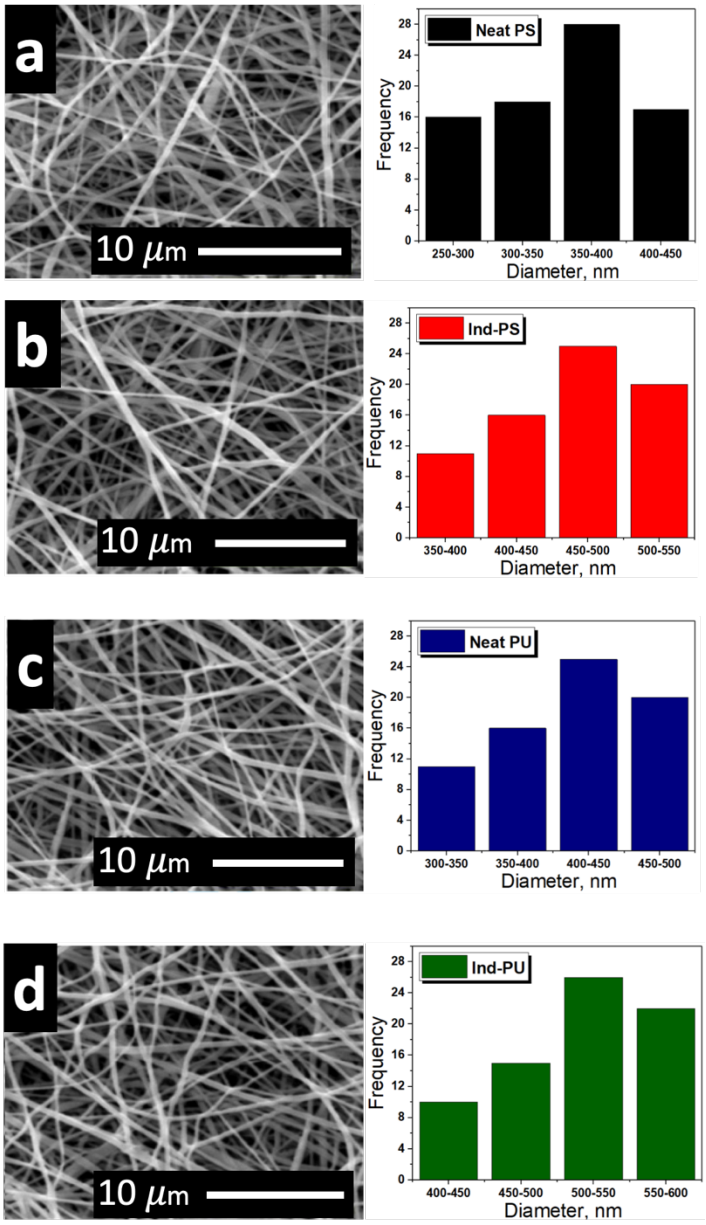

Fig. 5. 5. SEM Images of (a) PS ENM, (b) PS/Indole ENM, (c) PU ENM and (d) PU/Indole ENM.

5.3.5. Chemical structure of PU and PS ENMs before and after dye incorporation

Fig. 5. 6 shows the FTIR spectra of PU and PS before and after incorporation of Indole dye. The FTIR spectrum of PS and Ind-PS can be seen in Fig. 5. 6(A) which are similar in chemical composition, the peaks at the spectrum 2936 cm^{-1} and 2856 cm^{-1} reveals C-H and

CH_2 respectively present in chemical composition of Neat PS and Ind-PS nanofibers. The peak at 1695 cm^{-1} represents C=O and the peaks at 1522 cm^{-}confirms the availability of C=C(Aromatic), the small bending peaks at 1370 cm^{-1} and 1306 cm^{-1} reveals C-H_2, the stretching peaks at 1219 cm^{-1} 1106 $cm^{-1}$and 1073 cm^{-1} reveals the availability of C-O (Esters), the small bending peaks at 813 cm^{-1} and 770 cm^{-1} also corresponds to C-H in Neat PS and Ind-PS, conclusively there is no influence in the chemical structure of PS with Indole dye incorporation[28].

Fig. 5. 6(B) shows the FTIR spectrum of Neat PU and Ind PU nanofibers. The peaks at 3336 cm^{-1} corresponds to the stretching (-NH) and the peak at 2958 cm^{-1} are associated to stretching vibration of CH_2. The spectrum at 1735 cm^{-1} and 1689 cm^{-1} corresponds to C=O urethane and the peak at 1535 cm^{-1} spectrum bending shows the amide-II. The band at 1226 cm^{-1} and 1076 cm^{-1}corresponds to asymmetric stretching of Esters and a small bending peak at 771 cm^{-1} represents C-H available in both Neat PU and Ind-PU. FTIR results confirmed that there is also no any influence on the chemical structure of PU wih Indole dye incorporation, the probale reason behind may be due to small amount of Indole dye incarporation within PS and PU ENMs respectively [27].

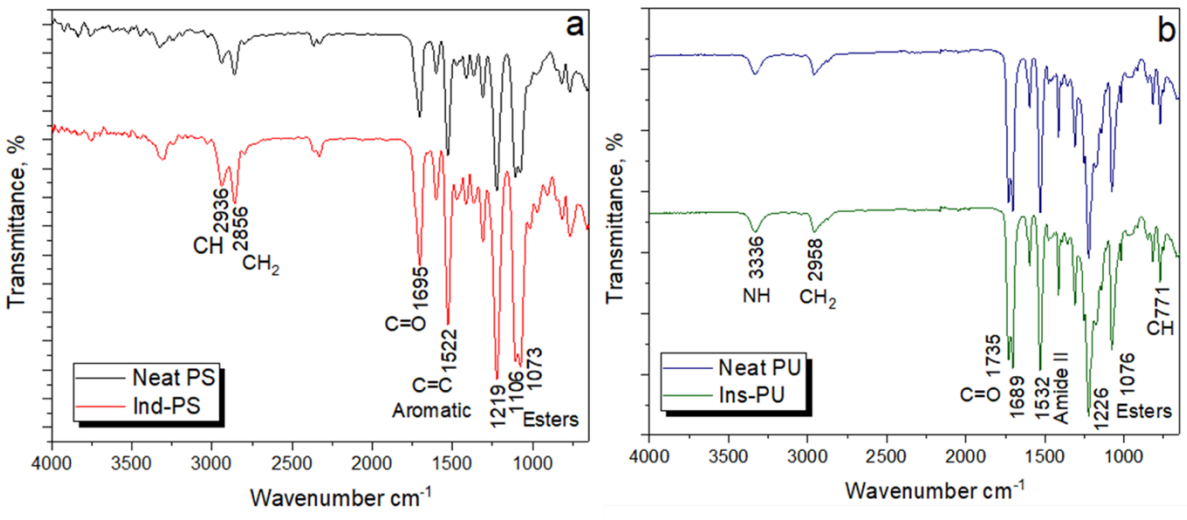

Fig. 5. 6. FTIR spectrum of (A) Neat PS and Ind-PS, (B) Neat PU and Ind-PU

5.4. Conclusion

The Ind-PS ENM and Ind-PU ENM were successfully prepared via electrospinning technique for application of quick-response code recording/ erasing multiple times. The recorded quick-response code on newly prepared ENMs were easily readable via Smartphone at the small area of 1x1 square cm. These ENMs and their solutions loaded with indole dyes were found to be photo-switchable upon alternating UV and visible light irradiations. The rate of photo coloration was observed faster than the rate of decoloration for both nanofibers. Additionally, use of indole compound in PS and PU matrices increased average nanofiber diameter. The Ind-PU ENMs showed better color yield and have potential to be used multiple times due to its shape memory where Ind-PS ENMs can only be used for few times. Only few reports can be found on such application of ENMs and this is the first time the application of hydrophobic polymeric nanofibers with delay in rate of decoloration of both type of photosensitive ENMs have been explored for textile applications.

5.5. References

[1] Xue, J., Wu, T., Dai, Y., & Xia, Y. (2019). Electrospinning and electrospun nanofibers: methods, materials, and applications. Chemical reviews, 119(8), 5298-5415.

[2] J. Lee, C. W. Lee and J.M Kim, Fabrication of patterned images in Photosensitive Organic Microfibers, Macromol. Rapid Comm.,**31**(2010)1010-1014.

[3] Y. S. Nam, I. Yoo, O. Yarimaga, I. S. Park, D. H. Park, S. Song and C .W. Lee, Photosensitive spiropyran-embedded PDMS for highly sensitive and tunable optochemical gas sensing. Chem. Comm., 50(2014) 4251-4254.

[4] L.Shuiping, T. Lianjiang, H. Weili, L. Xiaoqiang and C. Yanmo, Cellulose acetate nanofibers with photosensitive property: Fabrication and characterization ,Mater. Lett., 64(2010) 2427.

[5] W. Hu, S. Liu, S. Chen and H. Wang, Preparation and properties of photosensitive bacterial cellulose nanofibrous membranes, Cellulose., 18(2011) 655-661.

[6] F. B. De Sousa, J. D. Guerreiro, M. Ma, D. G. Anderson, C. L. Drum, R. D. Sinisterra and R. Langer, Photo-response Behavior of Electrospun Nanofibers Based on Spiropyrancyclodextrin Modified Polymer, J Mater. Chem., **20** (2010) 9910-9917.

[7] F. Di Benedetto, E. Mele, A. Camposeo, A. Athanassiou, R. Cingolani and D. Pisignano, Photoswitchable organic nanofibers, Adv. Mater.,**20**(2008) 314-318.

[8] M. Wang, S. A. Vail, A. E. Keirstead, M. Marquez, D. Gust and A. A. Garcia, Preparation of photosensitive poly(vinylidene fluoride-co-hexafluoropropylene) fibers by electrospinning, Polymer., **50**(2009) 3974-3980.

[9] Z. Khatri, S. Ali, I. Khatri, G. Mayakrishnan, S. H. Kim and I. S. Kim, UV-responsive polyvinyl alcohol nanofibers prepared by electrospinning Appl. Surf. Sci., **342** (2015) 64-68

[10] J. M. Meruga, W. M. Cross, P. S. May, Q. Luu, G. A. Crawford and J. J. Kellar, Security printing of covert quick response codes using upconverting nanoparticle inks

[11] Nanotechnology.,23 (2012) 395201.

[12] S. M. R. Billah, R. M. Christie and R. Shamey, Direct coloration of textiles with photosensitive dyes. Part 1 : Application of spiroindolinonaphthoxazines as disperse dyes to polyester, nylon and acrylic fabrics. Color. Technol.,124(2008) 223-228.

[13] Che, Y., Liu, L., Zhao, J., Yu, Y., & Zhao, X. (2019). Photosensitive behavior and mechanism of indole thiosemicarbazide derivates in amorphous powder, solution and nanofiber. Dyes and Pigments, 169, 105-110.

[14] Pinto, T. V., Cardoso, N., Costa, P., Sousa, C. M., Durães, N., Silva, C., ... & Freire, C. (2019). Light driven PVDF fibers based on photosensitive nanosilica@ naphthopyran fabricated by wet spinning. Applied Surface Science, 470, 951-958

[15] Hu, J., & Zhang, K. Q. (2019). Electrospun Nanofibers for Optical Applications. In Electrospinning: Nanofabrication and Applications (pp. 603-617). William Andrew Publishing.

[16] Galvez, P., Abenojar, J., & Martinez, M. A. (2019). Durability of steel-CFRP structural adhesive joints with polyurethane adhesives. Composites Part B: Engineering, 165, 1-9.

[17] J., Zhao, J., Yu, X., Liu, L., Yu, J., & Ding, B. (2019). Electrospun Nanofibers for Waterproof and Breathable Clothing. In Electrospinning: Nanofabrication and Applications(pp. 543-570). William Andrew Publishing.

[18] Zhang, S., Rind, N. A., Tang, N., Liu, H., Yin, X., Yu, J., & Ding, B. (2019). Electrospun nanofibers for air filtration. In Electrospinning: Nanofabrication and Applications (pp. 365-389). William Andrew Publishing

[19] Khatri, M., Qureshi, U. A., Ahmed, F., Khatri, Z., & Kim, I. S. (2018). Dyeing of Electrospun Nanofibers. Handbook of Nanofibers, 1-16.

[20] Khatri, M., Ahmed, F., Jatoi, A. W., Mahar, R. B., Khatri, Z., & Kim, I. S. (2016). Ultrasonic dyeing of cellulose nanofibers. Ultrasonics sonochemistry, 31, 350-354.

[21] Khatri, M., Ahmed, F., Shaikh, I., Phan, D. N., Khan, Q., Khatri, Z., ... & Kim, I. S. (2017). Dyeing and characterization of regenerated cellulose nanofibers with vat dyes. Carbohydrate polymers, 174, 443-449.

[22] Jatoi, A. W., Ahmed, F., Khatri, M., Tanwari, A., Khatri, Z., Lee, H., & Kim, I. S. (2017). Ultrasonic-assisted dyeing of Nylon-6 nanofibers. Ultrasonics sonochemistry, 39, 34-38.

[23] Khatri, Z., Ahmed, F., Khatri, A., Khatri, M., Qureshi, U. A., & Kim, I. S. (2017). Screen-printed electrospun cellulose nanofibers using reactive dyes. Cellulose, 24(10), 4561-4568.

[24] Khatri, A., Ali, S., Jhatial, A. K., & Kim, S. H. (2015). Dyeability of polyurethane nanofibres with disperse dyes. Coloration Technology, 131(5), 374-378.

[25] Cao, Z. J., Liao, W., Wang, S. X., Zhao, H. B., & Wang, Y. Z. (2019). Polyurethane foams with functionalized graphene towards high fire-resistance, low smoke release, superior thermal insulation. Chemical Engineering Journal, 361, 1245-1254.

[26] Chan, J. P., Battiston, K. G., & Santerre, J. P. (2019). Synthesis and characterization of electrospun nanofibrous tissue engineering scaffolds generated from in situ polymerization of ionomeric polyurethane composites. Acta Biomaterialia

[27] Urbina, L., Alonso-Varona, A., Saralegi, A., Palomares, T., Eceiza, A., Corcuera, M. Á., & Retegi, A. (2019). Hybrid and biocompatible cellulose/polyurethane nanocomposites with water-activated shape memory properties. Carbohydrate polymers, 216, 86-96.

[28] Arráez, F. J., Arnal, M. L., & Müller, A. J. (2019). Thermal degradation of high-impact polystyrene with pro-oxidant additives. Polymer Bulletin, 76(3), 1489-1515.

CHAPTER 6

Zein nanofibers via deep eutectic solvent electrospinning: Tunable morphology with super hydrophilic properties

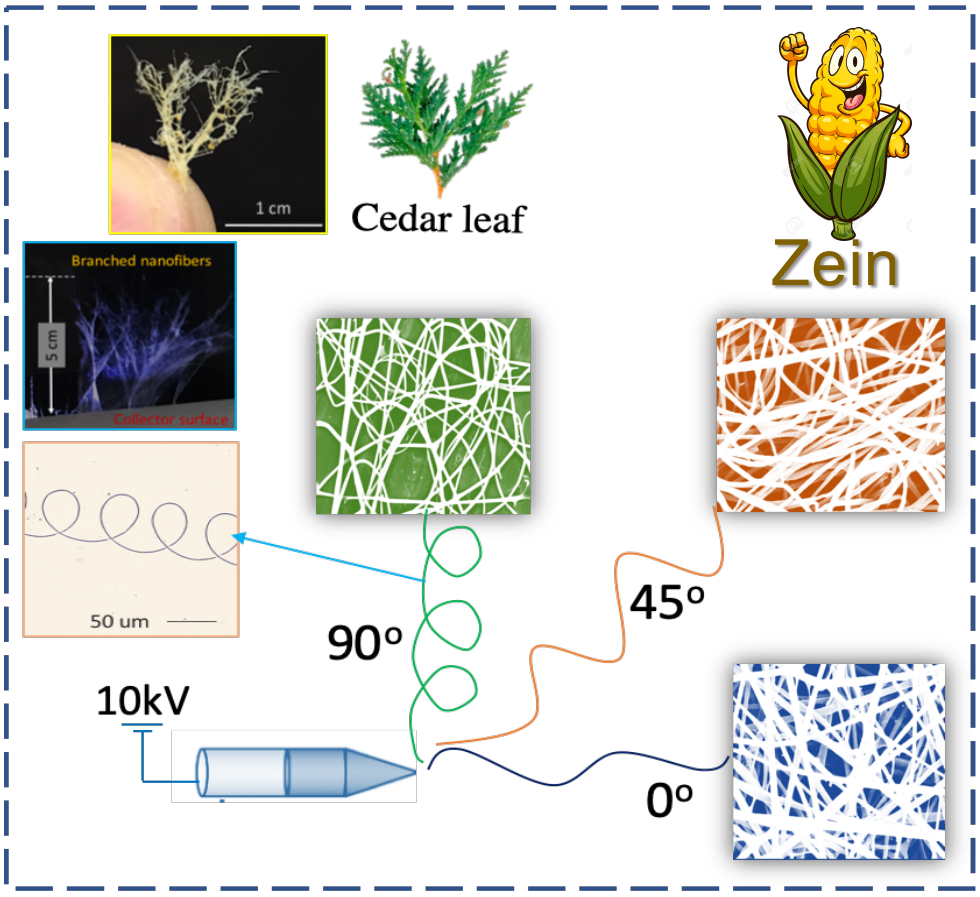

6.1. Introduction

With a full background of electrospinning development to project the question is better to list several organic solvents such as dimethylformamide (DMF) [1], chloroform [2], trifluoracetic-acid [3] and tetra hydro-furan [4], electrospinning is developing from fluid blending process to fluid coaxial 1 and side-by-side [5], and to tr-fluid coaxial [6] and other multi-fluid processes [7,8].

However, all these developments are based on the application of organic solvents for preparing working fluids, which is harmful to environment and health [9].

In contrast, Deep Eutectic Solvents (DES) offers a valuable alternative to overcome the limitations of conventional volatile solvents. DES are widely acknowledged as an ultimate class of Ionic Liquids (ILs) having distinctive chemical properties [10,11].

The prominent applications of DES have initially emerged in the 21st [12], such as bioengineering [13], electrochemical synthesis [14], targeted green extraction [15], hydrogen transfer [16], bio-catalysis [17] and Lithium ion batteries [18].

The DES based on quaternary salt (choline chloride) as a hydrogen bond acceptor (HBA) and (furfuryl alcohol) as a hydrogen bond donor (HBD) has intensively been in the field of green chemistry allowing a cost-effective synthesis of different green materials and utilization for the extraction of bioactive natural materials [19-23].

Zein has attracted a great deal of attention due to its biocompatibility, biodegradability, non-toxicity and its wide abundance on earth [18]. Electrospinning of Zein has yet been challenged by the limitation of reusability of the polymer solution and frequent clogging of spinneret when its dissolution occurs in aqueous-ethanol (Aq-EtOH) [24,25], or its preparation using hazardous solvents, such as DMF [26-28].

Direct electrospinning of water stable Zein nanofibers have remained a challenging task, due to post-treatments such as longer exposure to Ultraviolet or higher temperatures have been considered as an unavoidable step [29-31].

Solvents have direct impact on the morphology of resultant fibers and various morphologies of polymeric nanomaterials have been investigated recently, by using different solvent types [32-35].

The DES have been previously incorporated as a guest molecule used for conveying specific characteristics into chitin nanofibers only, nonetheless direct electrospinning of Zein nanofibers using DES (DES-Zein) has not been reported [36].

In this article, we attempted to fabricate Zein nanofiber using DES directly by electrospinning technique and achieved super hydrophilic Zein nanofibers without any post-treatment. DES used for electrospinning was based on choline chloride (HBA) and furfuryl alcohol (HBD) with a ratio of 1:2 was effectively.

The prepared solution was utilized for the preparation of bead-free Zein nanofibers using 45% (w/w) polymer concentration having the extended shelf life for up to three days. Super hydrophilic DES-Zein nanofibers were compared against the hydrophobic conventional Zein nanofibers (C-Zein) prepared in Aq-EtOH.

DES-Zein nanofibers showed finer average diameter and a unique cedar leaf morphology tuned by varying the spreading angle between the tip and the collector. Precisely, an increase in angle creates alternate coils that leads to a cedar leaf morphology [37-39].

Super hydrophilicity of C-Zein and DES-Zein nanofibers were confirmed by the wicking test and the water contact angle test [40,41,42] and effectively utilized for faster adsorption of impurities present in water [43-45].

The resultant DES-Zein nanofibers were checked for adsorption capability by removal of the Reactive Black 5 dye. Super hydrophilicity, finer diameter and cedar leaf morphology, all attributed to increased adsorption rate and adsorption capability of DES-Zein nanofibers giving them an edge over C-Zein nanofibers.

The DES-Zein nanofibers can effectively be utilized where faster adsorption and super hydrophilicity is required such as biosensor, biomedical strip, controlled drug release, heavy metal and dye adsorption [46].

6.2. **Experimental**

6.2.1. Materials

Zein produced from maize having a melting point of (266-283 °C), Choline chloride (>98%) with molecular weight 139.62 g/mol and Furfuryl alcohol (98%) with molecular weight 98.10 g/mol were supplied by Sigma-Aldrich, USA. Ethanol (99.8%) with molecular weight 46.07 g/mol was supplied by Merck, Japan. CI reactive black 5 bis(sulphatoethylsulphone) (Mw = 991.82 g/mol) purchased from Sumitomo Chemical Co., Ltd., Japan.

6.2.2. Preparation of DES-Zein nanofibers

Zein Nanofibers were prepared separately in conventional and deep eutectic solvent using (Har-100*12, Matsusada Co., Tokyo, Japan) Electrospinning machine. Zein 25% (w/v) in 80% of Aq-EtOH was stirred for 2h at 80 °C [21]. The DES was prepared by mixing Choline chloride and Furfuryl alcohol with molar ratio 2:1 and stirred well until a clear transparent solution was obtained. Zein polymer was then added into DES solution with different concentrations (20, 25, 30, 35, 40, 45, 50 and 55% w/w) and well stirred up to 2h at 80 °C. Each electrospinning solution was poured into a syringe of 5mL attached to a tip of 0.6 mm internal diameter and the flow rate was set to 0.2 mL/h. Copper wire was used as an anode dipped into the Zein solution, and the ground collector was connected as a cathode. The electrospinning parameters were optimized to produce uniform and consistent DES-Zein nanofibers.

The voltages supplied for electrospinning of DES-Zein and C-Zein were optimized as 10 kV and 25 kV respectively and the distances between the tip and the collector for DES-Zein and C-Zein were optimized as 14 cm and 17 cm respectively. The DES-Zein nanofibers were

consistently deposited on a stationary collector at different angles between the tip and the collector from 0° to 90°. After electrospinning, the obtained samples were dried overnight at room temperature to remove residual solvents before subjecting to other characterizations.

6.2.3. Characterizations

Polymer solution properties of DES-Zein such as pH and conductivity were assessed using (WTW MultiLine IDS multi-parameter portable meter). The surface morphology examined under SEM (S-3000N by Hitachi, Japan), C-Zein and DES-Zein were sputtered with Pb-Pt under vacuumed environment prior to take SEM images and the average diameter of was calculated using ImageJ software.

The chemical structure of DES-Zein was assessed through Fourier Transform Infrared (FTIR) spectroscopy (IR Prestige-21 by Schimadzu, Japan) using ATR mode and Xray Photoelectron spectroscopy (XPS) by AXIS Ultra (Schimadzu) with dual-anode X-ray source Al/Mg, HSA hemispherical sector analyzer and the detector, vacuum pressure was maintained at 1.4×10^{-9} torr, and Mg Kα X-ray source (1253.6 eV) was used.

Wide-angle Xray diffractometer (WAXD) Rigaku Miniflex 300 from Japan was used to compare the crystallinity of C-Zein and DES-Zein where the range was 10-80° at the scanning speed $2\theta = 2°$/min. The WCA test was carried on FACE model CA-VP, Kyowa interface science, Japan, five readings were assessed from each sample. The wicking behavior of DES-Zein nanofibers was checked by previously reported methods [35,36,37].

6.2.4. Adsorption studies

The residual values of reactive black 5 after adsorption on DES-Zein nanofibers were analyzed by using Lambda 35 UV-vis spectrophotometer from Perkin Elmer USA.

The absorbance values were taken at λ_{max} 590 nm. The average-thickness of DES-Zein nanofibers was 35 μm. The DES-Zein nanofiber samples were checked for dye adsorption capability, 50 g/L Reactive black 5 was used to check the dye adsorption on novel DES-Zein. The mass 40± 0.2 mg of DES-Zein nanofibers was shacked in glass tube filled with 5 ml of Reactive black 5 dye solution at room temperature. Dye adsorption values were then checked at different intervals (0, 5, 8, 12 ,15 ,18, 20, and 25) min [44,45].

6.3. **Results and discussion**

6.3.1. Effect of solution properties of C-Zein and DES-Zein on morphology

Solution properties have direct impact on the morphology of nanofibers [47-49], more specifically polymer ratio, solvent concentration, pH and electro-conductivity (EC) have been studied before electropinning.

EC and pH of DES-Zein and C-Zein polymer solutions were studied by varying the concentrations of Zein in respective polymer solutions, viz. Aq-EtOH, C-Zein, neat DES, DES-Zein 45%, DES-Zein 22.5% and DES-Zein 15% as given in Table 6. 1.

Neat DES obtained an EC of 1770 micro-symon/centimeter (mS/cm) and pH 4.8. An EC of DES-Zein 15% was observed and 1380 mS/cm and pH 5.0. DES-Zein 22.5% having an EC of 450 mS/cm with pH 6.8 and DES-Zein 45% having an EC of 233 mS/cm with pH 7.3 which is near to neutral pH.

The influence of each polymer solution on electrospinnability and their morphology is revealed in Fig. 6. 1. DES-Zein electropun at concentrations (25%, 35% and 45%) with beads, beaded nanofibers and bead-free nanofibers respectively as shown in Fig. 6. 1(a-c).

On the other hand, Fig. 6. 1(d) shows bead-free ribbon like morphology of C-Zein nanofibers electrospun at 25% polymer concentration [28]. Fig. 6. 1(e,f) showed average diameter of DES-Zein nanofibers (350±50 nm) and C-Zein nanofibers (550±70 nm).

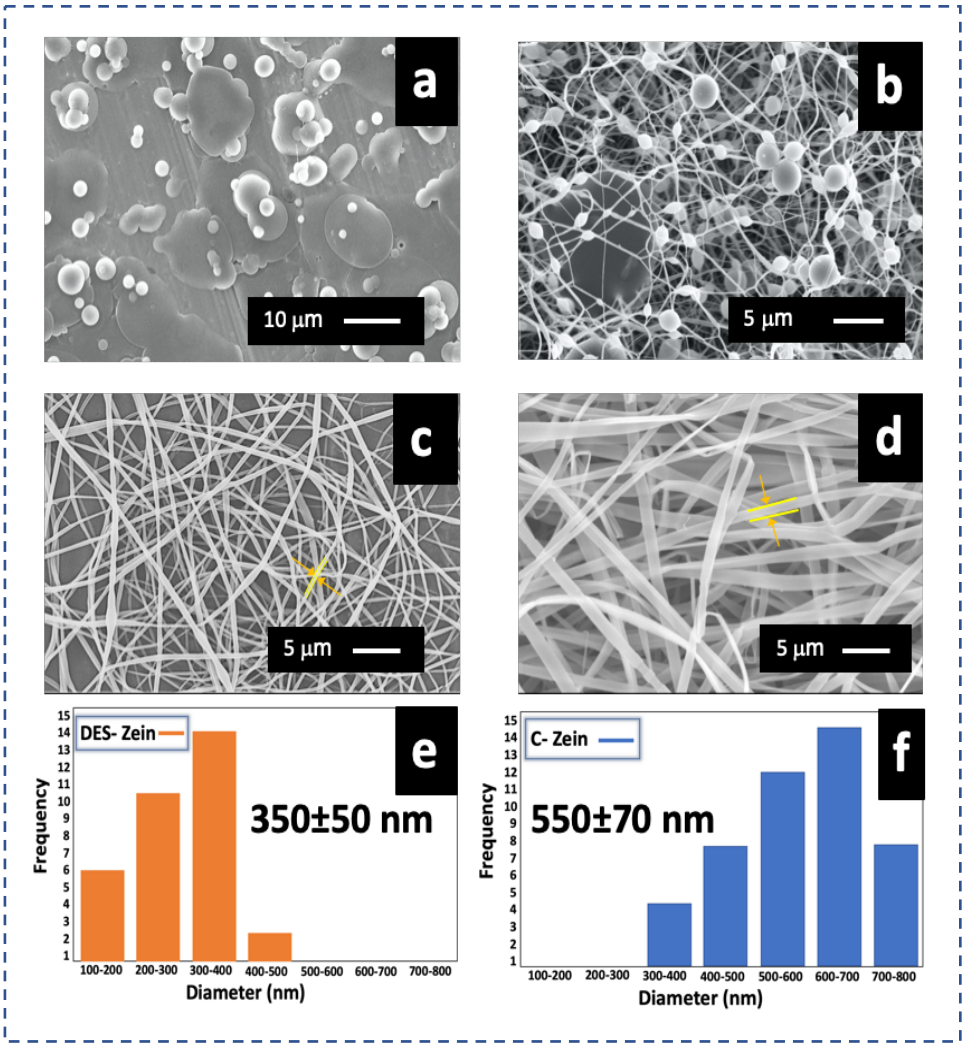

Fig. 6. 1. SEM images of (a) DES-Z 25% (b) DES-Z 35% (c) DES-Z 45% (d) C-Zein 25%, diameter distribution graphs of (e)DES-Zein 45% and (f) C-Zein 25%

Table 6. 1. Solution properties of Neat DES, DES-Zein 25%, DES-Zein 35% and DES-Zein 45%, Aq-EtOH and C-Zein

Solution (10-ml)	Neat DES	DES-Zein 25%	DES-Zein 35%	DES –Zein 45%	Aq-EtOH	C-Zein 25%
pH	4.8	5.6	6.5	7.3	8.0	5.8
mS/cm	1770	1380	450	233	5.7	140

6.3.2. Influence of electrospinning parameters on morphology of DES-Zein nanofibers

The quantitative analyses for the fast preparation of nanofibers via electrospinning is totally depended on the basic parameters of the processing which includes, Taylor cone, straight fluid jet and unstable region which are useful for predicting and manipulating a direct link to the quality of resultant nanofibers [48].

Fig. 6. 2 shows the SEM images of dimeter distribution graphs of DES-Zein nanofibers prepared at different tip-collector distances and supplied voltages. Fig. 6. 2(a-c) show the DES-Zein nanofibers prepared at 20 cm, 14 cm and 8 cm tip-collector distance with average diameters 350±50 nm, 400±70 nm and 450±60 respectively, a slight increase in average diameter observed when decreasing the tip-collector distance and minimum diameter distributions observed at maximum distance 20 cm as revealed in the respective inset images, which was optimized to carry further experiments. Whereas Fig. 6. 2 (d-f) show that the supplied voltage has no significant influence on the morphology of DES-Zein nanofibers.

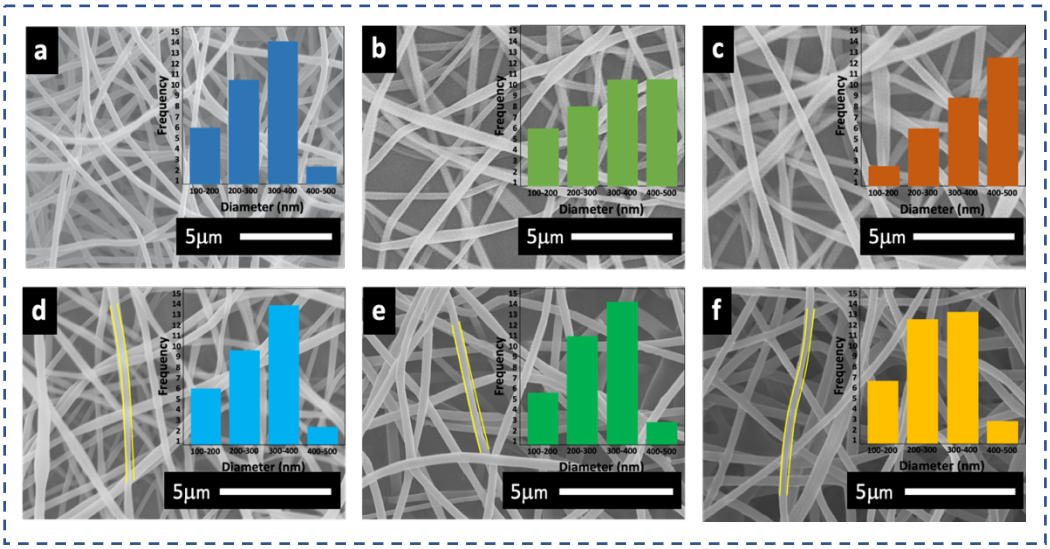

Fig. 6. 2. SEM images of DES-Z 45% with voltage 17 kV at tip-collector distance (a) 20 cm, (b) 14 cm and (c) 8 cm, The DES-Z 45% at tip-collector distance 20 cm and voltage (d) 10 kV, (e) 17 kV and (f) 19 kV

The spreading angle during electrospinning of DES has a significant influence on nanofiber`s morphology with a very unique and interestingly different than what usually obtained in conventional electrospinning. Therefore, we set different angles at 90°, 45° and 0° to investigate the extent of tunability of nanofibers morphology during electrospinning. Fig. 6. 3(a) illustrates that how nanofiber morphology from straight to coiled can directly be formed by tuning spreading angle from 0° to 90°, coil-less morphology obtained at 0°, semi-coil morphology observed at 45° and at 90° a coiling morphology was achieved. In contrast, the DES-Zein nanofibers, C-Zein did not demonstrate any change in morphology by variation of spreading angle.

Furthermore, Fig. 6. 3(b) shows the coiling configuration of coil shaped morphology of DES-Zein nanofibers having a gap of 85±5 µm between two neighboring coils. Fig. 6. 3(c) shows microscopic image of the consistent coil formation in different directions from a divergent point ultimately resulting a cedar leaf effect. Fig. 6. 3(d) shows coil shaped

nanofibers collected on a stationary collector. Fig. 6. 3(e) shows the image of electrospun DES-Zein nanofibers over a stationery metallic collector that resulted in a “tweed like” structure and further prolonged corrugation of four hours resulted into a 3D cedar leaf morphology as shown in Fig. 6. 3(f, g). The probable reason for coils formation during electrospinning was due to α-helix of amino acid series present in the native Zein, the DES with the hydrogen bonding assistance actually preserves the α-helix configuration of Zein during electrospinning of DES-Zein nanofibers. Another reason for coil formation may be the higher conductivity of DES due to the presence of Choline chloride as a salt that may create gaps at the perpendicular collector angle for electrospinning [28,29].

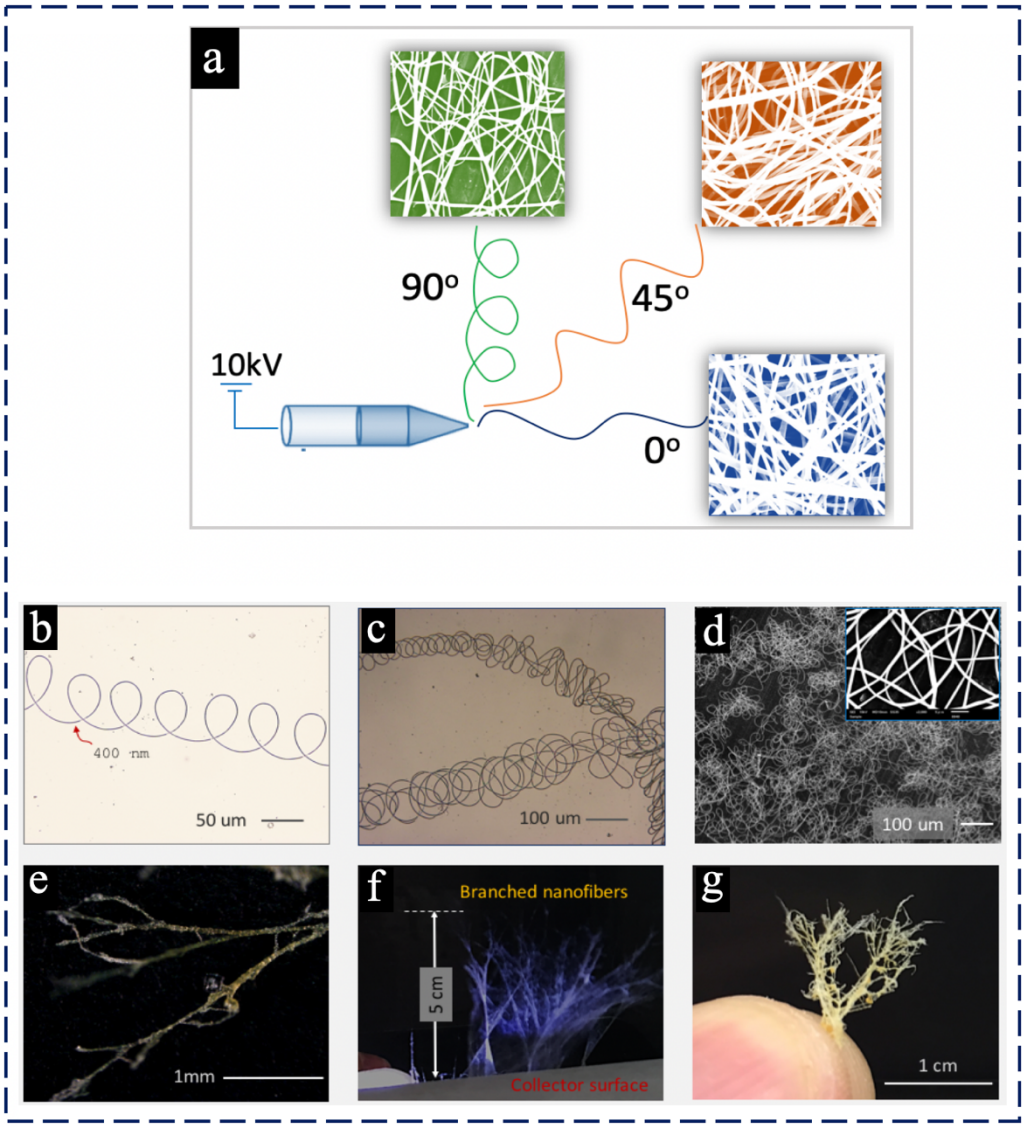

Fig. 6. 3. (a) Tunability of morphology by varying the spreading angle, Microscopic images of b) helical loops, (c) multiple alternative helical loops, (d) multilayered nanofibers, (e) multilayered nanofibers with branches, (f) Photograph of branched nanofibers growth, (g) Cedar leaf morphology of DES-Zein.

6.3.3. Chemical structure of C-Zein and DES-Zein

Fig. 6. 4 shows the FTIR spectrum of electrospun C-Zein and DES-Zein nanofibers. C-Zein showed a significant peak at 3289 cm^{-1} due to -NH stretching, while DES-Zein showed intensive and broad stretching peak at 3303 cm^{-1} due to the strong hydrogen bonding

between -OH from Choline chloride/furfuryl-alcohol moiety and -NH from Zein polymer [15,16,22],

The intense bands at 2875 cm^{-1} and 2960 cm^{-1} due to the asymmetric and symmetric C-H stretching in the spectrum of DES-Zein nanofibers, which may be due to the induced dipole moment caused by the change in solvent polarity comparing to C-Zein nanofibers. Peaks at 1647 cm^{-1} and 1661 cm^{-1} clearly show the amide I (C=O) stretching, the bands at 1540 cm^{-1} in both C-Zein and DES-Zein may be due to presence of amide II (angular deformation vibration of -NH bond). The band at 1240 cm^{-1} in DES Zein and 1170 cm^{-1} in C-Zein reveal the axial deformation of C-N vibration and no peaks found in C-Zein at 1662 cm^{-1}, 1631 cm^{-1} and 1614 cm^{-1}.

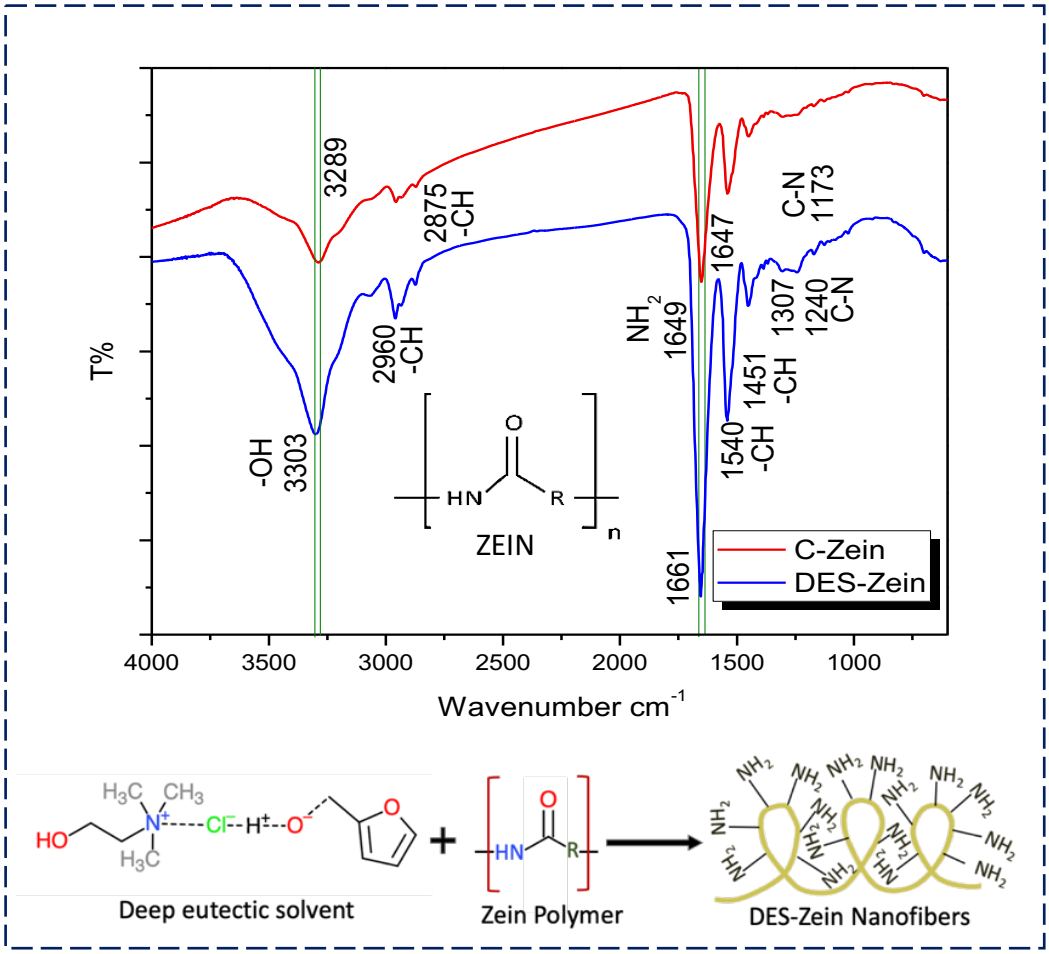

Fig. 6. 4. FTIR spectrum of C-Zein and DES-Zein with proposed chemical structure

Zein nanofibers obtained either from a conventional solvent or a DES, do not have any profound difference in chemical composition as shown in Fig. 6. 5(a), wide scan XPS spectrum of electropun nanofibers was obtained for both samples (C-Zein and DES-Zein), which contain C1s (284eV), N1s (399 eV) and O1s (530 eV). Peak fitting of every component showed a similar composition as C-Zein nanofibers obtained from conventional solvents [28].

Fig. 6. 5(b) shows the deconvolution of C1s peak from DES-Zein revealing three main components C-C, C-N and O=C-N at 284 eV, 285 eV and 287 eV respectively. Fig. 6. 5(c) shows the deconvolution of O1s indicating two different peaks at 529.3 eV and 529.9 eV indicating the presence of O-C and O=C-N respectively. Furthermore, Fig. 6. 5(d) shows the deconvolution of N1s revealing the presence of N in three chemical states N-C, N-C=O and -NH at 398 eV, 399 eV and 400 eV respectively. This finding suggests that the DES solvent do not bring any substantial changes to the chemical composition of Zein polymer.

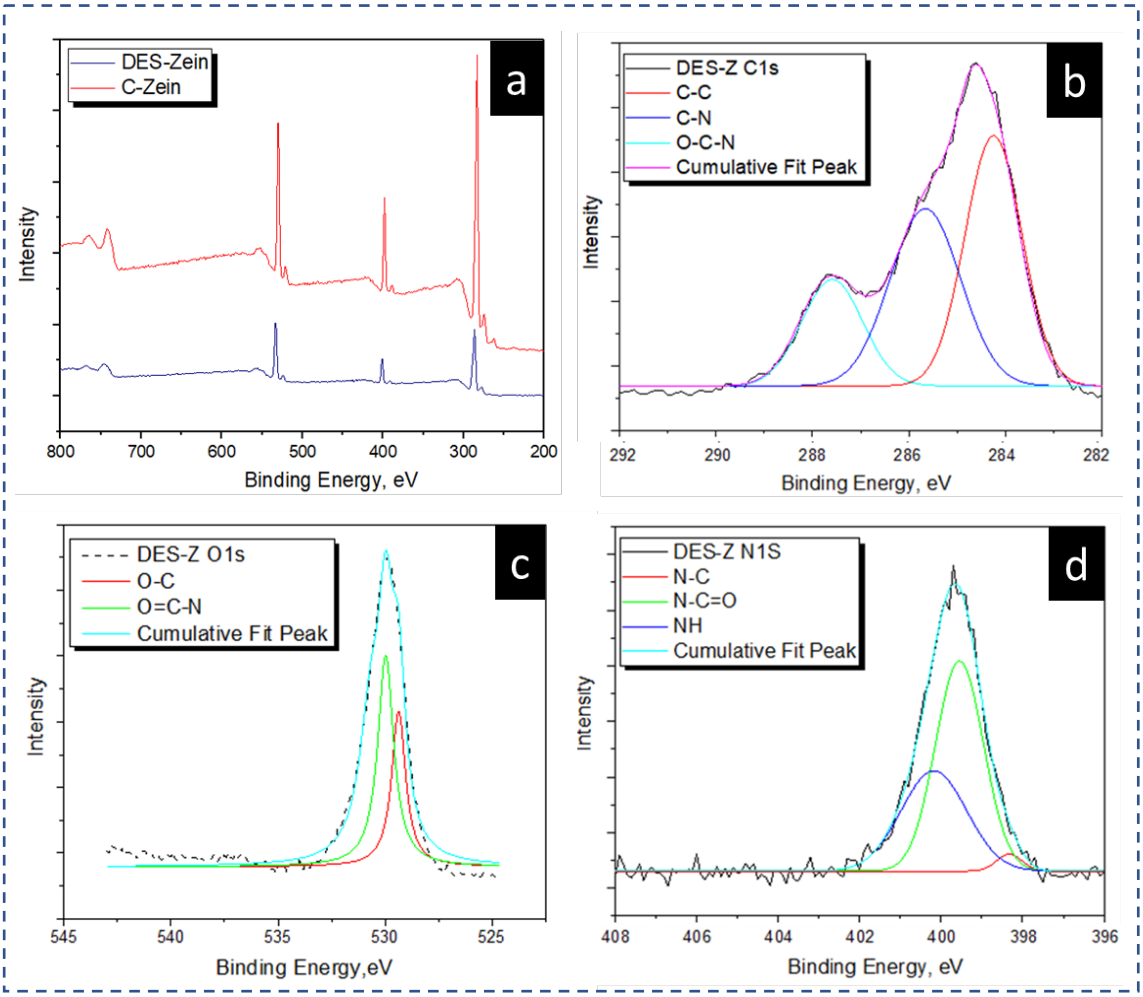

Fig. 6. 5 (a) Wide XPS spectrum of DES-Zein and C-Zein, XPS spectra of (b) DES-Zein C1s, (c) DES-Zein O1s and (d) DES-Zein N1s

6.3.4. Comparison of crystallinity between DES-Zein and C-Zein nanofiber

Fig. 6. 6 shows the XRD patterns of C-Zein and DES-Zein nanofibers. C-Zein shows intensive peak at 9.5° with d-spacing (9.3 Å) and some small peaks at angles 16.6°,18.3°, 22.04°, 22.8° with d-spacing (5.3 Å) , (4.8 Å), (4.0 Å), (3.8 Å) respectively, whereas DES-Zein shows intensive peaks at 8.7° with d-spacing (10.2 Å) and some highly intensive

peaks at 19.8°, 20.1°, 20.9° with d-spacing (4.48 Å), (4.42 Å), (4.2 Å) respectively and an additional small peak also observed at 35.9° with d-spacing (2.4 Å).

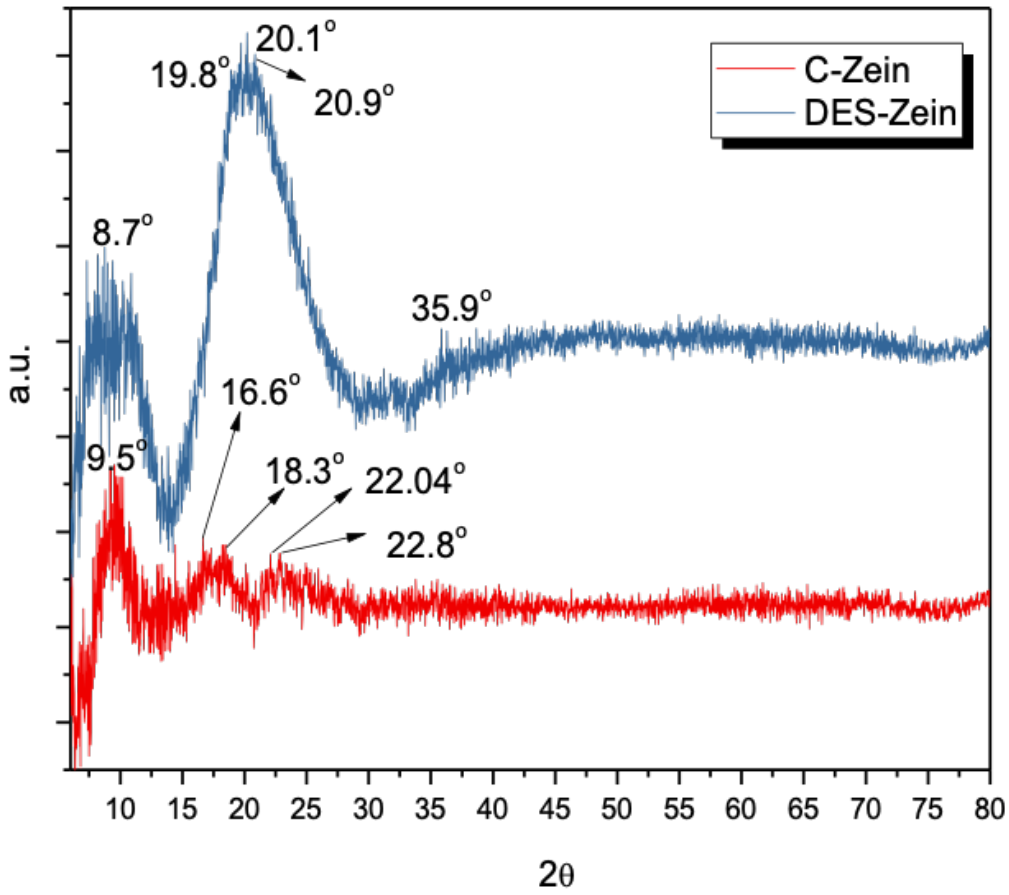

Fig. 6. 6. XRD Comparison of C-Zein and DES-Zein

6.3.5. Hydrophilicity of DES-Zein nanofibers

Water contact angle (WCA) of C-Zein and DES-Zein is demonstrated in Fig. 6. 7. The WCA of in Fig. 6. 7(a) shows, C-Zein takes 70 ±3 seconds to reach the angle from 115° ±10° to 2° ± 2°, whereas, Fig. 6. 7(b) shows that DES-Zein takes only 3 ±1 second to decrease in angle from 122° ±10° to 0°.

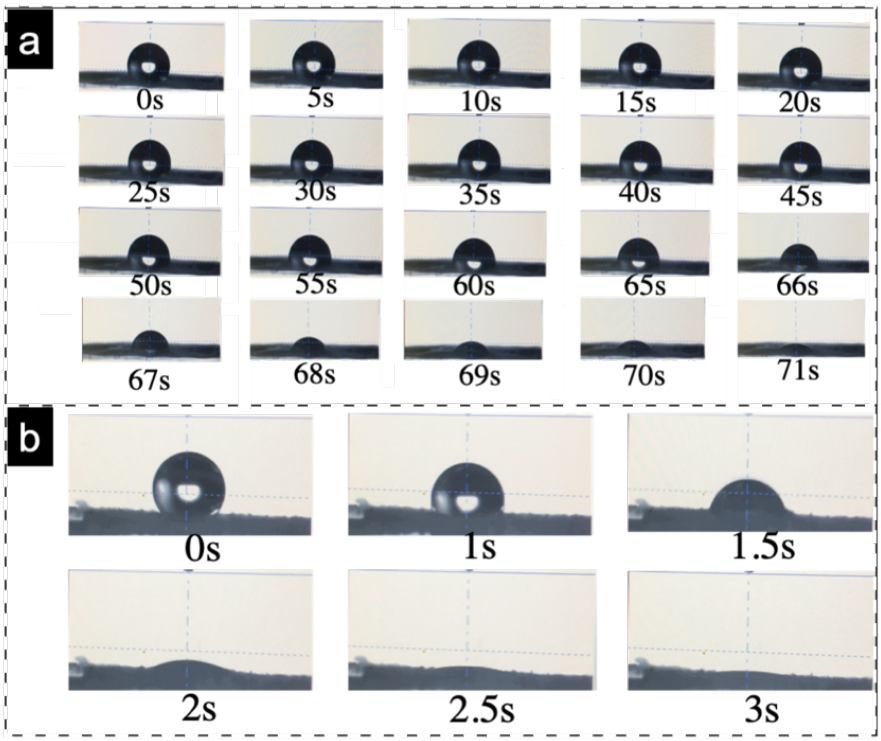

Fig. 6. 7. Water contact angle of (a) C-Zein and (b) DES-Zein

6.3.6. Wicking and Dye adsorption capability of DES-Zein nanofibers

Hydrophobic behavior of C-Zein and super hydrophilic behavior of DES-Zein nanofibers further confirmed by rate of wicking as shown in Fig. 6. 8(a). C-Zein shows the wicking height of 2 mm at initial dipping into dye solution and no more wicking observed until 90 sec. However, DES-Zein reached the wicking height of >16 mm in first 30 sec and slowly reached to the wicking height of 20 mm within 75 sec, confirming the super hydrophilic behavior of DES-Zein nanofibers.

Fig. 6. 8(b) shows the dye removal efficiency of DES-Zein nanofibers. Reactive black 5 dye was used to check the dye removal capability of DES-Zein nanofibers because C-Zein has been previously well studied for selective removal of reactive black 5 dye [28].

This study reveals UV-vis spectrophotometry in which absorbance values of dye solutions were individually checked at different time intervals after dye adsorption on DES-Zein. Increase in dye adsorption on DES-Zein was the result of decreased absorption peaks of UV spectrophotometer with respect to time. DES-Zein nanofibers have capability to remove 60% of the dye within first 3 minutes, whereas the C-Zein nanofiber have a slower removal capability with 45% in the same time, which confirms the rapid adsorption of DES-Zein. The removal efficiency of DES-Zein observed 98.29 ±1 % within 18 minutes and (99 ±1) % in 20 minutes, whereas the removal efficiency of C-Zein observed 97.19 ±1 % in 20 minutes which is lesser than the removal efficiency of DES-Zein achieved within 18 minutes. Increased dye removal efficiency was achieved by DES-Zein at pH 3.9-7.3 as compared to the dye removal efficiency C-Zein at pH 2-6.

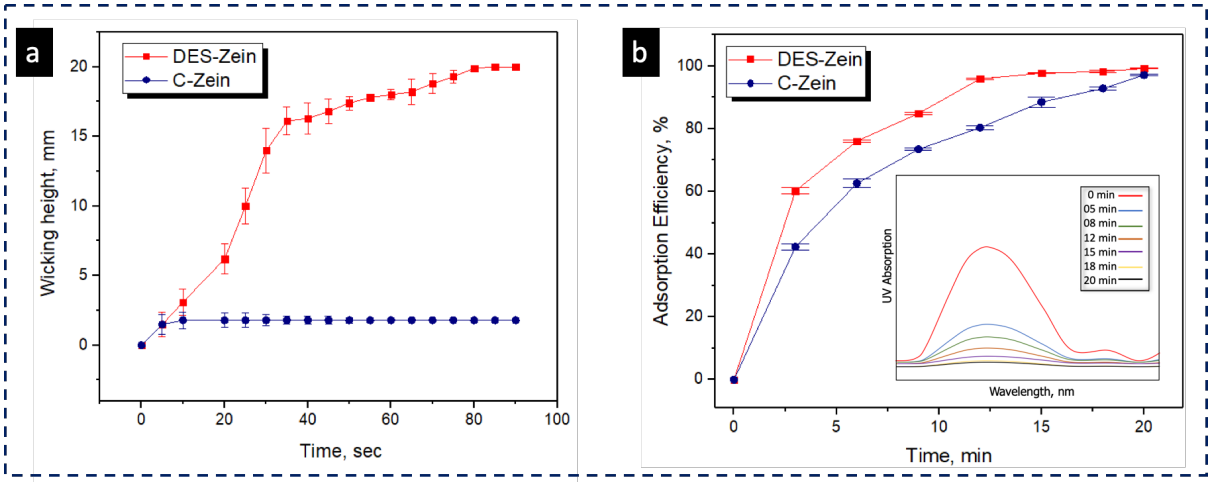

Fig. 6. 8. (a) Wicking profile of DES-Zein and C-Zein (b) Adsorption efficiency graph with inset UV-vis profile

6.3.7. Discussion

DES can directly be utilized for electrospinning of Zein at optimized concentration 45% (w/w) at pH 7.3 having an EC of 233 mS/cm, offering the solution stability for further electrospinning up to three days. The EC values decreased with increasing Zein concentration into DES and the pH was increased due to the protonation of Zein in acidic medium (DES) which can be stabilized through salt bridges of Choline chloride.

On contrary, the addition of Zein polymer into Aq-EtOH resulted increased EC 140 mS/cm and decreases pH in comparison to the Aq-EtOH solution, the obvious reasons for this is because of the less free hydrogens of C-Zein and polyelectrolytic behavior of Aq-EtOH after solubilizing Zein polymer in it [33,50].

No difference in DES-Zein nanofiber morphology was observed by varying voltage supply of 10-19 kV during electrospinning, above 19kV the charges induced were so high that did not allow the polymer solution to pass through the tip, therefore no nanofiber formation observed. Therefore, the lowest 10kV was selected as optimized voltage for electrospinning of DES-Zein, on the other hand preparation of C-Zein in Aq-EtOH requires voltage supply of 22-25 kV for nanofabrication which is quite higher than the voltage required for preparation of DES-Zein nanofibers.

The average diameter of DES-Zein nanofibers (350±50 nm) was observed as around 200nm finer than the average diameter of C-Zein nanofibers (550±70 nm). Also, in contrast to cedar leaf tunable morphology of DES-Zein nanofibers, C-Zein did not demonstrate any change in morphology by variation of spreading angle.

The basic reason for unique morphology was helices and branched coil formation of DES-Zein during electrospinning at angle 90°, the probable reason for coils formation during electrospinning was due to α-helix of amino acid series present in the native Zein.

The deep eutectic solvent with the hydrogen bonding assistance actually preserves the α-helix configuration of Zein during electrospinning of DES-Zein nanofibers.

Another reason for coil formation may be the higher conductivity of DES due to the presence of Choline chloride as a salt that may create gaps at the perpendicular collector angle for electrospinning [34,35].

The chemical spectra of FTIR also proposed some chemical changes of protonation of Zein due to inter/intra hydrogen bonding between -NH groups in the Zein polymer when dissolved in DES [51]. No peak was found in C-Zein at 1662 cm^{-1}, 1631 cm^{-1} and 1614 cm^{-1} which clearly reveals a major presence of α helices in DES-Zein rather than β sheets or β turns [52]. α helices in the chemical structure of DES-Zein can be one of the reasons for the tweed-like morphology formed during electrospinning.

Evidently, DES-Zein showed increased crystallinity compared to C-Zein due the bulk presence of -OH bonds as supported by FTIR results, which was the reason of decreased distance between the molecules in the molecular chain and increased diffraction angles [52]. The d-spacing of ~4.5 Å is considered to be the average backbone distance within the α-helix of Zein structure. However, in parallel the larger d-spacing of ~10Å is believed to be the spacing of the inter-helix packing or the mean distance approach to the neighboring helices [50,52].

The increase in its intensity implies the irruption of DES-Zein molecular aggregation because of increased d-spacing and more inter-helix packing of DES-Zein [47].

The faster adsorption achieved by DES-Zein was due to the electrostatic interactions between the -NH and -OH and their abundancy on surface of nanofibers resulted from the protonation by DES.

WCA and wicking confirmed the super hydrophilic nature of DES-Zein nanofibers in contrast to hydrophobic conventional Zein, due to presence of more amines and hydrogen bonds on the surface of ribbons, that was the reason that DES-Zein nanofibers showed faster and increased dye removal efficiency, Hence, DES-Zein can potentially be considered for the applications where faster adsorption is required such as biosensors and selective adsorption of impurities present in environment.

6.4. Conclusion

Zein nanofibers were successfully electrospun using DES. The optimized parameters to produce bead free nanofibers were 45% (w/w) polymer concentration with pH 7.3 and EC 233 mS/cm. The resultant DES-Zein nanofibers showed aligned to tweed like cedar leaf morphology tuned by varying the spreading angle from 0° to 90°. The average diameter of DES-Zein nanofibers was 350±50 nm, about 200 nm finer than the average diameter of C-Zein nanofibers 550±70 nm. In contrast to hydrophobic C-Zein nanofibers, DES-Zein nanofibers showed super hydrophilic character confirmed by WCA, the drop from 122°±10° promptly sunk to 0° within 3 seconds. Additionally, DES-Zein nanofiber showed higher wicking rate, thanks to the cedar leaf morphology and the abundant presence of -NH and -OH groups on the surface of DES-Zein nanofibers, which allow it to be used where super hydrophilicity is required.

6.5. References

[31] X. Zhou, W. Jin, C. Sun, S.H. Gao,C. Chen, Q. Wang, & Q.Wang, "Microbial degradation of N, N-dimethylformamide by Paracoccus sp. strain DMF-3 from activated sludge." Chemical Engineering Journal 343 (2018): 324-330.

[32] K. Baskar, J. Ananthi & S. Ignacimuthu, "Toxic effects of Solanum xanthocarpum Sch &Wendle against Helicoverpa armigera (Hub.), Culex quinquefasciatus (Say.) and Eisenia fetida (Savigny, 1826)." Environmental Science and Pollution Research 25.3 (2018): 2774-2782.

[33] Viglianisi, C., Scarlini, A., Tofani, L., Menichetti, S., Baschieri, A., & Amorati, R. (2019). Magnetic nanoantioxidants with improved radical-trapping stoichiometry as stabilizers for inhibition of peroxide formation in ethereal solvents. Scientific reports, 9(1), 1-7.

[34] Zhou, H., Shi, Z., Wan, X., Fang, H., Yu, D. G., Chen, X., & Liu, P. (2019). The relationships between process parameters and polymeric nanofibers fabricated using a modified coaxial electrospinning. Nanomaterials, 9(6), 843.

[35] Yu, D. G., Li, J. J., Zhang, M., & Williams, G. R. (2017). High-quality Janus nanofibers prepared using three-fluid electrospinning. Chemical Communications, 53(33), 4542-4545.

[36] Zhao K, Wang W, Yang Y, Wang K, Yu DG. From Taylor cone to solid nanofiber in tri-axial electrospinning: Size relationships. Results in Physics. 2019 Dec 1;15:102770.

[37] Riley, R. S., and E. S. Day. "Wiley Interdiscip." Rev.: Nanomed. Nanobiotechnol 9.4 (2017): 1449.

[38] Yu, D. G., Wang, M., Li, X., Liu, X., Zhu, L. M., & Annie Bligh, S. W. (2019). Multifluid electrospinning for the generation of complex nanostructures. Wiley Interdisciplinary Reviews: Nanomedicine and Nanobiotechnology, e1601.

[39] E.L. Smith, A.P. Abbott, K.S. Ryder, Deep eutectic solvents (DESs) and their applications." Chemical reviews 114.21 (2014): 11060-11082.

[40] C.A. Nkuku, R.J. J. LeSuer. "Electrochemistry in deep eutectic solvents." The Journal of Physical Chemistry B 111.46 (2007): 13271-13277.

[41] A. Paiva, R. Craveiro, I. Aroso, M. Martins, R.L. Reis, A.R.C. Duarte, "Natural deep eutectic solvents–solvents for the 21st century." ACS Sustainable Chemistry & Engineering 2.5 (2014): 1063-1071.

[42] Y.P Mbous, M. Hayyan, A. Hayyan, W.F.Wong, M.A. Hashim, M. A., & C.Y. Looi, , "Applications of deep eutectic solvents in biotechnology and bioengineering—promises and challenges." Biotechnology advances 35.2 (2017): 105-134.

[43] A. Abo-HamadM. Hayyan, M.A. AlSaadi, M. A. Hashim, ”Potential applications of deep eutectic solvents in nanotechnology." Chemical Engineering Journal273 (2015): 551-567.

[44] Chatterjee, M., Ishizaka, T., & Kawanami, H. (2018). Accelerated decarbonylation of 5-hydroxymethylfurfural in compressed carbon dioxide: a facile approach. Green chemistry, 20(10), 2345-2355.

[45] Paulino, P. N., Perez, R. F., Figueiredo, N. G., & Fraga, M. A. (2017). Tandem dehydration–transfer hydrogenation reactions of xylose to furfuryl alcohol over zeolite catalysts. Green Chemistry, 19(16), 3759-3763.

[46] L. Millia, V. Dall'Asta, C. Ferrara, V. Berbenni, E. Quartarone, F.M. Perna & P. Mustarelli, "Bio-inspired Choline chloride-based deep eutectic solvents as electrolytes for lithium-ion batteries." Solid State Ionics 323 (2018): 44-48

[47] Wang, Y., Niu, Z., Zheng, Q., Zhang, C., Ye, J., Dai, G., ... & Zhang, X. (2018). Zn-based eutectic mixture as anolyte for hybrid redox flow batteries. Scientific reports, 8(1), 5740

[48] Li, G., Li, N., Zheng, M., Li, S., Wang, A., Cong, Y., ... & Zhang, T. (2016). Industrially scalable and cost-effective synthesis of 1, 3-cyclopentanediol with furfuryl alcohol from lignocellulose. Green Chemistry, 18(12), 3607-3613.

[49] Perez, R. F., & Fraga, M. A. (2014). Hemicellulose-derived chemicals: one-step production of furfuryl alcohol from xylose. Green Chemistry, 16(8), 3942-3950.

[50] M.W. Nam, J. Zhao, M.S. Lee, J.H. Jeong, & J. Lee, "Enhanced extraction of bioactive natural products using tailor-made deep eutectic solvents: application to flavonoid extraction from Flos sophorae." Green Chemistry 17.3 (2015): 1718-1727.

[51] A.P. Abbott, S. Cihangir, & K.S. Ryder, "Redox fusion of metal particles using deep eutectic solvents." Chemical Communications 54.24 (2018): 3049-3052.

[52] Wang, H. J., Cao, Y., Wang, C. F., Cui, S. Z., Mi, L. W., & Miyazawa, T. (2016). Green self-assembly of zein-conjugated ZnO/Cd (OH) Cl hierarchical nanocomposites with high cytotoxicity and immune organs targeting. Scientific reports, 6, 24387.

[53] Lu, M., Han, G., Jiang, Y., Zhang, X., Deng, D., & Ai, N. (2015). Solubilities of carbon dioxide in the eutectic mixture of levulinic acid (or furfuryl alcohol) and Choline chloride. The Journal of Chemical Thermodynamics, 88, 72-77.

[54] Wang, M., Hai, T., Feng, Z., Yu, D. G., Yang, Y., & Annie Bligh, S. W. (2019). The relationships between the working fluids, process characteristics and products from the modified coaxial electrospinning of zein. Polymers, 11(8), 1287.

[55] Wang, Q., Yu, D. G., Zhang, L. L., Liu, X. K., Deng, Y. C., & Zhao, M. (2017). Electrospun hypromellose-based hydrophilic composites for rapid dissolution of poorly water-soluble drug. Carbohydrate polymers, 174, 617-625.

[56] L.I. Tomé, V. Baião, W. da Silva, & C.M Brett,. "Deep eutectic solvents for the production and application of new materials." Applied Materials Today 10 (2018): 30-50.

[57] N. Amiri, A. Moradi, S.A.S. Tabasi, & J. Movaffagh, "Modeling and process optimization of electrospinning of chitosan-collagen nanofiber by response surface methodology." Materials Research Express 5.4 (2018): 045404.

[58] U.A. Qureshi, Z. Khatri, F. Ahmed, M. Khatri & I.S. Kim, "Electrospun zein nanofiber as a green and recyclable adsorbent for the removal of reactive black 5 from the aqueous phase." ACS Sustainable Chemistry & Engineering 5.5 (2017): 4340-4351.

[59] Yao, C., Li, X., & Song, T. (2007). Electrospinning and crosslinking of zein nanofiber mats. Journal of applied polymer science, 103(1), 380-385.

[60] Lu, H., Wang, Q., Li, G., Qiu, Y., & Wei, Q. (2017). Electrospun water-stable zein/ethyl cellulose composite nanofiber and its drug release properties. Materials Science and Engineering: C, 74, 86-93.

[61] G. W., Woods, K. K., Sessa, D., & Biswas, A. (2008). Electrospun zein fibers using glutaraldehyde as the crosslinking reagent: Effect of time and temperature. Macromolecular Chemistry and Physics, 209(10), 1003-1011

[62] Anbukarasu, P., Sauvageau, D., & Elias, A. (2015). Tuning the properties of polyhydroxybutyrate films using acetic acid via solvent casting. Scientific reports, 5, 17884

[63] Samuel, C., Raquez, J. M., & Dubois, P. (2013). PLLA/PMMA blends: A shear-induced miscibility with tunable morphologies and properties. Polymer, 54(15), 3931-3939.

[64] Ravati, S., & Favis, B. D. (2013). Tunable morphologies for ternary blends with poly (butylene succinate): Partial and complete wetting phenomena. Polymer, 54(13), 3271-3281.

[65] Zhang, X., Zhu, J., Haldolaarachchige, N., Ryu, J., Young, D. P., Wei, S., & Guo, Z. (2012). Synthetic process engineered polyaniline nanostructures with tunable morphology and physical properties. Polymer, 53(10), 2109-2120.

[66] C. Mukesh, D. Mondal, M. Sharma, & K. Prasad. "Choline chloride–thiourea, a deep eutectic solvent for the production of chitin nanofibers." Carbohydrate polymers 103 (2014): 466-471.

[67] Du, C., Zhao, B., Chen, X. B., Birbilis, N., & Yang, H. (2016). Effect of water presence on Choline chloride-2urea ionic liquid and coating platings from the hydrated ionic liquid. Scientific reports, 6, 29225.

[68] Yao, T., Li, X., Lin, Q., Jie, W., Ren, Z., Wang, C., ... & Yang, B. (2009). Patterns of conducting polypyrrole with tunable morphologies. Polymer, 50(16), 3938-3942.

[69] Huan, W., Zhang, J., Qin, H., Huan, F., Wang, B., Wu, M., & Li, J. (2019). A magnetic nanofiber-based zwitterionic hydrophilic material for the selective capture and identification of glycopeptides. Nanoscale, 11(22), 10952-10960.

[70] F. Ahmed, A. A Arbab, A.W. Jatoi, M. Khatri, N. Memon, Z. Khatri, & I.S.Kim, "Ultrasonic-assisted deacetylation of cellulose acetate nanofibers: A rapid method to produce cellulose nanofibers." Ultrasonics sonochemistry 36 (2017): 319-325.

[71] M. Khatri, F. Ahmed, A.W. Jatoi, R.B. Mahar, Z. Khatri & I.S. Kim, "Ultrasonic dyeing of cellulose nanofibers." Ultrasonics sonochemistry 31 (2016): 350-354.

[72] Khatri, M, F. Ahmed, I. Shaikh, D.N. Phan, Q. Khan, Z. Khatri, H. Lee, H. and I.S Kim, "Dyeing and characterization of regenerated cellulose nanofibers with Vat dyes." Carbohydrate polymers 174 (2017): 443-449

[73] Zang, L., Lin, R., Dou, T., Ma, J., & Sun, L. (2019). Electrospun superhydrophilic membranes for effective removal of Pb (II) from water. Nanoscale Advances, 1(1), 389-394.

[74] U.A. Qureshi, Z. Khatri, F. Ahmed, A.S. Ibupoto, M.Khatri ,F.K. Mahar, R.Z. Brohi, R.Z. and I.S. Kim, "Highly efficient and robust electrospun nanofibers for selective removal of acid dye." Journal of Molecular Liquids 244 (2017): 478-488.

[75] A.S. Ibupoto, U.A. Qureshi, F. Ahmed, Z. Khatri, M.Khatri, M. Maqsood, R.Z. Brohi and I.S. Kim, "Reusable carbon nanofibers for efficient removal of methylene blue from aqueous solution." Chemical Engineering Research and Design 136 (2018): 744-752.

[76] Yang, Y., Zhu, T., Liu, Z., Luo, M., Yu, D. G., & Bligh, S. A. (2019). The key role of straight fluid jet in predicting the drug dissolution from electrospun nanofibers. International journal of pharmaceutics, 569, 118634.

[77] M.C. Morris, H.F. Mc Murdie, E.H. Evans, B. Paretzkin, H.S. Parker, N.C. Panagiotopoulos & C.R. Hubbard, "Standard X-ray Diffraction Powder Patterns, NBS Monograph 25, Section 18, Data for 58 Substances." Gaithersburg: National Bureau of Standards (1981): 64-65.

[78] Son, W. K., Youk, J. H., Lee, T. S., & Park, W. H. (2004). The effects of solution properties and polyelectrolyte on electrospinning of ultrafine poly (ethylene oxide) fibers. polymer, 45(9), 2959-2966.

[79] Shen, L., & Huang, X. (2019). Tuning the morphologies and electrical properties of azobenzene-4, 4′-dicarboxylate-doped polypyrrole via ultraviolet light irradiation and medium pH alteration. Polymer, 176, 188-195.

[80] S. Ali, Z. Khatri, K.W. Oh, I.S. Kim, & S.H. Kim, "Zein/cellulose acetate hybrid nanofibers: Electrospinning and characterization." Macromolecular Research 22.9 (2014): 971-977.

[81] K.Shi, J.L. Kokini, & Q. Huang, "Engineering zein films with controlled surface morphology and hydrophilicity." Journal of agricultural and food chemistry 57.6 (2009): 2186-2192.

[82] C.D. Mejia, D.C. Gonzalez, L.J. Mauer, O.H. Campanella& B.R. Hamaker, "Increasing and stabilizing β-sheet structure of maize zein causes improvement in its rheological properties." Journal of agricultural and food chemistry 60.9 (2012): 2316-2321.

[83] I. Erdogan, M. Demir, O. Bayraktar, "Olive leaf extract as a crosslinking agent for the preparation of electrospun zein fibers." Journal of Applied Polymer Science132.4 (2015).

CHAPTER 7

Conclusion

In this dissertation, energy efficient and environment friendly approaches have been studied for advanced textile applications. Different nanofiber types including cellulose, silk, Zein, polyurethane and polystyrene were prepared using electrospinning technique. Cellulose nanofibers were formed by means of deacetylation of electrospun cellulose acetate nanofibers. Silk fibroin nanofiber were prepared by complex dissolution followed by dialysis and electrospinning. Cellulose nanofibers with reactive dyes and silk fibroin nanofibers with acid dyes were individually dyed under ultrasonication and several dyeing parameters (temperature, time and dye concentration) were optimized. In parallel to improving color yield, color fastness properties of cellulose nanofibers were improved using vat dyes which ultimately reduced drainage of dye effluent to the environment during washing process. Photo responsive polyurethane and polystyrene nanofibers were prepared using dope-dyeing technique and the indole-based material was doped to achieve photo responsive function. Polyurethane due to its shape memory showed very good dyeability and mechanical properties having an edge over stiff polystyrene nanofibers. These nanofibers have potential to be used to assess the temperature during food or drugs transportation. We for the first time prepared Zein nanofibers using deep eutectic solvents (DES-Zein). The novel DES-Zein nanofibers showed super hydrophilic behavior and a unique cedar leaf morphology with finer diameter compare to conventional Zein. New attributes of DES-Zein allows it to be used for the environmental and biomedical applications.

Accomplishments

(a) Publications

[1] Muzamil Khatri, Zeeshan Khatri*, Sofia El-Ghazali, Nadir Hussain, Umair Ahmed Qureshi, Shunichi Kobayashi, Farooq Ahmed and Ick Soo Kim* "Zein nanofibers via deep eutectic solvent electrospinning: tunable morphology with super hydrophilic properties"
Scientific Reports 10, 1-11, (2020)
https://doi.org/10.1038/s41598-020-72337-4 (IF: 4.120)

[2] Muzamil Khatri, Farooq Ahmed, Shamshad Ali, Mujahid Mehdi, Sana Ullah, Phan Duy Nam ,Zeeshan Khatr*i and Ick Soo Kim*
"Photosensitive nanofibers for data recording and erasing"
The Journal of the Textile Institute. 1754-2340, (2020)
https://doi.org/10.1080/00405000.2020.1761681 (IF: 1.239)

[3] Muzamil Khatri, Farooq Ahmed, Abdul Wahab Jatoi, Rasool Bux Mahar, Zeeshan Khatri* and Ick Soo Kim*
"Ultrasonic Dyeing of cellulose nanofiber"
Ultrasonics sonochemistry 31, 350-354, (2016)
https://doi.org/10.1016/j.ultsonch.2016.01.020 (IF: 7.630)

[4] Muzamil Khatri, Nadir Hussain, Sofia El-Ghazali, Takayuki Yamamoto, Shunichi Kobayashi, Zeeshan Khatri*, Farooq Ahmed, and Ick Soo Kim*
"Ultrasonic-assisted dyeing of silk fibroin nanofibers: an energy-efficient coloration at room temperature"
Applied Nanoscience 1-14, (2019)
https://doi.org/10.1007/s13204-019-01191-2 (IF: 2.88)

[5] Farooq Ahmed, Alvira Ayoub Arbab, Abdul Wahab Jatoi, Muzamil Khatri, Najma Memon, Zeeshan Khatri* and Ick Soo Kim*
"Ultrasonic-assisted deacetylation of cellulose acetate nanofibers: A rapid method to produce cellulose nanofibers"
Ultrasonics sonochemistry 36, 319-325, (2017)
https://doi.org/10.1016/j.ultsonch.2016.12.013 (IF: 7.630)

[6] Muzamil Khatri, Farooq Ahmed, Irfan Shaikh, Phan Duy Nam, Qamar Khan, Zeeshan Khatri*, Hoik Lee and Ick Soo Kim*
"Dyeing and characterization of regenerated cellulose nanofibers with vat dyes"
Carbohydrate Polymers (2017), 174, 443-449, (2017)
https://doi.org/10.1016/j.carbpol.2017.06.125 (IF: 7.182)

[7] Zeeshan Khatri*, Farooq Ahmed, Awais Khatri, Muzamil Khatri, Umair Ahmed Qureshi and Ick Soo Kim*
"Screen-printed electrospun cellulose nanofibers using reactive dyes"
Cellulose, 24, 4561-4568 (2017)
https://doi.org/10.1007/s10570-017-1428-1 (IF: 3.90)

[8] Mujahid Mehdi, Faraz Khan Mahar, Umair Ahmed Qureshi, Muzamil Khatri, Zeeshan Khatri*, Farooq Ahmed, Ick Soo Kim*
"Preparation of colored recycled polyethylene terephthalate nanofibers from waste bottles: Physicochemical studies"
Advances in Polymer Technology 37 (8), 2820-2827, (2018)
https://doi.org/10.1002/adv.21954 (IF: 1.137)

[9] Umair Ahmed Qureshi, Zeeshan Khatri*, Farooq Ahmed, Muzamil Khatri and Ick Soo Kim*
"Electrospun Zein Nanofiber as a Green and Recyclable Adsorbent for the Removal of Reactive Black 5 from the Aqueous Phase"
ACS Sustainable Chemistry & Engineering 5(5), 4340-4351, (2017)
https://doi.org/10.1021/acssuschemeng.7b00402 (IF: 7.632)

[10] Umair Ahmed Qureshi, Zeeshan Khatri*, Farooq Ahmed, Abdul Sameeu Ibupoto, Muzamil Khatri, Faraz Khan Mahar, Rafi Zaman Brohi and Ick Soo Kim*
"Highly efficient and robust electrospun nanofibers for selective removal of acid dye"
Journal of Molecular Liquids, 244, 478-488, (2017)
https://doi.org/10.1016/j.molliq.2017.08.129 (IF: 5.065)

[11] Abdul Sameeu Ibupoto, Umair Ahmed Qureshi, Farooq Ahmed, Zeeshan Khatri*, Muzamil Khatri, Maryam Maqsood, Rafi Zaman Brohi and Ick Soo Kim*
"Reusable carbon nanofibers for efficient removal of methylene blue from aqueous solution"
Chemical Engineering Research and Design , 136, 744-752 , (2018)
https://doi.org/10.1016/j.cherd.2018.06.0351 (IF: 3.35)

[12] Phan Duy Nam, Rina Afiani Rebia, Yusuke Saito, Davood Kharaghani, Muzamil Khatri, Toshihisa Tanaka, Hoik Lee and Ick-Soo Kim*
"Zinc oxide nanoparticles attached to polyacrylonitrile nanofibers with hinokitiol as gluing agent for synergistic antibacterial activities and effective dye removal"
Journal of Industrial and Engineering Chemistry , 85, 258-268 , (2020)
https://doi.org/10.1016/j.jiec.2020.02.008 (IF: 5.09)

[13] Abdul Wahab Jatoi, Farooq Ahmed, Muzamil Khatri, Anwaruddin Tanwari, Zeeshan Khatri*, Hoik Lee and Ick Soo Kim*
Ultrasonic-assisted dyeing of Nylon-6 nanofibers
Ultrasonics Sonochemistry , 39, 34-38, (2017)
https://doi.org/10.1016/j.ultsonch.2017.04.010 (IF: 7.630)

[14] Muhammad Qamar Khan, Hoik Lee, Zeeshan Khatri*, Davood Kharaghani, Muzamil Khatri, Takahiro Ishikawa, Seung-Soon Im and Ick Soo Kim* Fabrication and characterization of nanofibers of honey/poly (1,4-cyclohexane dimethylene isosorbide terephthalate) by electrospinning"
Materials Science and Engineering: C , 81, 247-251 (2017)
,https://doi.org/10.1016/j.msec.2017.08.011 (IF: 5.88)

[15] Motahira Hashmi, Sana Ullah, Azeem Ullah, Muhammad Qamar Khan, Nadir Hussain, Muzamil Khatri, Xinyu Bie, Jungsoon Lee and Ick Soo Kim*
"An optimistic approach from hydrophobic to super hydrophilic nanofibers for enhanced absorption properties."
Polymer Testing, 90, 106683, (2020)
https://doi.org/10.1016/j.polymertesting.2020.106683 (IF: 3.275)

[16] Phan Duy Nam, Muhammad Qamar Khan, Ngoc-Thang Nguyen, Thanh-Thao Phan, Azeem Ullah, Muzamil Khatri, Nguyen Ngoc Kien and Ick Soo Kim*
"A review on the fabrication of several carbohydrate polymers into nanofibrous structures using electrospinning for removal of metal ions and dyes"
Carbohydrate Polymers 252, 117175, (2020)
https://doi.org/10.1016/j.carbpol.2020.117175 (IF: 7.182)

[17] Aamir Abbasi, Sheeraz Ahmed Memon, Raja Fahad Qureshi, Mujahid Mehdi, Muzamil Khatri, Farooq Ahmed, Zeeshan Khatri*, Ick Soo Kim*
"Adsorptive defluoridation from aqueous solution using a novel blend of eggshell powder and chitosan nanofibers"
Materials Research Express, 7, 125005, (2020) (IF: 1.929)

(b) Conferences

[1] Muzamil Khatri*, Abdul Wahab Jatoi, Farooq Ahmed Arain, Zeeshan Khatri and Ick Soo Kim
"Dyeing of nanofibers using ultrasonic energy"
4th International Conference on Energy, Environment and Sustainable Development 2016 (EESD 2016), Jamshoro, Pakistan November 1st to 3rd, 2016
https://www.muet.edu.pk/news/4th-international-conference-energy-environment-and-sustainable-development-2016-eesd-2016-organised

[2] Muzamil Khatri*, Zeeshan Khatri and Ick Soo Kim
"Ultrasonic-Assisted treatments of nanofibers"
Textile Summit 2017, USA NCSU March 20th to 21st , 2017
https://sites.textiles.ncsu.edu/textilesummit/

[3] Muzamil Khatri*, Zeeshan Khatri and Ick Soo Kim
"Deacetylation of Cellulose acetate using ultrasonication"
The 70th Annual Meeting of The Textile Machinery Society of Japan, Osaka, Japan June 1st to 3rd, 2017
http://tmsj.or.jp/annual/70/index.html

[4] Muzamil Khatri*, Zeeshan Khatri and Ick Soo Kim
"Effect of ultrasonication on dyeing of nanofibers",
2017 International Conference on Nanostructures, Nanomaterials and Nanoengineering (ICNNN 2017) Tokyo, Japan October 26th to 29th, 2017
http://www.wikicfp.com/cfp/servlet/event.showcfp?eventid=61279&copyownerid=13881

[5] Muzamil Khatri* and Ick Soo Kim
"Recent trends of nanofibers innovation and commercialization perspective"
International Conference on Nano science and Technology, Dubai, United Arab Emirates September 24th to 25th, 2018
https://www.meetingsint.com/conferences/nanoscience/2018

[6] Muzamil Khatri*, Zeeshan Khatri, Nadir Hussain and Ick Soo Kim
"Electrospinning of nanofibers using green deep eutectic solvents"
Korean Fiber Society 2019 Spring Conference, Daegu, Korea April 17th to 20th, 2019

[7] Muzamil Khatri*, Zeeshan Khatri, Nadir Hussain and Ick Soo Kim, "Preparation of super-hydrophilic Zein nanofibers using green deep eutectic solvents", 14th International Conference on Materials Chemistry (MC14), Birmingham, United Kingdome July 08th to 11th, 2019
https://www.rsc.org/events/detail/31760/14th-international-conference-on-materials-chemistry-mc14

(c) Book Chapter

[1] Authors: Muzamil Khatri, Umair Ahmed Qureshi, Farooq Ahmed, Zeeshan Khatri and Ick Soo Kim*
"Dyeing of Electrospun Nanofibers Handbook of Nanofibers"
Nature- Springer Publishing (2018), Pages (1-16)
https://doi.org/10.1007/978-3-319-42789-8_55-1

(d) Prize/Award

[1] **Muzamil Khatri***, Zeesshan Khatri, Nadir Hussain and Ick Soo Kim. **"Best poster presentation Award"** Korean Fiber Society Spring Conference, EXCO, Daegu, **South Korea**
2019-04-17 to 2019-04-20

Acknowledgements

All praises to almighty Allah, the most gracious and the most merciful.
I am thankful to my parents and my wife Ms. Sofia El-Ghazali for their continuous support and encouragement. I would like to say special thanks to my advisor Prof. Ick Soo Kim for being supportive consistently for 5 years with kind guidelines like my parents.

My sincere appreciation is for Prof. Zeeshan Khatri, who has remained my mentor from my University life, Prof. Zeeshan guided and supported me to enter Japan and encouraged me to go for higher studies and helped me to take right decision on right time.

I am indebted to Prof. Michael James Andrew Honywood and Rassool Omar for counseling and help at each easy or difficult part of my 5 years in Japan.

My profound gratitude would be to Prof. Makoto Shimosaka - Program Director and Dean of the Faculty of Textile Science and Technology for his contributions to the Leading Program. I am deeply thankful to Prof. Mikihiko Miura and Prof. Tsutomu Ishiwatari, Prof. Hiroaki Ishizawa, Prof. Yasushi Tamada, Prof. Masayuki Takatera and Prof. Shigeru Inui, Prof. Farooq Ahmed Arain for their guidance, counselling and help.

I would like appreciate Ms. Akiko Kubota, Ms. Tomoko Ikeda and Ms. Naoko Suguta, from Leading Program staff, they supported me in all my difficult conditions and helped like family members during my studies at Shinshu University.

My sincere thanks are to Prof. Chwee Teck Lim and Prof. Hisatoshi Kobayashi for accepting me guiding me during my academic and business internships.

I am thankful to my friends, Mr. Hussain Nadir, Mr. Mujahid Mehdi Abro, Mr. Uchikado Rikito, Mr. Phan Duy Nam, Mr. Kim Sukjoo, Pakistani community including Mr. Azeem Ullah, Mr. Sana Ullah, Ms. Motahira Hashmi and Mr. Nauman Sarwar for their kind support.

Special thanks to Mr. Kousei Wada, who assisted me to prepare necessary documentation at Shinshu University and I am grateful to all Leading Program student and Kim lab members (Mr. Naoki Uemura, Mr. Takahiro Ishikawa, Mr. Yusuke Saito, Mr. Inoue Yuma, Mr. Murai Masaaki, Mr. Nishino Masayoshi, Mr. Hasegawa Yohei, Mr. Yuko Kaneta, Mr. Yohei, Mr. Otani Hiziri, Hasegawa, Mr. Takayuki Yamamoto, Mr. Dawood Kharaghani, Mr. Mohammad Qamar Khan, Mr. Takato Matsuhisa, Ms. Wang Qianyu, Ms. Bie Xinyu, Mr. Kosuke Hidaka, Mr. Yasunari Yamauchi, Mr. Yuji Suzuki, Mr. Yuki Kikuchi, Mr. Takami Yamaguchi, Ms. Wang Feifei, Mr. Sun Lei, Mr. Md. Kaiser Haider) for spending such a great time for 5 years.